Université de Montréal

Élaboration de couches minces de diamant à partir d'un plasma d'onde de surface non conventionnel

par

Carlos Fernando de Mello Borges
Département de Physique
Faculté des arts et des sciences

Thèse présentée à la Faculté des études supérieures
en vue de l'obtention du grade de
Philosophiae Doctor (Ph.D)
en Physique

Avril, 1996

Université de Montréal

Faculté des études supérieures

Cette thèse intitulée:

Élaboration de couches minces de diamant à partir d'un plasma d'onde de surface non conventionnel

présentée par:
Carlos Fernando de Mello Borges

a été évaluée par un jury composé des personnes suivantes:

Professeur **John L. Brebner**	**président-rapporteur**
Professeur **Michel Moisan**	**directeur de recherche**
Professeur **Michel Wertheimer**	**membre du jury**
Professeur **Jean-Luc Meunier**	**examinateur externe**

Thèse acceptée le: 19 juin 1996

À *Andressa*

Sommaire

Nous avons réalisé des couches minces de diamant polycristallin par une méthode faisant appel à la chimie en phase gazeuse dans un plasma. Le plasma est créé par le champ micro-onde d'une onde de surface électromagnétique utilisée dans une configuration non conventionnelle. Le réacteur à plasma ainsi obtenu possède des proprietés supérieures à celles des réacteurs micro-onde les plus courants.

L'étude paramétrique du réacteur a en effet montré que le flux micro-onde est totalement absorbé par le plasma, ce qui permet un ajustement indépendant et avec une distribution uniforme de la température du porte-substrat: il est également possible d'atteindre des densités volumiques de puissance absorbée très élevées; enfin le réglage de la distance du substrat au plasma s'effectue de façon fine et reproductible.

Nous avons en recours à de nombreux moyens de diagnostic pour caractériser. pendant la phase initiale de nucléation et pendant le processus ultérieur de dépôt. la contamination de la couche de diamant par le Si du substrat et par celui des parois du réacteur.

Nous avons examiné l'influence de l'orientation des plans cristallins du substrat de silicium sur la densité de nucléation, sur la taille des cristaux et sur la rugosité moyenne de la surface du dépôt diamant. Ceci nous a permis de mieux comprendre les mécanismes influant sur l'adhérence de la couche mince au substrat.

Enfin, nous nous sommes penchés sur les mécanismes permettant d'obtenir les rugosités moyennes les plus faibles possible. Ainsi, nous avons mis au point diverses techniques de préparation du substrat avant dépôt. Nous avons aussi

montré que la diminution de la taille des grains de la poudre de diamant utilisée dans le prétraitement et l'accroisement de la densité de puissance absorbée dans le plasma conduisaient à une augmentation de la densité de nucléation et à une décroissance de la taille des cristaux et en conséquence, à une réduction de la rugosité moyenne.

Mots clé: diamant, couche mince, plasma, plasma micro-onde, onde de surface, densité de nucléation, rugosité, adhérence.

TABLE DES MATIÈRES

LISTE DES TABLEAUX

Chapitre 1

Chapitre 4

Chapitre 5

Chapitre 6

LISTE DES FIGURES

Chapitre 1

Chapitre 2

Chapitre 3

Chapitre 4

Chapitre 5

Chapitre 6

LISTE DES ABRÉVIATIONS UTILISÉES DANS LES ARTICLES

CVD	Chemical Vapor Deposition
SW	Surface Wave
ERD-TOF	Elastic Recoil Detection - Time-of-flight
SIMS	Secondary Ion Mass Spetrometry
EMA	Electron Microprobe Analysis
SEM	Scanning Electron Microscopy
XPS	X-Ray Photon-electron Spectroscopy

CHAPITRE 1

Introduction générale

Chapter 1

Introduction générale

Parmi tous les solides cristallins, le diamant occupe une place particulière. Son nom est dérivé du grec $\alpha\delta\alpha\mu\alpha\varsigma$, acier le plus dur, diamant; l'adjectif correspondant signifie inébranlable, inflexible.

Dès 1772, le français Antoine Lavoisier avait mis en évidence le comportement similaire du diamant et du charbon à la combustion [1]. Ses expériences consistaient à dissoudre les gaz de combustion dans du lait de chaux qui, dans les deux cas, provoquaient la précipitation de carbonate de calcium. Il classa ces matériaux dans la famille des corps inflammables. Ce n'est qu'en 1797 que S. Tennant établit que le diamant correspond à une forme allotrope du carbone au même titre que le graphite [1]. Il arriva à cette conclusion en constatant que la même masse de charbon et de diamant conduisait exactement à la même quantité de carbonate de calcium. Cette découverte a orienté par la suite de nombreuses études dans le but de réaliser la synthèse du diamant en laboratoire.

Parmi les nombreux chercheurs prétendant avoir réussi cette synthèse, les plus connus sont J. B. Hannay [2] en 1880 et H. Moissan [3] en 1894. Les expériences de J. B. Hannay ont consisté à chauffer au rouge de l'huile de paraffine (carbure d'hydrogène saturé) enfermée dans des tubes scellés en présence de lithium. La plupart de ces tubes ont explosé ou fui, mais quelques-uns ont résisté et les substances qu'ils renfermaient étaient selon lui du diamant. Cependant, en 1959, K. Lonsdale émit l'hypothèse, ensuite confirmée en 1975 par A. T. Collins à l'aide de cathodoluminescence, que les différentes pierres de Hannay comportaient du diamant mais n'avaient pas toutes la même origine [4]. H. Moissan avait prévu pour sa part de réaliser ses expériences à des pressions élevées. Pour cela, il adjoignit de la fonte (parfois de l'argent) à du charbon fossile et le porta à des températures

très élevées. Comme la fonte dissout plus de carbone à haute température, les précipités de cet élément, formés et comprimés lors d'un brusque refroidissement, devaient selon lui conduire à la formation de diamant. Les particules obtenues après dissolution de la fonte dans des acides furent considérées comme du diamant. Malheureusement, ces échantillons n'ont pas été conservés et ils n'ont donc jamais pu être authentifiés.

On a par la suite pensé utiliser des très hautes pressions pour obtenir une phase plus dense du carbone. La compréhension de la thermodynamique chimique de ce procedé en fonction du domaine de pression et de température n'a été developpée qu'aux 19^{eme} et 20^{eme} siècles. Ce n'est qu'en 1955 que l'on fait état de façon non ambiguë de la synthèse de diamant par cette méthode avec le dépôt d'un brevet par la compagnie General Electric [5]. Cette synthèse s'effectue dans les conditions de stabilité de la phase diamant (et de métastabilité du graphite) sous des pressions statiques de 15 GPa et à des températures de l'ordre de 1500 °C. Cette transformation se fait en présence de plusieurs catalyseurs, tels que le fer ou le nickel, qui jouent le rôle de solvant pour le carbone. Celui-ci diffuse et précipite ensuite sous la forme diamant dans une zone de plus faible pression (inhomogénéité de la compression) ou lors d'une légère détente. Ce procédé, qui au départ ne permettait que de réaliser des poudres contenant une quantité importante d'impuretés, a été affiné par la suite, notamment par le choix des catalyseurs, le contrôle précis des champs de pression et de température et par la géométrie de compression. Ces techniques, regroupées sous le terme générique de haute pression haute température (HPHT), permettent de nos jours la réalisation avec une bonne pureté de cristaux de taille microscopique. Ce terme regroupe également des techniques de compression par ondes de chocs à l'aide d'explosions qui conduisent également à la réalisation de composés diamantés.

La possibilité de former du diamant dans des conditions métastables fut émise pour la première fois en 1911 par W. van Bolton [6]. Cependant l'étude plus approfondie de ce principe de dépôt ne commença que dans les années 1950 avec les travaux de Eversole chez General Electric [7], auquel fut attribuée l'invention de la croissance de diamant sur des poudres par décomposition thermique d'hydrocarbures. Du diamant était alors déposé en même temps que du graphite, et dans une seconde étape du processus, le graphite était regazéifié dans une atmosphère hydrogénée, un cycle dépôt-gravure étant donc nécessaire à l'obtention de la croissance de diamant. Ces expériences ne permettaient qu'une croissance

d'environ 0.1 μm/jour, ce qui n'avait pas convaincu les financiers américains à l'époque. En même temps, l'équipe du professeur B. V. Derjaguin en URSS poursuivait de nombreux essais de synthèse de diamant par différentes techniques [8]. Au cours des années 60 et 70, ce fut pratiquement la seule équipe à travailler sur le sujet avec J. C. Angus [9] aux Etats-Unis. L'équipe russe a ainsi mis en évidence le rôle de l'hydrogène atomique dans la gravure sélective du carbone de lien d'hybridation sp^2.

La synthèse de couches polycristallines de diamant par plasma fut d'abord proposée par les soviétiques [10] suivant une technique non précisée à l'époque mais utilisant des proportions importantes d'hydrogène atomique dans la décharge. Par la suite, seuls les japonais crurent réellement aux résultats annoncés et lancèrent dès le début des années 80 un important programme dans ce domaine, en particulier avec Matsumoto en 1982 [11]. En 1982 et 1983, cette équipe, dont les principaux chercheurs sont S. Matsumoto, M. Kamo et Y. Sato, a publié plusieurs articles sur la synthèse du diamant par plasma micro-onde [12,13] ou par décomposition thermique à l'aide d'un filament chaud [14,15]. La porte était alors ouverte à la synthèse de couches diamant sur substrats pour des applications tant dans le domaine des outils de coupe que dans celui de l'optique et de l'électronique du fait des propriétés multiples du diamant.

Les différents procédés de synthèse de couches diamant sont généralement classés en fonction de la pression dans l'enceinte réactive. À part les très basses pressions, par exemple 5 mtorr, utilisées surtout en recherche, les pressions de travail sont soit comprises entre 1 et 300 torr (pressions dites réduites), soit voisines de la pression atmosphérique. Les techniques à pressions réduites conduisent à une assez bonne uniformité et à une grande pureté des couches; les vitesses de croissance de ces films sont comprises entre 0.5 à 5 μm/heure. Les techniques développées à la pression atmosphérique sont avantageuses du point de vue de la vitesses de croissance (100 à 930 μm/heure pour un film [16,17]) mais la faible pureté et la non uniformité des couches en limitent l'utilisation.

De nombreuses techniques de dépôt diamant ont été mises au point mais elles nécessitent toutes l'obtention d'une dissociation efficace de H_2 en H monoatomique. Les techniques d'activation les plus utilisées sont principalement le plasma micro-onde [12,18] et le filament chaud [19]; nous citerons également celles utilisant un chalumeau [20] et une torche à plasma [21,22].

La quasi totalité des études expérimentales de dépôt diamant par chimie en phase gazeuse (CPG) assistée par plasma micro-onde a été effectuée soit dans une cavité résonnante dont le mode est tel que l'intensité maximale du champ électrique se trouve sur l'axe du tube [23], soit dans un système constitué d'une cloche en silice vitreuse au travers de laquelle passe l'onde électromagnétique entretenant la décharge [17]. Ces deux techniques utilisent les propriétés d'une onde stationnaire.

Ces contingences géométriques et les dimensions limitées qui en découlent ne sont guère compatibles avec une exploitation industrielle d'un procéde de dépôt. Pour nous libérer de ces contraintes et aussi tenter de résoudre certains autres problèmes, nous avons conçu et caractérisé un nouveau type de décharge micro-onde. Ce nouveau réacteur permet d'obtenir des couches de très grande pureté avec une taille de grains de l'ordre de quelques nanomètres seulement si on le souhaite et des vitesses de croissance supérieures à celles des réacteurs à cavité résonnante; un avantage très important de notre système est de permettre le découplage de la température du porte-substrat de la puissance micro-onde incidente, à l'inverse des systèmes à cavité résonnante où très souvent le porte-substrat est même utilisé comme plan réflecteur des micro-ondes. Ce nouveau réacteur fonctionne grâce aux propriétes des ondes de surface. Une onde électromagnétique de surface peut se propager en étant guidée par l'interface entre la colonne de plasma et le matériau diélectrique qui l'entoure. Ce phénomène a été découvert dans les années 60 [24] mais son utilisation pour entretenir des colonnes de plasma est plus récent [25]. Nous allons revenir sur cette question à la section I.3.

Afin de situer notre travail, nous allons maintenant rappeler les différentes formes allotropes du carbone, les propriétés et applications du diamant et les caractéristiques des ondes de surface.

1.1 Les différentes formes allotropes du carbone

Le carbone peut se cristalliser sous différentes formes, à savoir le diamant, la Lonsdaléite, le graphite, le carbone microcristallin mais aussi se retrouver sous une forme amorphe. Nous allons décrire brièvement chacune de ces formes [26,27].

1.1.1 Diamant

Le diamant est une phase thermodynamiquement métastable à l'ambiante: il correspond à une hybridation sp^3, ordonnée dans un réseau CFC (cubique à faces centrées) dont quatre sites tétraédriques sont occupés. La symétrie spatiale de la liaison sp^3 ainsi que la rigidité de la liaison (83 kcal mol^{-1}) en font un matériau ultra-dur dont la dureté Vickers est estimée à 10.000 kg mm^{-2}; le tableau 1 montre qu'il s'agit du corps le plus dur existant. La constante de réseau est de 3.56 $\AA$ et la longueur de liaison de 1.54 $\AA$. La signature Raman du diamant à forme cubique est donnée par un pic à 1332 cm^{-1} pour le carbone 12 et à 1284 cm^{-1} pour le carbone 13.

Tableau 1. Comparaison des duretés Vickers d'un ensemble de matériaux durs.

Matériau	Dureté Vickers (Kg mm^{-1}) (*298 K*)
Diamant	5.700-10.400
Carbone adamantin	6.200
cBN	4,500
BC	2.250
WC	2.190
TiC	2.190
Al_2O_3	2.000
SiC	1.875-3.980
TiN	1,800
Cu	40

1.1.2 Lonsdaléite

La Lonsdaléite possède la forme hexagonale de l'hybridation sp^3 du diamant et l'orientation spatiale de ses plans cristallins est (*111*). Cependant alors que le diamant (*111*) est caracterisé par des plans inclinés les uns par rapport aux autres, la Lonsdaléite donne lieu à un empilement de plans (*111*) quasi parallèles (mais liés entre eux): elle a été trouvée dans certaines météorites. Sa densité est identique à celle du diamant. Ce matériau conduit à un pic Raman à 1315 - 1325 cm^{-1}.

1.1.3 Graphite

Le graphite est la forme cristallisée stable du carbone dans les conditions normales

de pression et de température: il correspond à une hybridation sp^2 dont les liaisons sont coplanaires. Il est composé de feuillets d'atomes liés de façon covalente, ces feuillets étant reliés entre eux par des forces de type Van der Waals. Cette structure a une densité théorique de 2.27. La signature Raman s'exprime par un pic à 1580 cm^{-1}.

1.1.4 Carbone microcristallin

Cette forme vient d'un diamant synthétique de petite taille (liaisons sp^3 dans un micro volume), en liaison sp^2 aux joints de grain avec d'autres micro-cristaux semblables. Un tel matériau est caracterisé par une signature Raman centrée à 1355 cm^{-1}.

1.1.5 Carbone amorphe

Il existe différents types de phases amorphes du carbone suivant la proportion d'atomes en hybridation sp^3 et sp^2 et suivant leur arrangement à courte distance. Par ailleurs, ces phases peuvent le cas échéant contenir une quantité variable d'hydrogène, engendrant différentes familles de composés. Nemanich et al [28] ont montré que leur signature Raman donne lieu à un pic à 1140 cm^{-1} pour la partie du carbone amorphe en liaison sp^3 alors que le pic Raman à 1500 cm^{-1} provient des liaisons sp^2.

1.1.6 Carbone adamantin

Aussi appelé quasi-diamant (*en anglais Diamond-Like Carbon - DLC*), ce matériau est caracterisé en Raman par une seule bande asymétrique vers 1500 cm^{-1}, bande qui n'est pas assignée à une phase précise. Elle ne peut être attribuée à une phase amorphe de carbone sp^2 car son énergie de vibration est supérieure à celle du diamant et inférieure à celle du graphite.

Le carbone adamantin est un composé de grande dureté et stable en témperature jusqu'à 300-350°C environ, dont la concentration en hydrogène est inférieure à 1% et la densité proche de celle du diamant. Il présente une bande interdite de l'ordre de 3 eV, semblant issu d'une configuration de sites sp^3. Ceci serait dû au fort bombardement

ionique (pendant le dépôt) induisant une densification importante de la couche et une grande dureté.

1.2 Propriétés et applications du diamant

Les applications des films diamant peuvent être classées en quatre grandes catégories suivant la propriété particulière dont elles découlent. ce qui donne:

1. les applications mécaniques,
2. les applications optiques,
3. les applications électroniques.
4. les applications biologiques.

Nous allons maintenant considérer brièvement chacune de ces applications.

1.2.1 Applications mécaniques

Le diamant est caractérisé par une conductivité thermique cinq fois plus grande que celle de l'argent ($20\ W/cm$ à $30°C$), une contrainte à la rupture relativement forte variant entre 3.44×10^9 et $9.65 \times 10^{10} Pa$; son coefficient de frottement, η_k. qui dépend de la nature de la face cristalline considérée, est faible et se situe autour de 0.2 en moyenne. Ce frottement dépend de la température et de la teneur en air adsorbé. Ainsi. à $10^{-5} torr$. pour des températures allant de 300 jusqu'à $850°C$, la friction augmente de façon monotone jusqu'à $\eta_k = 0,7$ et reste constante par la suite: après refroidissement, η_k diminue jusqu'à sa valeur initiale.

Les couches minces de diamant possèdent généralement des propriétes voisines de celles du diamant monobloc; ainsi leur conductibilité thermique peut même atteindre celle du diamant monobloc suivant la nature des joints de grain. Cette haute conductibilité thermique, associée à une grande dureté et à une grande résistance chimique. semble particulièrement appropriée, par exemple, à la protection et au bon fonctionnement des thermocouples en milieu chimiquement et mécaniquement hostile. Ces couches peuvent également être utilisées en protection tribologique dans des structures soumises à l'usure.

comme c'est le cas par exemple d'éléments en forme de pointe. Par rapport au carbure de titane, déjà très bon mécaniquement, les couches diamant présentent des caractéristiques supérieures de friction et d'usure. D'autres paramètres sont également à prendre en compte sur le plan des propriétés mécaniques, telles que la rugosité de la surface, la qualité du dépôt obtenu (sphérulitique ou bien cristallisé), ainsi que l'adhérence de la couche au substrat. Ces diverses propriétés confèrent aux couches de diamant une potentialité d'applications dans plusieurs industries, en particulier dans celle de l'automobile.

Les progrès récents concernant l'obtention de couches diamant de granulométrie très faible, ainsi que les post-traitements en plasma d'oxygène capables de graver ces couches de telle sorte à les rendre lisses, sont aussi des atouts pour certaines applications mécaniques (prothèses médicales, résistance à l'usure des têtes de boîtes de vitesses en automobile ou autre). La possibilité d'accroître à volonté la taille des grains et la rugosité moyenne de ces surfaces intéresse haut plus au point l'industrie des outils de coupe et de forage [29].

1.2.2 Applications optiques

Les propriétes optiques du diamant sont également importantes du point de vue industriel. La plupart des diamants naturels ont une raie d'absorption à $8\,\mu m$ mais celle-ci est probablement due à la présence d'hydrogène [30]. Il existe de façon générale une absorption infrarouge due à la création de phonons qui se situe entre 1400 et $2500\,cm^{-1}$ ($6.7\,\mu$m et $4.2\,\mu$m) [31,32]. Enfin, une des plus remarquables propriétés du diamant est l'énergie de sa bande interdite: 5.45 eV. Ceci signifie qu'aucune absorption par transition électronique entre la bande de valence et la bande de conduction ne peut avoir lieu à des énergies inférieures à 5.45 eV, i.e. à des longueurs d'ondes supérieures à environ 248 nm. En résumé, le diamant pur serait donc transparent:

- dans le proche *UV* (tout le domaine de longueurs d'onde compris entre 248 nm et 400 nm):
- dans le visible et
- dans l'*IR*, sauf dans la bande d'absorption comprise entre 4.2 et $6.7\,\mu m$.

La présence d'impuretés modifie cependant ces propriétés, faisant notamment apparaître des bandes d'absorption dans la région *IR*. Les diamants peuvent être dopés par le *bore (B)* qui introduit un niveau accepteur, donnant une couleur *bleue* au diamant, ou par *l'azote (N)*, élément donneur qui leur confère une couleur *jaune* [32]. Une classification en fonction du degré de pureté du diamant naturel a été établie: les moins purs (soit 98% de ce qui est extrait des mines) sont des diamants de **type I** qui peuvent contenir jusqu'à 0.1% *d'azote* et ont une absorption supplémentaire dans le domaine de l'*IR* (6-13 μm) ainsi que dans l'*UV* pour des longueurs d'onde inférieures à 300 nm. Les plus purs sont les diamants de **type II** qui n'absorbent qu'aux longueurs d'ondes inférieures à 248 nm [33]. Les couches diamant synthétisées par plasma en phase gazeuse et non dopées à l'azote ou au bore, grâce à un indice de réfraction relativement important et sans pertes dans le visible, constituent un matériau idéal pour la protection d'éléments optiques dans le visible et comme guide d'onde dans ce même domaine. Ce type de diamant est utilisable en optoélectronique à condition que la couche soit ou bien monocristalline ou bien nanocristalline (de façon à éviter la diffusion de lumière aux joints de grain). On peut aussi s'en servir comme mono-couche antiréfléchissante dans le domaine *IR* pour les détecteurs en *Si*.

Les applications optiques des diamants synthétiques obtenus par la méthode *HPHT* ne paraissaient pas très viables à cause de leur prix de fabrication très elevé. Par contre, l'apparition des techniques de chimie en phase gazeuse assistées par une décharge électrique ou par d'autres moyens permet d'envisager un développement économique important de ce secteur. Dans ces applications optiques, on est non seulement intéressé par les propriétés de transparence au rayonnement électromagnétique du diamant, mais aussi par sa haute conductibilité thermique (cependant très sensible aux variations de réseau et donc aux impuretés telles que *N*), par son faible coefficient de dilatation ($10^{-6}/°C$) et par sa forte résistance aux chocs thermiques ($10^7 W/m$) ainsi que par sa grande dureté. L'utilisation des films diamant comme revêtement tribologique sur des matériaux optiques très ductiles en infra-rouge, pour les fenêtres par rayons-X et pour la lithographie par rayons-X forme autant de sujets d'étude importants. La taille des grains et la morphologie (polycristalline ou amorphe) de ces couches minces constituent les paramètres limitatifs des applications optiques. Ainsi, l'obtention de films de faible granulométrie.

donc d'une faible rugosité moyenne, est-elle très importante car elle réduit la dispersion optique et l'absorbance.

1.2.3 Applications électroniques

La température maximum d'utilisation d'un semi-conducteur est d'autant plus grande que l'énergie de sa bande interdite est élevée puisque le nombre d'électrons passant de la bande de valence à la bande de conduction varie comme:

$$n = N_c e^{-\frac{E_g - E_f}{\kappa T}} \tag{1.1}$$

où N_c est la densité d'état dans la bande de conduction. E_g est l'énergie de la bande interdite, E_f est l' énergie du niveau de *Fermi* (approximativement $\frac{E_g}{2}$). κ est la constante de Boltzmann et T, la température.

La limite d'utilisation en température du diamant en qualité de semi-conducteur est estimée à $500°C$; elle est deux fois plus élevée que celle de l'$AsGa$ et du quasi-diamant ($250°C$), et *3.3* fois plus élevée que celle du Si ($150°C$). De plus, sa conductibilité thermique elevée permet une transmission efficace d'une importante partie de l'énergie dissipée par les semi-conducteurs, et son utilisation comme radiateur thermique devrait notamment conduire à doubler la puissance des transistors générateurs de micro-ondes [34].

La qualité d'isolant électrique remarquable du diamant (résistivité allant de 10^{13} à $10^{16}\Omega.cm$) vient de ce que sa bande interdite est élevée; ainsi le champ électrique minimum avant claquage est de $10^7 V/cm$, propriété que l'on peut mettre à profit pour se servir du diamant comme isolant dans les amplificateurs de puissance.

D'autres applications électroniques sont aussi envisageables du fait de la faible permittivité diélectrique du diamant dans le domaine des fréquences radio et des micro-ondes.

En resumé les applications des couches diamant sont nombreuses, notamment:

- on peut les utiliser comme revêtements antiréfléchissants pour les détecteurs IR en Si [35] et comme fenêtres pour les rayons-X;
- on peut se servir de ces couches dopées P au bore par B_2H_6 dans des transistors [36] ou dans des diodes *Schottky* [37];

- ils peuvent constituer des diaphragmes acoustiques grâce à leur très grand module de *Young* ($9.2\,N/m^2$) et par conséquent du fait de la grande vitesse du son (*18.2 km/s*) qui s'y propage [38].

1.2.4 Applications biologiques

Le diamant est extrêmement hydrophobe. À cause de cette propriété, le tissu biologique qui comprend près de 98% d'eau, n'adhèrera pas facilement au diamant: ainsi les bactéries et virus peuvent difficilement s'accrocher à sa surface. La combinaison du caractère hydrophobe du diamant avec sa non toxicité, sa non corrosion et sa dureté en fait un candidat idéal, par exemple, pour la réalisation de valvules cardiaques artificielles. Le plus grand problème des matériaux non hydrophobes est en effet la présence de sites de nucléation qui entraînent la coagulation du sang; les porteurs de valvules artificielles hydrophiles doivent prendre des médicaments leur vie durant pour éviter ce problème de coagulation.

1.3 Les ondes de surface

Le plasma de notre réacteur est produit par le champ électrique d'une onde de surface électromagnétique.

1.3.1 Caractéristiques des ondes de surface

Les ondes de surface électromagnétiques peuvent se propager en utilisant l'interface entre deux diélectriques, de formes diverses, comme structure de guidage; dans une enceinte diélectrique contenant un gaz, le champ électrique de cette onde peut produire un plasma qui constitue en même temps un élément de sa structure de propagation (voir 1.3.3). Le flux de puissance de l'onde décroît à partir de l'excitateur d'où elle émerge parce qu'elle est absorbée par la décharge, qu'elle l'entretienne ou non. La propagation ne peut plus avoir lieu quand la densité électronique est inférieure à une densité minimale n_c:

$$n_c = 1.2 \times 10^{-8} \times (1 + \epsilon_g) \times F^2\,(cm^{-3}), \tag{1.2}$$

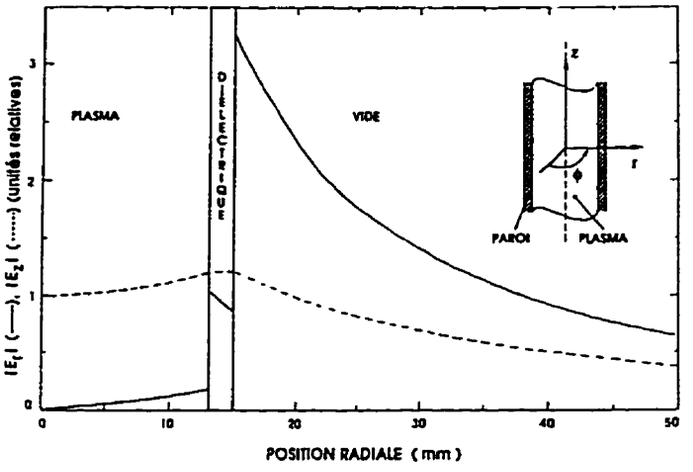

Figure 1.1: Distribution théorique radiale des composantes radiale E_r et axiale E_z du champ électrique d'une onde de surface dont le milieu de propagation est une colonne cylindrique de plasma supposé spatialement uniforme, entouré d'un tube diélectrique lui-même situé dans le vide Ref. 39.

où ϵ_g est la permitivité relative du tube (4.52 pour le Pyrex, 3.78 pour la silice) et F, la fréquence de l'onde en Hz. Pour un tube en silice et une décharge micro-onde à $F = 2.45$ GHz, $n_c = 3.44 \times 10^{11} cm^{-3}$.

Une caractéristique essentielle des ondes de surface réside dans la distribution de leur champ électrique dans la direction perpendiculaire à l'interface. Comme le montre la figure 1.1 [39], l'intensité de ce champ est évanescente de part et d'autre du matériau diélectrique de l'enceinte à décharge. L'onde de surface peut se propager sur différents modes. Ceux-ci s'identifient par un nombre entier ($m = 0,1,2,3,...$) provenant de l'expression en coordonnées cylindriques de l'intensité du champ qui fait apparaître le facteur $exp(jm\varphi)$ (φ = angle azimutal; $j = (-1)^{\frac{1}{2}}$). Dans la gamme de fréquences et de diamètres de tubes que nous avons utilisée, grâce à l'accord d'impédance de l'excitateur, nous pouvons choisir entre le mode $m = 0$ (symétrie azimutale) et le mode $m = 1$ (symétrie dipolaire), lequel présente, en fonction de l'angle azimutal φ, deux maximums et deux minimums d'intensité du champs produisant respectivement des maximums et des minimums d'ionisation. Dans ce cas, la densité électronique n'est pas uniforme azimutalement, ce qui est une source d'inhomogénité lors d'un processus de dépôt à partir d'une chimie en phase gazeuse.

1.3.2 Caractéristiques des ondes de surface entretenant une colonne de plasma

À la section précédente, nous avons présenté les principales caractéristiques des ondes de surface utilisant une colonne de plasma comme milieu de propagation, sans préciser si le plasma était entretenu ou non par le champ de l'onde; pour une onde de faible flux de puissance, la colonne de plasma est nécessairement préexistante (par exemple, la colonne positive d'une décharge en courant continu). Si, par contre, le flux de puissance de l'onde est suffisant, celle-ci pourra produire une décharge; des conditions plus restrictives s'appliquent alors aux ondes de surface, comme nous allons le montrer.

Coefficients de propagation et d'atténuation

Une onde progressive est caractérisée par un coefficient de propagation β qui apparaît dans l'expression de l'amplitude du champ électrique sous la forme

$$E = E_o\, e^{j(\omega t - \beta_z z)} e^{-\alpha z} \tag{1.3}$$

où z est la coordonnée axiale de la colonne de plasma et ω, la pulsation du champ de l'onde; β_z est le coefficient axial de propagation et $\beta_z = 2\pi/\lambda$ où λ est la longueur d'onde le long de l'axe z. Le vecteur $\vec{\beta}$ (aussi appelé vecteur d'onde) n'est dirigé suivant z que dans le cas limite où le milieu de propagation est sans perte; le vecteur $\vec{\beta}$ est d'autant plus orienté vers la normale à l'axe de la colonne (en pointant vers le plasma) que l'absorption de l'onde est grande. Dans ce cas, β_z diminue d'autant et λ augmente donc. L'atténuation du flux de puissance $P(z)$ se représente par le coefficient α dans 1.3. L'expression 1.3 fait l'hypothèse que le milieu de propagation est axialement uniforme. La densité électronique décroît généralement de façon linéaire de l'applicateur micro-onde vers la fin de la décharge le long d'un tube de section constante [40]; dans ce cas, il faut remplacer $\beta_z z$ par $\int_0^z \beta_z(z')dz'$, et $\alpha(z)$ par $\int_0^z \alpha(z')dz'$ dans 1.3.

Bilan local de puissance

La distribution spatiale du champ de l'onde de surface est telle que la puissance de l'onde absorbée dans la décharge entre les plans z et $z + dz$ provient de l'atténuation du

flux de l'onde dans ce même intervalle le long de la colonne. Nous pouvons donc écrire localement que

$$P(z)\,\alpha(z) \equiv \frac{1}{2}\frac{dP(z)}{dz} = \pi \int_0^R \sigma(n)\,E^2(r)\,r\,dr, \tag{1.4}$$

où le membre de droite montre que le champ E de l'onde *chauffe* la décharge par effet Joule; σ est la conductivité électronique du plasma et R, le rayon de la colonne de plasma. Pour des conditions de décharge données (nature et pression du gaz, ω, m et R), la valeur de α ne dépend, en première approximation, que de la densité électronique n. L'équation (1.4) est le *bilan local de puissance*.

Modes de propagation

Margot-Chaker et al [41] ont montré que l'on peut en principe entretenir une colonne de plasma avec une onde de surface de mode $m = 0$ sans restriction sur F et R au contraire de ce qui se passe avec les modes supérieurs. Ainsi, le mode $m = 1$ ne peut servir à entretenir une décharge que si $F \times R \geq 2\,\mathrm{GHz\,cm}$, alors que l'on peut observer sa propagation sur la colonne positive d'une décharge en courant continu pour des valeurs de F et R quelconques.

Stabilité de la décharge

Pour des décharges entretenues par des ondes progressives en général, la colonne de plasma sera stable, i.e. ne pourra exister, que si la condition [42]

$$\frac{d\alpha(\overline{n})}{\alpha(\overline{n})} < \frac{d(\overline{n})}{\overline{n}} \tag{1.5}$$

est verifiée; $\overline{n}$ est le valeur moyenne de $n(r)$ sur la section du plasma en z donné. Dans le cas d'un plasma d'onde de surface, cette condition conduit au fait expérimental bien connu que $\frac{d\overline{n}}{dz} < 0$ en comptant z à partir de l'excitateur; ce critère élimine la partie *onde inverse* du diagramme de phase de l'onde de surface qui s'observe le long d'un plasma de colonne positive.

Fin de colonne et force pondéromotrice

On appelle fin de colonne, la position axiale à laquelle se termine le plasma d'onde de surface du fait soit que $\overline{n} < n_c$, soit que le flux de puissance n'est plus suffisant pour ioniser même si $\overline{n} > n_c$. On observe alors en ce point une variation brusque de $\mid E(z) \mid$, i.e. une forte valeur de $\mid \nabla E \mid^2$ [43]. Ce gradient crée une force dite pondéromotrice qui va accélérer les électrons vers la région sans plasma; le champ de charges d'espace qui en résulte lance les ions positifs dans la même direction.

La configuration du plasma d'onde de surface que nous utilisons favorise l'existence de cette force pondéromotrice. En effet, par suite d'une rupture abrupte de la structure de propagation au passage d'un tube à décharge d'un certain diamètre à un second tube de plus grand diamètre (voir plus loin la Fig. 1.3), l'onde de surface ne peut plus se propager. Nous constatons expérimentalement que très peu de champ micro-onde demeure au-delà du plasma, ce qui montre bien l'existence d'un fort $\mid \nabla E \mid^2$.

1.3.3 Schéma et principes de fonctionement d'une source de plasma à onde de surface

Schéma de la source de plasma

La figure 1.2(a) montre les éléments essentiels d'une source de plasma à onde de surface dans sa forme classique. Le tube à décharge, de forme cylindrique droite, est entouré de l'applicateur de champ sur une certaine distance axiale (qui peut être de quelques centimètres seulement si nécessaire); l'applicateur a pour mission de lancer l'onde de surface. Entre la ligne d'alimentation amenant la puissance HF du générateur, P_I, et l'applicateur se trouve un système d'adaptation d'impédance qui fait en sorte que P_I se rende le plus complètement possible jusqu'à l'interstice de lancement de l'applicateur (voir plus loin); il s'agit de faire tendre vers zero la puissance réfléchie à l'entrée de la source, P_R (figure 1.2(b)), avec en même temps le moins de pertes possible dans ce système d'accord [44]. Nous appelerons *lanceur d'onde* l'ensemble formé par l'applicateur de champ et le système d'adaptation d'impédance.

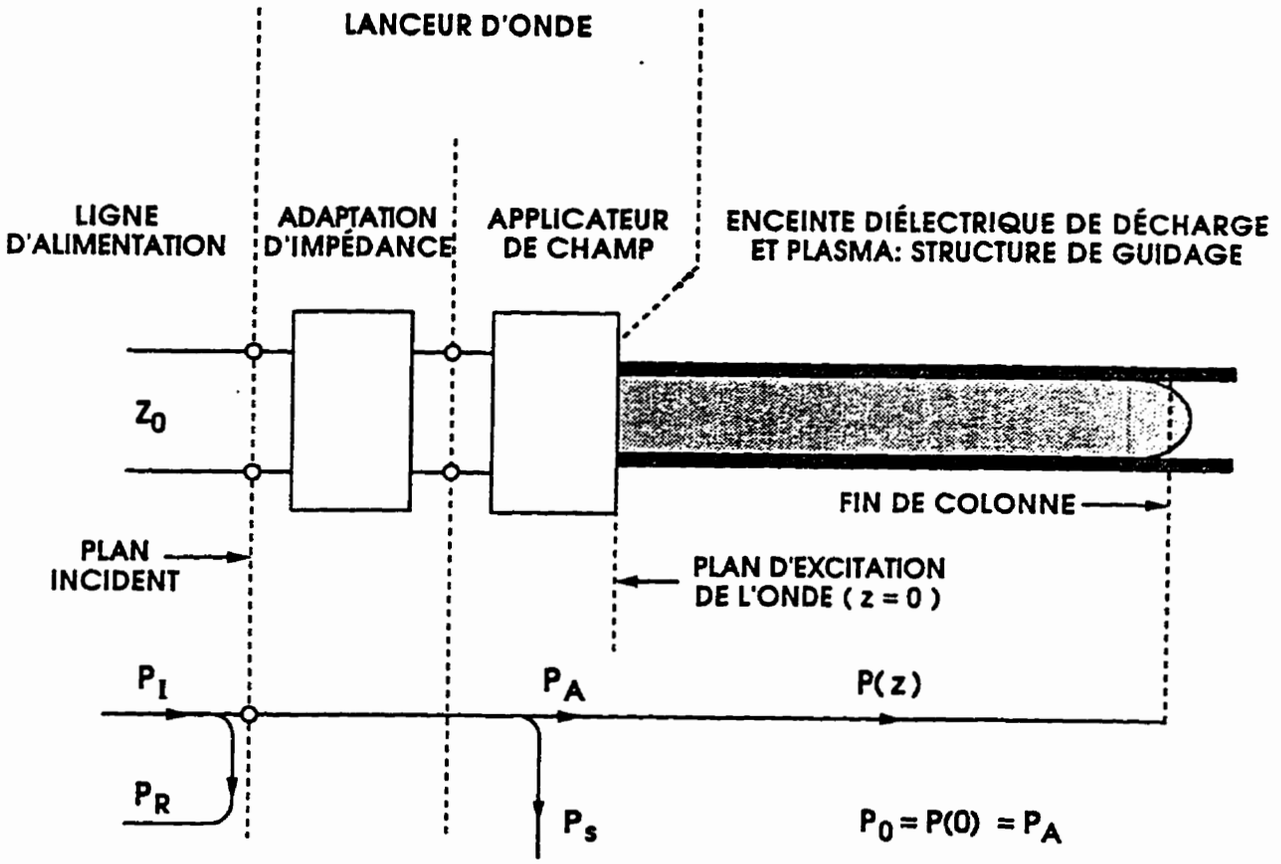

Figure 1.2: (a) Schéma type d'une source de plasma à onde de surface faisant apparaître ses éléments essentiels: le tube à décharge, l'applicateur de champ et le système d'accord d'impédance; (b) chemin suivi par la puissance incidente (P_I): puissance absorbée dans le plasma (P_A), transportée par le flux $P(z)$; pertes par réflexion à l'entrée de la source de plasma (P_R), pertes par rayonnement électromagnétique (P_S) Ref. 44.

Configuration des tubes à décharge

L'augmentation de P_I entraîne l'allongement de la colonne de plasma; c'est une caractéristique essentielle d'un plasma d'onde de surface. Dans notre Groupe, on a ainsi créé des colones de plasma de plusieurs mètres de longueur. Pour une longueur donnée du tube à décharge et une puissance P_0 suffisante (figure 1.2(b)), le plasma atteint l'extrémité du tube. Si celui se termine par un obstacle, l'onde de surface est réfléchie vers l'excitateur. Dans son "trajet de retour", l'onde dispense son flux de puissance à la décharge, ce qui contribue à réduire le gradient axial caractéristique de la colonne de plasma entretenue par une onde de surface progressive (§1.3.2).

Il est possible de produire une décharge d'onde de surface dans des tubes de configurations différentes de celle de la figure 1.2(a). Ainsi, on peut lancer l'onde dans un tube de diamètre 2R donné (respectant, par exemple, la condition FR pour l'excitation du mode $m=0$) pour réaliser ensuite une décharge dans une enceinte de plus grand diamètre: il faut dans ce cas s'assurer que le diamètre du tube s'évase doucement vers le diamètre plus grand à atteindre, comme le montre la figure 1.3(a), de façon à ce qu'il y ait peu de réflexion vers l'excitateur; le mode de l'onde de la région du "petit" tube se conserve dans le "grand" tube. Par contre, si l'extremité du tube est ouverte, ainsi qu'il arrive lorsqu'on passe de façon abrupte sur un diamètre plus grand comme sur la figure 1.3(b), alors l'onde ne peut se propager au-delà de cette extrémité: une partie du flux est réfléchie et l'autre partie est transmise sous forme d'onde évanescente. Dans un gaz comme H_2, à la différence de l'argon par exemple, il se forme alors un hémisphère de plasma en cette extrémité ouverte, dans l'enceinte de plus grand diamètre. C'est en mettant à profit cette configuration non conventionnelle du plasma d'onde de surface que nous avons pu réaliser le réacteur original et avantageux qui est à la base de nos travaux sur les couches de diamant.

L'interstice de lancement et le mode de propagation de l'onde

Notre Groupe de physique des plasmas a mis au point au cours des années passées toute une famille de lanceurs d'onde de surface (Fig. 1.4) qui permettent d'entretenir efficacement des colonnes de plasma. Ces dispositifs ont en commun la forme de leur

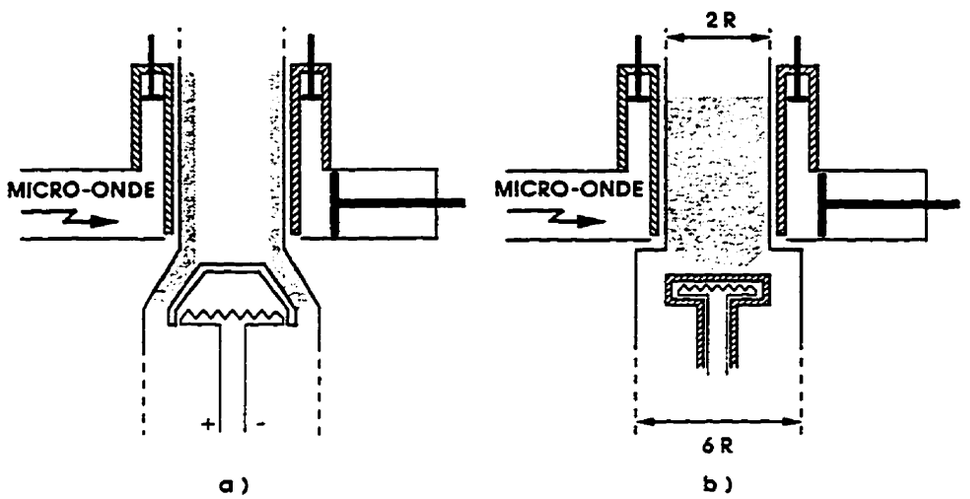

Figure 1.3: Exemple de tubes à décharge utilisés dans une source de plasma à onde de surface: (a) tube s'évasant doucement vers un plus grand diamètre, (b) tube avec transition abrupte sur un plus grand diamètre.

applicateur de champ HF, qui est constitué par l'interstice de lancement schématisé à la figure 1.5. Cet interstice est manifestement de symétrie azimutale ($m = 0$); il faut cependant savoir que l'arrivée de puissance dans l'applicateur ne se fait pas de façon azimutalement symétrique, de sorte que le flux de puissance sortant de l'interstice n'est pas nécessairement de symétrie azimutale parfaite. On peut alors se demander dans quelle mesure l'applicateur de champ va autoriser la sélection d'un mode en particulier. La réponse se trouve dans ce qui est dit à la section 1.3.2: le mode qui va apparaître dépend, à une fréquence F donnée, du rayon 2 R de la portion du tube à décharge entourée par l'interstice de lancement, les caractéristiques de symétrie de l'applicateur de champ étant sans effets apparents.

Pour nous assurer de la formation d'une couche de diamant uniforme sur le substrat placé en regard de l'hémisphère de plasma et perpendiculairement à l'axe du tube à décharge, il faut recourir au mode $m = 0$ de l'onde de surface. Dans la pratique, nous avons trouvé que nous pouvions fonctionner avec le mode $m = 0$ pour R aussi grand que 13 mm à 2.45 GHz. En nous rappelant le critère $F \times R \leq 2$ GHz cm enoncé en §1.3.2 pour s'assurer du mode $m = 0$, nous constatons qu'avec cette valeur de R, le produit $F \times R$

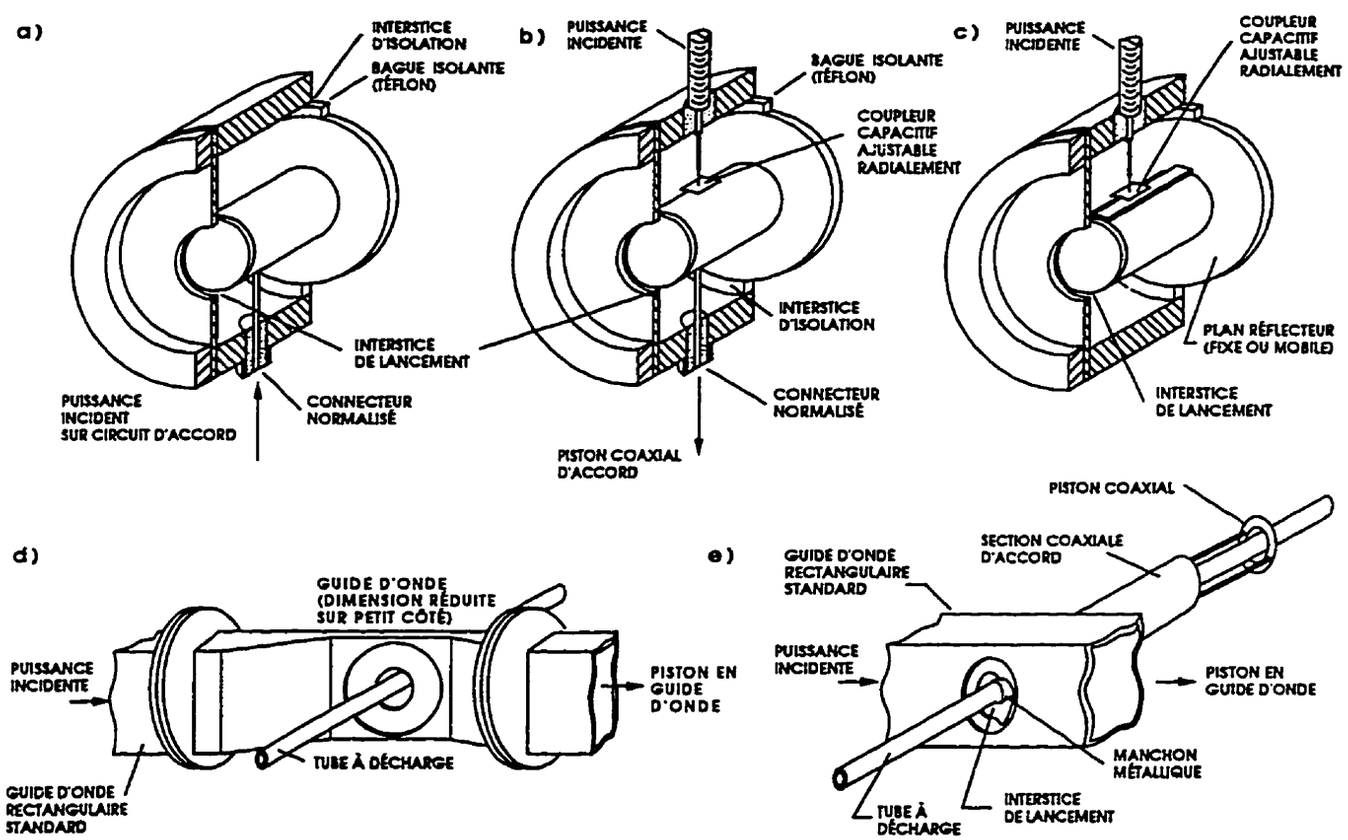

Figure 1.4: Schéma de différents types de lanceurs d'ondes de surface: Ro-Box avec accord par circuit LC (a), Ro-Box avec piston coaxial d'accord (b), Surfatron (c), Surfaguide (d), Surfatron-guide (e) Ref. 45.

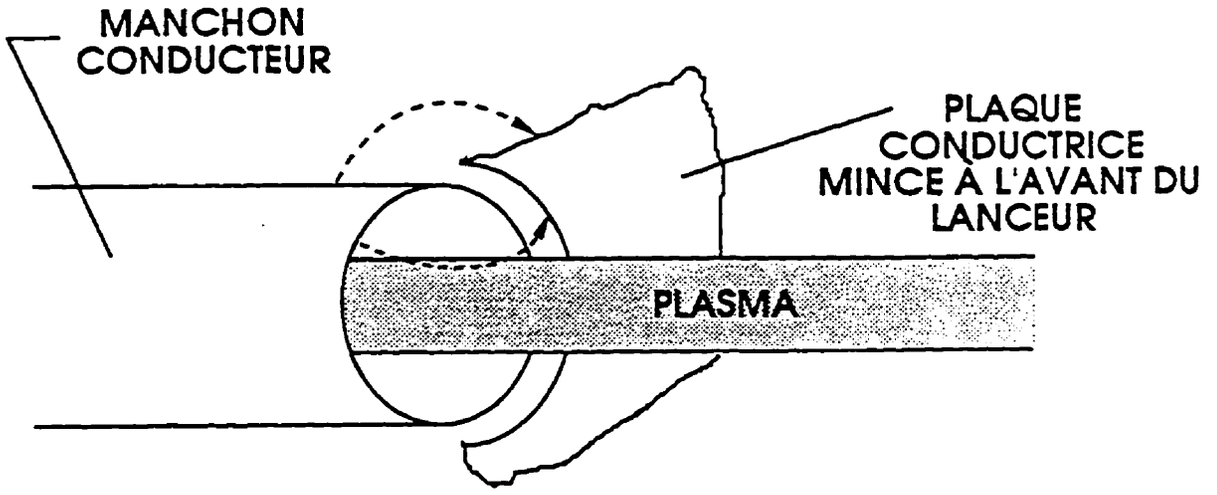

Figure 1.5: Schéma de l'interstice de lancement des excitateurs d'onde de surface mis au point par le Groupe de physique des plasmas de l'université de Montréal Ref. 45.

donne 3.2 GHz cm. De façon concrète, ceci signifie que les modes $m = 0$ et $m = 1$ peuvent être excités l'un et l'autre, mais que les moyens d'accord d'impédance du lanceur utilisé nous permettent d'éliminer le mode $m = 1$ au profit du mode $m = 0$. Pour FR un peu plus grand, disons $F \times R \simeq 4$ GHz cm, on ne peut plus faire apparaître le mode $m = 0$, et dans ce cas, ce sont les modes $m = 1$ et $m = 2$ qui sont en compétition.

Le surfatron-guide, le lanceur d'onde de surface de notre réacteur

Parce que nous devions utiliser des puissances de 1 à 6 kW pour entretenir la décharge, il a fallu éliminer l'utilisation du Ro-box et du surfatron (Fig. 1.4(b) et (c))limités à 300-500 W à cette fréquence. Pour exciter avec efficacité de grandes diamètres de plasma et pouvoir sélectionner le mode $m = 0$, il a fallu rejeter le surfaguide (Fig. 1.4(d)) doté d'un seul moyen d'accord d'impédance, et utiliser plutôt le surfatron-guide (Fig. 1.4(e)). Celui-ci est représenté de façon plus précise à la figure 1.6. Le cheminement de la puissance micro-onde à travers ce dispositif vers la colonne de plasma peut s'analyser par la *méthode du circuit équivalent.* Les différents éléments d'un tel circuit représentent des processus de transmission, d'accumulation et de pertes d'énergie. Cette méthode, beaucoup plus

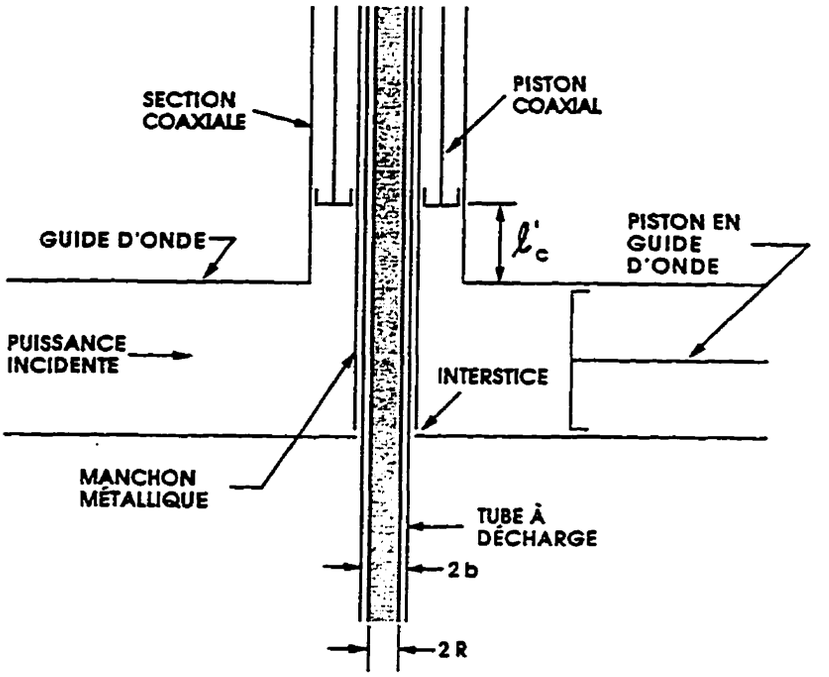

Figure 1.6: Coupe schématique d'un surfatron-guide Ref. 41.

simple que le recours aux équations de Maxwell avec les conditions aux limites appropriées, permet néanmoins de bien comprendre les propriétés de la source et d'en prédire les caractéristiques d'accord d'impédance.

La figure 1.7 montre le circuit équivalent de notre source. La colonne de plasma qui consomme la puissance P_0 émise par l'interstice de lancement est décrite par une impédance complexe Z_g; les impédances Z_c et Z_t sont ajustables et respectivement liées au piston court-circuit coaxial et au piston court-circuit en guide d'onde; quant à Z_s, elle tient compte de la partie du manchon conducteur entourant le tube à décharge qui se trouve dans la partie en guide d'onde de l'excitateur; Z_0 est l'impédance caractéristique de la ligne de transmission venant du générateur qui, dans notre cas, est constituée d'un guide rectangulaire WR-430 (4.3″ pour le grand coté à l'intérieur du guide). Ce circuit équivalent est le même que celui du surfatron d'où le terme surfatron-guide pour désigner le présent dispositif. Moisan et al. [45] ont considéré dans leur analyse que le diamètre de la ligne coaxiale dans laquelle se meut le piston court-circuit était plus petit que le grand coté du guide WR-430, ce qui permet de définir un même plan de référence (en pointillé sur la figure 1.7); de plus, ils ont fait l'hypothèse que les seules pertes de la source de plasma étaient la puissance absorbée dans la décharge, ce qui fait que l'impédance Z_0 est

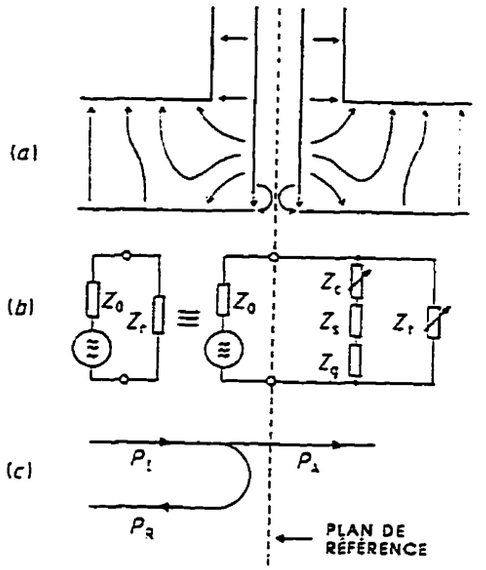

Figure 1.7: Répartition approximative du champ électrique dans un surfatron-guide (a); circuit électrique équivalent (b); désignation des puissances incidente (P_I), réfléchie (P_R) et absorbée (P_A) (c) Ref. 41.

réelle, que Z_g est complexe et que les autres sont imaginaires. La figure 1.8 montre le bon accord de cette analyse avec les résultats expérimentaux lorsqu'on fait varier la position l'_c du piston court-circuit coaxial: le piston en guide d'onde est ajusté à chaque fois pour minimiser P_R.

1.4 Le réacteur de dépôt

Le nouveau réacteur que nous avons conçu pour le dépôt de couches minces de diamant fait appel au surfatron-guide comme lanceur d'ondes de surface. Le choix d'un dispositif fonctionnant dans le domaine des micro-ondes a été dicté par le désir d'avoir à notre disposition un plasma de forte densité: on se rappelera que la densité du plasma d'onde de surface croît avec F, les autres conditions de fonctionnement étant fixées (voir par exemple l'equation 1.2). Le fait de retenir précisément $F = 2{,}45$ GHz vient de la disponibilité à cette fréquence de générateurs de puissance d'un coût moindre qu'à 915 MHz ou 5.8 GHz, qui sont aussi des fréquences autorisées pour des fins industrielles, médicales et scientifiques (ISM). Ce dispositif a été mis à l'épreuve à des puissances pouvant atteindre 6 kW.

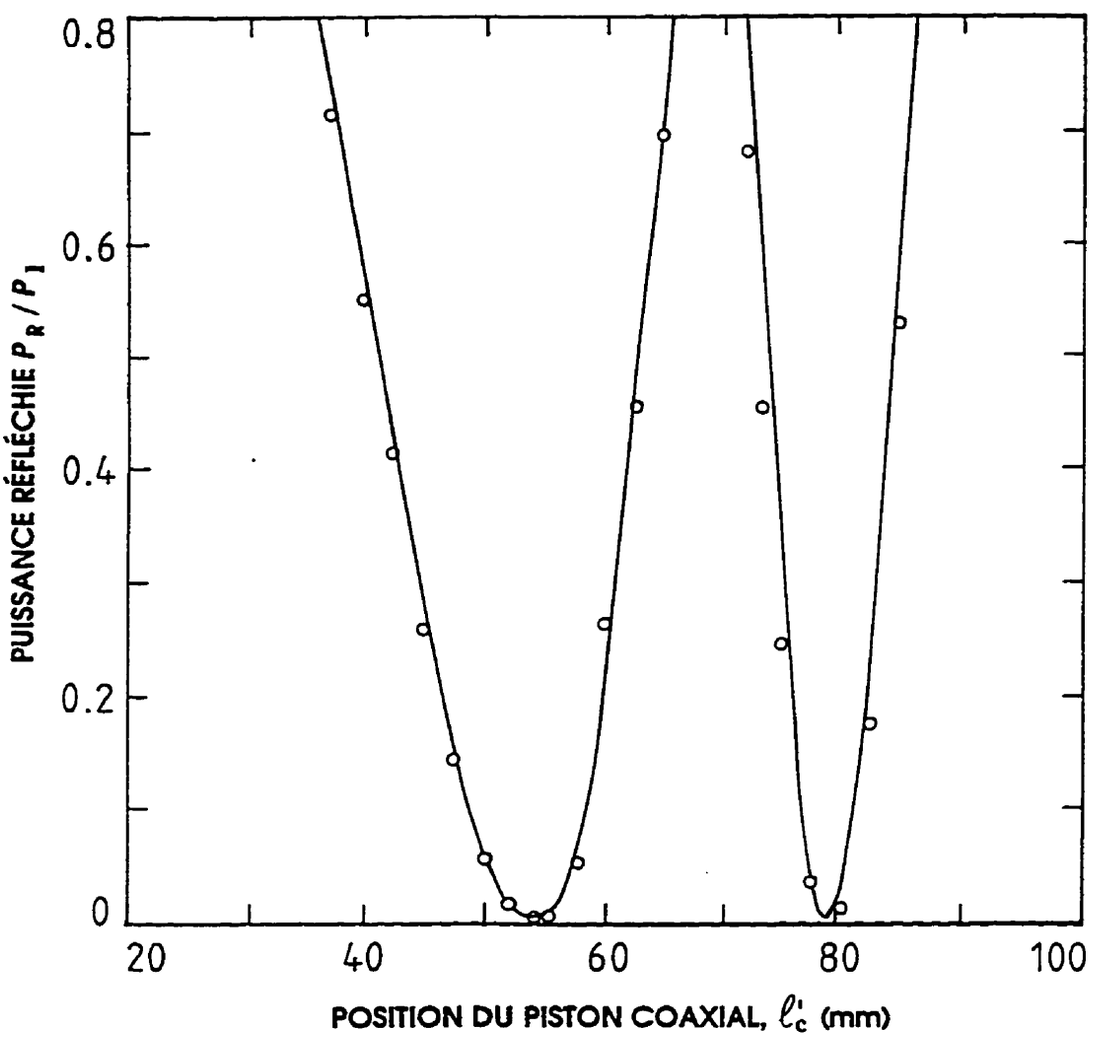

Figure 1.8: Caractéristiques d'accord d'impédance du surfatron-guide, à fréquence constante: puissance réfléchie en fonction de la position du piston coaxial. Comparaison entre les valeurs mesurées et le calcul selon le modèle du circuit équivalent Ref. 41.

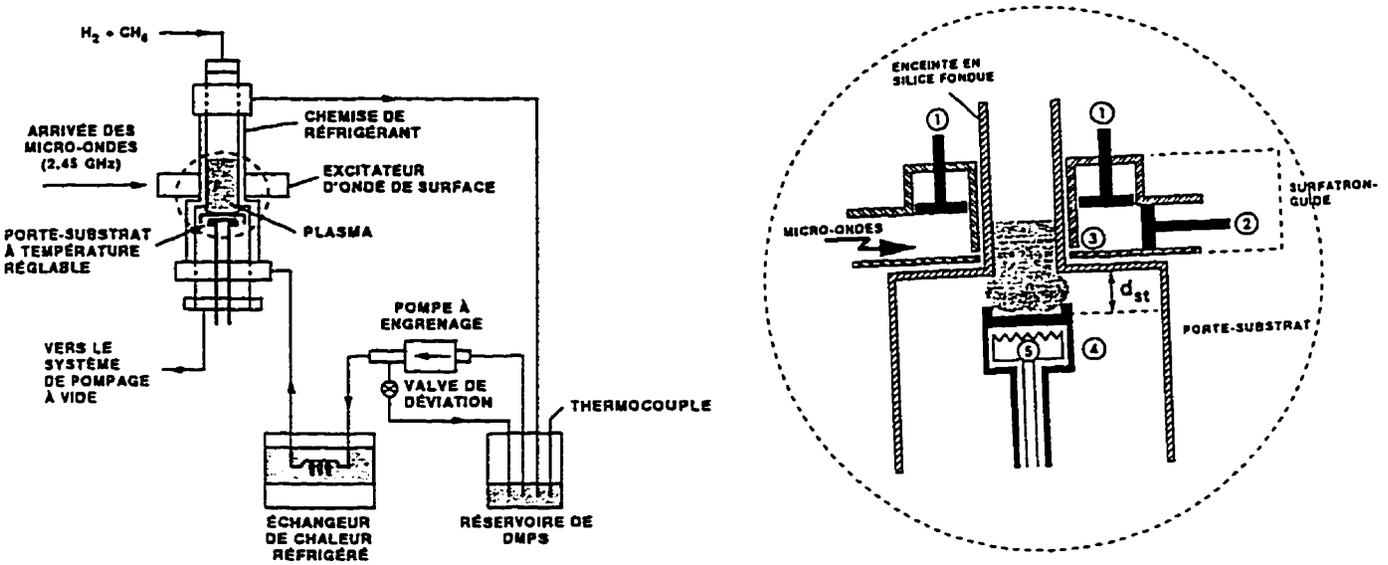

Figure 1.9: Schéma du réacteur micro-onde que nous avons conçu et mis au point: **1** piston d'accord de la ligne coaxiale. **2** piston d'accord dans le guide d'onde. **3** interstice de lancement. **4** porte-substrat de molybdène. **5** filament de tungstène. la distance d_{st} est ajustable.

1.4.1 Description du réacteur de dépôt

Le surfatron-guide entoure à un ou deux mm près, de façon bien centrée, un tube de silice fondue (quartz) de 30 mm de diamètre extérieur (figure 1.9). Pour s'assurer dans ces conditions du produit $F \times R$ conduisant à l'excitation du mode $m = 0$ plutôt qu'à celle du mode $m = 1$, nous ajustons le piston coaxial et le piston en guide d'onde de façon à ce que la couronne de luminosité localisée au voisinage de la paroi, telle que vue dans l'axe du tube par une extremité, soit d'une intensité le plus uniforme possible. Ce "petit" tube s'élargit par une transition abrupte sur un "grand" tube de 60 mm de diamètre externe (figure 1.9), de façon à empêcher l'onde de se propager et donner ainsi lieu au champ évanescent responsable de la formation de l'hémisphère de plasma en son extrémité. Le porte-substrat est placé perpendiculairement à l'axe du tube à décharge dans la continuation du grand tube (voir figure 1.9). Cette forme originale de réacteur a été mise au point à l'occasion de la présente thèse. Une pompe primaire assure l'évacuation des gaz que nous introduisons par le petit tube.

La paroi de l'enceinte à décharge et du réacteur est refroidie au moyen d'un liquide à

faibles pertes diélectriques, le diméthyle-poly-siloxane (DMPS), comme le montre la figure 1.9. L'emport de chaleur de ce liquide est voisin de celui de l'eau. Ce refroidissement protège le tube contre un échauffement excessif menaçant son intégrité et il diminue aussi la recombinaision de l'hydrogène atomique sur la paroi; la recombinaision de l'hydrogène atomique sur les parois du tube à décharge croît en effet de façon exponentielle avec la température de cette paroi [46].

Le système micro-onde est constitué de plusieurs éléments:

- Un générateur micro-onde dont la puissance est ajustable entre 0.4 et 3 kW: un circulateur permet de dériver sur une charge adaptée la puissance réfléchie par le source de plasma afin d'éviter la détérioration du magnétron du générateur:
- un dispositif à *trois vis d'accord* destiné à minimiser la puissance réfléchie n'ayant pas pu être résorbée par les dispositifs de réglages intrinsèques au surfatron:
- une transition en guide d'onde de la norme WR-340 (86×43 mm) à la norme WR-430 (109×55 mm);
- le surfatron-guide, dont la section coaxiale est refroidie par une circulation d'eau:
- un piston en guide d'onde de type quart-d'onde (sans contact).

1.4.2 Optimisation de l'hémisphère de plasma

La forme et le volume du plasma présent dans le réacteur dépendent de la nature du gaz, de la pression totale et de la puissance micro-onde incidente. Ajoutons que le centrage et le positionnement axial du tube dans l'ouverture de lancement du surfatron-guide sont également importants.

1.4.2.1 Amélioration de l'efficacité du couplage micro-onde et de la forme de l'hémisphère de plasma

L'efficacité du lancement de l'onde se juge en fonction de la valeur de la puissance réfléchie (qui doit être le plus faible possible) et de la forme du plasma en regard du substrat (qui doit être hémisphérique et sans contact avec la paroi du grand tube). Dans cette optique, plusieurs réglages doivent être optimisés:

1. **Le réglage de l'interstice de lancement:** Si celui-ci est trop faible, des arcs électriques apparaissent qui peuvent aller jusqu'à fondre une épaisseur de 4 mm de silice en quelques secondes, et souder le manchon métallique à la lèvre du guide d'onde qui lui fait face.

2. **Le réglage des deux pistons d'accord:** Comme le montre la figure 1.8. une position particulière du piston coaxial (pour une composition et une pression donnée du gaz) correspond à un minimum de puissance réfléchie et à une optimisation de la forme du plasma en regard du porte-substrat.

3. **Le réglage des trois vis:** Leur mise en oeuvre permet l'annulation quasi totale de la puissance réfléchie (mesurée par un bolomètre lié à une ligne directionnelle). Cependant ce réglage ne doit intervenir qu'une fois les deux pistons d'accord en position optimale. En effet, on peut annuler la puissance réfléchie par l'action de ces trois vis sans que le lancement de l'onde n'ait été optimisé par les moyens de réglage intrinsèques au lanceur. Un système d'ondes stationnaires peut alors s'établir entre l'interstice de lancement et les trois vis: une quantité non négligeable d'énergie micro-onde est perdue en chauffage de la structure métallique dans les multiples "allées et venues" de l'onde dans le guide, et des points chauds se créent au niveau des maxima d'intensité du champ électrique, pouvant mener jusqu'à la déformation du guide d'onde.

L'optimisation du lancement de l'onde est important pour bien définir l'hémisphère de plasma mais aussi pour éviter tous les inconvénients liés à la puissance réfléchie circulant dans le système micro-onde, y compris la fusion du quartz dans le cas où un mauvais lancement est effectué.

1.4.2.2 Optimisation du milieu de propagation

Le coefficient d'attenuation de l'onde de surface dépend principalement des trois paramètres suivants:

- La densité électronique. Le coefficient α diminue lorsque $\overline{n}$ augmente; une bonne approximation (en excluant la fin de colonne) est de considérer le produit $\alpha(\overline{n})\overline{n}$ comme étant constant pour des conditions de décharge données [47].

- La fréquence ν des collisions électron-neutre pour le transfert de la quantité de mouvement [47]. Le coefficient α augmente avec ν qui dépend de l'énergie moyenne des électrons; en général, ν croît avec la pression. Les pertes dues aux collisions entre les électrons et la paroi du tube n'interviennent qu'aux pressions suffisamment basses pour que le libre parcours moyen des électrons soit comparable ou inférieur au rayon R du tube à décharge. Dans nos conditions de pression, le libre parcours moyen est de l'ordre du dixième de millimètre.

- Les pertes dans le matériau diélectrique du tube à décharge. Ces pertes sont de deux ordres: *i)* les pertes liées à la polarisation du diélectrique: elles croissent avec le valeur de la permittivité et avec le fréquence du champ HF; *ii)* les pertes liées aux charges libres dans le matériau. Celles-ci s'expriment en général par le rapport de la partie imaginaire ε_i sur la partie réelle ε_r du diélectrique, rapport aussi appelé "tangente δ" où $\tan\delta = \frac{\varepsilon_i}{\varepsilon_r}$. L'avantage de recourir, par exemple, à la silice par rapport au Pyrex est le suivant: la valeur ε_r de la silice (3.78) est plus faible que celle du Pyrex (4.52 pour du Dow Corning 707), la tangente δ de la silice ($\simeq 10^{-4}$) est aussi plus faible que celle du Pyrex ($\simeq 10^{-3}$) et, enfin, la permitivité de la silice n'augmente avec la température que pour des valeurs très élevées de celle-ci, au contraire du Pyrex et de la céramique (Al_2O_3) qui peuvent être victimes d'un emballement thermique conduisant à la fusion du tube. Il faut donc éviter à tout prix des matériaux où la tangente de pertes est élevée. Ainsi, Ilic et al [48] ont montré que les pertes dans un mauvais diélectrique, $\tan\delta = 0.014$, pouvaient atteindre 50% des pertes dues aux collisions électrons-neutres dans ce cas précis. Il est clair que le choix d'un tube à décharge adéquat est nécessaire pour l'emploi de puissances micro-ondes aussi élevées que 3 kW, afin d'éviter une perte importante de la puissance micro-onde et la destruction du tube à décharge. Dans notre système, non seulement nous utilisons de la silice fondue comme matériau mais nous refroidissons le tube avec du DMPS pour éviter tout emballement thermique.

Les motifs et les grandes lignes de l'étude poursuivie

Le Groupe de physique des plasmas au sein duquel a été élaborée la présente thèse est réputé par ses travaux expérimentaux et théoriques sur les décharges électriques entretenues par des champs HF. Il avait été décidé par le professeur Moisan de mettre ces connaissances à profit pour tenter d'innover dans le domaine du dépôt de couches de diamant par plasma. Au moment d'entreprendre nos travaux, il existait deux méthodes principales de dépôt diamant par des plasmas HF à pression réduite: le réacteur à cavité résonnante [49] et le réacteur de type *cloche à vide* [50]. Lors d'un stage France-Québec de formation auprès de la professeure A. Gicquel (Université Paris-XIII), nous avons eu l'occasion de comprendre les difficultés inhérentes à ces systèmes. De retour dans notre laboratoire, après divers essais, nous avons réalisé un réacteur à plasma micro-onde fonctionnant aussi à pression réduite, qui utilise une décharge à onde de surface dans une configuration tout à fait originale. Ce nouveau réacteur possède, comme nous aurons l'occasion de le développer dans les articles présentés, des avantages importants par rapport aux systèmes existants; il a permis ainsi une étude plus systématique et plus fine de l'influence des conditions opératoires sur la qualité du diamant et sur son adhérence au substrat. De nouveaux phénomènes ont également été mis en évidence relativement à la rugosité, à l'adhérence et à la pureté des couches diamant. Une conséquence de nos travaux est la réalisation prochaine, dans le cadre d'une subvention dite stratégique obtenue par le pofesseur Moisan, d'un réacteur de même type que celui que nous avons mis au point mais de plus grande taille de façon à traiter des substrats de 150 mm de diamètre et plus.

Nous allons maintenant résumer les grandes lignes de la démarche que nous avons adoptée et présenter les résultats essentiels de nos travaux en guise d'introdution au contenu détaillé des cinq articles qui vont suivre, articles dont nous sommes le premier auteur.

Description du nouveau réacteur et présentation de ses principaux avantages

Le premier article (chapitre 2), publié dans Diamond and Related Materials (1995), montre l'avantage de la configuration originale que nous avons conçue par rapport à une

décharge d'onde de surface conventionnelle quant à l'uniformité du dépôt. Le plasma produit dans ce réacteur conduit à un hémisphère de plasma en regard du substrat, de façon analogue aux systèmes à cavité résonnante et à cloche à vide; cependant, à la différence de ces systèmes, aucun rayonnement micro-onde ne s'échappe de ce plasma pour venir chauffer le substrat. Nous pouvons ainsi réaliser un contrôle indépendant de la température T_s du substrat par rapport au niveau de puissance micro-onde utilisé; l'uniformité de T_s sur le substrat dépend du dispositif de chauffage externe utilisé. Pour une densité de puissance aussi élevée que 100 W/cm^3, la valeur de T_s due à la température du gaz de la décharge est de 580 °C, ce qui dans la pratique nous permet un réglage indépendant de T_s de 600 à 1000 °C. De plus, l'hémisphère de plasma est très peu affecté par la position relative du porte-substrat, à la différence des systèmes classiques. Par suite de ces bonnes propriétés, les conditions de fonctionement de notre réacteur sont parfaitement reproductibles. Par ailleurs, nous avons observé, sans doute pour le première fois, que la rugosité moyenne, R_q, de la couche de diamant diminuait lorsque la puissance absorbée croissait; ce phénomène ne se retrouve pas dans les systèmes conventionnels, sans doute par suite du chauffage micro-onde à la surface du substrat.

Étude paramétrique du nouveau réacteur

Le deuxième article (chapitre 3), paru dans le numéro de Thin Solid Films daté de mars 1996, a été consacré à l'influence des conditions opératoires (p, T_s, distance du substrat au plasma, densité de puissance absorbée, concentrations relatives de CH_4 et O_2 dans H_2) sur la température du gaz, la concentration d'hydrogène atomique et finalement sur les propriétés des couches diamant (qualité cristalline, vitesse de croissance, densité de nucléation et taille des cristaux). On retiendra de cet article la grande souplesse et l'indépendance des moyens de réglage de notre réacteur en comparaision des réacteurs classiques.

Détermination des impuretés et origine de la contamination en Si observée dans les couches de diamant de notre réacteur

Dans ce troisième article (chapitre 4), paru dans la revue Journal of Applied Physics, nous avons utilisé toute une panoplie de diagnostics pour identifier les principales impuretés de nos couches de diamant polycristallines. Le contaminant principal est le silicium, qui provient suivant les conditions en partie des parois du réacteur (en silice fondue) et en partie du substrat en silicium; dans ce dernier cas, c'est la gravure du substrat de Si dans les instants initiaux du dépôt qui en est responsable. Nous avons montré, semble-t-il pour la première fois, que la présence, même très faible, de Si dans la couche diamant provoquait une fluorescence autour de la raie du diamant du spectre Raman: l'absence de cette fluorescence est donc un moyen simple et pratique de s'assurer que la contamination en Si est faible, notamment dans des réacteurs dont les parois sont en silice fondue.

Adhérence des couches diamant sur les substrats de silicium de différentes orientations cristallines

Ce quatrième article (chapitre 5), accepté pour publication le 4 juin 1996 à la revue Diamond and Related Materials, s'intéresse aux mécanismes déterminant l'adhérence de la couche diamant au substrat. Notre approche de cette question a consisté à examiner l'adhérence de telles couches sur des substrats de silicium de trois orientations cristallines différentes. Les proprietés physiques (densité d'atomes/cm^2 dans le plan considéré, dureté) et chimiques (orientation spatiale des liaisons libres) de ces substrats varient en effet selon qu'il s'agit de Si(100), Si(110) et Si(111), les trois orientations cristallines étudiées. En traitant simultanément ces trois types de surface dans notre réacteur, nous avons pu faire ressortir les proprietés des couches obtenues qui sont liées à la nature de la surface, les conditions de la phase gazeuse étant les mêmes. Nous avons montré, semble-t-il pour le première fois, que l'adhérence de la couche diamant était, dans le cas présent, principalement déterminée par la gravure du silicium par l'hydrogène atomique de la décharge dans les premiers instants de nucléation du dépôt plutôt que par le prétraitement du substrat. Par ailleurs, nous avons observé que ce prétraitement dans un bain ultrason contenant de la poudre de diamant en suspension conduisait à une graphi-

tisation des particules de la poudre de diamant, la teneur en carbone laissé sur le substrat variant avec l'orientation cristalline. Finalement, nous avons constaté que la taille des cristaux de la couche diamant croissait avec la teneur en carbone dû au prétraitement.

Méthode pour obtenir des couches diamant de faible rugosité au moyen d'un plasma d'onde de surface

Cet article (chapitre 6), soumis le 28 mai 1996 à Journal Applied Physics, est une étude paramétrique visant à determiner les conditions de prétraitement du substrat et les conditions de fonctionnement du réacteur pour arriver à une surface diamant le plus lisse possible. Dans plusieurs applications, notamment en optique, il faut procéder à un polissage mécanique du dépôt pour éviter la diffusion de lumière en surface. Il semble que notre méthode, avec le réacteur que nous avons conçu, permette de s'affranchir d'un tel polissage. Notre étude montre que la rugosité moyenne R_a décroît avec: 1) la décroissance de la taille de la poudre diamant du prétraitement; 2) l'enlèvement par rinçage ultrason du résidu de poudre de diamant du prétraitement; 3) l'augmentation du pourcentage de CH_4 dans le mélange H_2-CH_4 (effet bien connu); 4) l'accroissement de la densité de puissance micro-onde absorbée dans le plasma. Nous sommes ainsi arrivés à une valeur de R_a inférieure au nanomètre, une première dans le domaine selon nos renseignements.

Le chapitre 7 présente la conclusion générale de notre thèse

Bibliographie

[1] S. Tennant, *Phil. Trans. Roy. Soc.* **87**, 123 (1797).

[2] J. B. Hanny, *Proc. Roy. Soc. London* **30**, 450 (1880).

[3] H. Moissan, *Comptes rendus des séances de l'Académie des Sciences* **118**, 320 (1894).

[4] Allan T. Collins, *Indus. Diam. Rev.* page 434 (1975).

[5] F. P. Bundy, H. T. Hall, H. M. Strong, and R. H. Wentorf, *Man-made Diamonds Nature* **4471**, 51 (1955).

[6] W. Von. Bolton, *Z. Elektrochem.* **17**, 971 (1911).

[7] Brevet: US Patent Number: 3,030,187 (23 Juillet 1958); US Patent Number: 3,030,188 (17 avril 1958).

[8] B. V. Derjaguin and B. V. Fedoseev, *Sci. Amer.* **233**, 102 (1975).

[9] J. C. Angus, H. A. Will, and W. S. Stanko, *J. Appl. Phys.* 39. 2915 (1968.

[10] B. V. Spitsyn, L. L. Bouilov, and B. V. Derjaguin, *J. Cryst. Growth* **52**, 219 (1981).

[11] S. Matsumoto and Y. Sato, *Jpn. J. Appl. Phys.* **21**, 219 (1982).

[12] M. Kamo, Y. Sato, S. Matsumoto, and N. Setaka, *J. Cryst. Growth* **62**, 642 (1983).

[13] Y. Matsui, S. Matsumoto, and N. Setaka, *J. Mater. Sci.* **2**, 532 (1983).

[14] S. Matsumoto, Y. Sato, M. Tsutsumi, and N. Setaka, *J. Mater. Sci.* **17**, 3106 (1982).

[15] S. Matsumoto, Y. Sato, M. Kamo, and N. Setaka, *Jpn. J. Appl. Phys.* **21**, L183 (1982).

[16] F. M. Creio and A. Weimer, *Rev. Sci. Instrum.* **63** (1992).

[17] N. Ohtake, H. Tokura, Y. Kuiyama, Y. Mashimo, and M. Yoshikawa, *The Electrochemical Soc. Inc.* **12, 93** (1989).

[18] Wei Zhu and B. Stoner, *Proceedings of the IEE* **79, 621** (1991).

[19] K. E. Spear, *J. Am. Ceram. Soc.* **72**, 171 (1989).

[20] Y. Matsui, H. Yabe, and Y. Hirose, *Jap. Appl. Phys.* **29**, 1552 (1990).

[21] S. Matsumoto, M. Hino, and T. Kobayasshi, *Appl. Phys. Lett.* **51**. 737 (1987).

[22] K. Kurihara, K. Sasaki, M. Kawarada, and N. Koshima, *Appl. Phys. Lett.* **52**. 437 (1988).

[23] K. E. Spear, *J. Amer. Chem. Soc.* **2**, 171 (1989).

[24] A.W. Trivelpiece and R. W. Gould, *J. Appl. Phys.* **30**, 1784 (1959).

[25] R. Claude, M. Moisan, M. R. Wertheimer, and Z. Zakrzewski, *Chem. Plasma Proc.* **7**, 451 (1987).

[26] Robert F. Davis. *Diamond Films and Coatings*. Noyes Publications. New Jersey. 1993.

[27] E. Anger. PhD thesis, LIMHP, Université Paris-XIII, 1994.

[28] R. J. Nemanich and S. A. Solin, *Phys. Rev. B* **20**, 392 (1979).

[29] S. Futaki et T. Chonan, *Poc. of the ISPC 9, IUPAC* **III**, L19 (1989).

[30] A. Gicquel, *Rapport SGDN*, (1989).

[31] Yves Catherine et Alix Gicquel, *Journées de Formation* **CIP91**. 333 (1991).

[32] A. Badzian et B. Simonton, *Proc. SPIE*, 1988).

[33] J.I. Pankove, *The Electro. Chem. Soc. Pennington NJ* page 269 (1989).

[34] R. Berman. *In The properties of diamond*, Academic Press, N.Y., 1979).

[35] A.L. Lin et M.G. Stapelbroek, *Proc. 1st. Int. Symp. on Diamond and Diamond like films. ed. by* J.P. Dismukes, The Electro. Chem. Soc. Pennington NJ, pp.261, 1989).

[36] D.D. Rathman M.W., *IEEE Electro. Device Letter* **EDL-8**[8], 341 (1987).

[37] G.S. Gildenblat et S.A. Grot, *Appl. Phys. Lett.* **53**[7], 568 (1988).

[38] Brevet: (Basic) JP 60141697 (850726) Pioneer Electronic Corp. Diamond vibration plate production by vapor phase growing on substrate, heating and pealing of diamond film.

[39] M. Moisan, A. Shwarova, and A. W. Trivelpiece, *Plasma Phys.* **24**, 1331 (1982).

[40] A. Ricard, C. Barbeau, A. Besner, J. Margot-Chaker J. Hubert, M. Moisan, and G. Sauvé, *Can. J. Phys.* **66**, 740 (1988).

[41] J. Margot-Chaker, M. Moisan, M. Chaker, V. M. M. Glaude, P. Lauque, J. Paraszczak, and G. Sauvé, *J. Appl. Phys.* 66, 4134 (1989).

[42] M. Moisan and Z. Zakrzewski, *Plasmas sustained by surface waves at microwave and rf frequencies: experimental investigations and applications, Série des volumes de l'OTAN*, volume **149**, page 381, Pitlochry, Ecosse, 1985. Radiative Processes in Discharges Plasmas.

[43] E. Bloyet, P. Leprince, M. Llamas Blasco, and J. Marec, *Phys. Lett. A* **83A**, 391 (1981).

[44] M. Moisan, M. Chaker, Z. Zakrzewski, and J. Paraszczak, *J. Phys. E: Sci. Instrum.* **20**, 1356 (1987).

[45] M. Moisan and J. Pelletier. *Microwave Exited Plasma*, Elsevier, Netherlands, 1992.

[46] L. St-Onge and M. Moisan, *Plasma Chem. Plasma Process.* **14**, 87 (1994).

[47] M. Moisan and Z. Zakrzewski, *J. Phys. D* **24**, 1025 (1991).

[48] D. B. Ilic and B. A. Anicin, *Int. J. Electron.* **28**, 41 (1970).

[49] A. R. Badzian, T. Badzian, R. Roy, R. Messier, and K. E. Spear, *Mater. Res. Bull.* **23**, 521 (1988).

[50] A. Gicquel, K. Hassouni, S. Farhat, Y. Breton, C. D. Scott, M. Lefebvre, and M. Pealat, *Diamond Relat. Mater.* **3**, 581 (1994).

CHAPITRE 2

A novel technique for diamond film deposition using surface wave discharges

C. F. M. Borges, M. Moisan, and A. Gicquel

Publié dans Diamond and Related Materials
Reçu: 16 juin 1994; Accepté: 6 septembre 1994

ELSEVIER

Diamond and Related Materials 4 (1995) 149–154

DIAMOND AND RELATED MATERIALS

A novel technique for diamond film deposition using surface wave discharges

C.F.M. Borges [a], M. Moisan [a], A. Gicquel [b]

[a] *Groupe de Physique des Plasmas, Université de Montréal, Succursale Centre-ville, Montréal H3C 3J7, Québec, Canada*
[b] *Laboratoire d'Ingéniérie des Matériaux et des Hautes Pressions (CNRS), Université Paris XIII, 93430 Villetaneuse, France*

Received 16 June 1994; accepted in final form 6 September 1994

Abstract

Surface-wave-sustained discharges are utilized in a non-conventional configuration to yield plasma with a hemispherical shape for diamond film deposition at gas pressures in the range 1–60 Torr. Compared with microwave-sustained plasma balls in "bell jar" reactors, microwave power absorption is more efficient: no power is left that would heat the substrate and, for given power to the reactor and gas conditions, higher power densities are obtained in the plasma. The roughness of the deposit decreases with increasing power density. Deposition rate on 4 cm^2 is typically 350 $\mu g\ cm^{-2}\ h^{-1}$.

Keywords: Diamond; Gas phase reactor; Microwave plasma CVD; Growth

1. Introduction

Diamond film deposition at pressures of the order of a few Torrs and at substrate temperatures as low as possible is of interest in many applications where delicate surfaces are to be coated. This can be achieved by plasma-enhanced chemical vapor deposition and, in that respect, microwave-produced plasmas are interesting candidates. The advantage of microwave discharges compared with the filament method [1] or with d.c. discharges [2] is essentially a lower contamination of the process because the powered electrode (field applicator here) is located outside the discharge vessel. A shortcoming of microwave tubular discharges in general is the radial non-uniformity of the deposit on large areas. It comes mainly from the radial non-uniformity of the density distributions of hydrogen atoms and carbon radicals in the gaseous phase, these distributions being related to the radial decay of the microwave electric field intensity toward the tube axis. At 2.45 GHz, for example, this effect shows up when the plasma diameter is typically larger than 20 or 30 mm. One known remedy is to achieve a plasma "ball", which has the further advantage of not being in contact with the discharge vessel wall; the most common method to produce it is to use as the discharge vessel a fused silica bell jar through which microwaves (out of a waveguide-based structure, for example) are directed from the outside onto a reflecting surface inside (the substrate holder or the metallic base on which the bell jar is resting) thereby forming a standing wave [3–5]. By proper adjustment of this system, a plasma ball is created, which leads to uniform and good quality diamond films.

In this paper, we disclose a method based on surface wave (SW) discharges to achieve a microwave-sustained plasma with a tip in the form of a hemisphere. The new reactor, its background and principles of operation are presented in Section 2 and a specific arrangement is described. Some operating results and the advantages of this reactor for diamond deposition are briefly compared in Section 3 with those of commonly encountered plasma ball systems. Section 4 is the conclusion.

2. Experimental details

2.1. Main features of classical surface wave discharges

Among the various types of microwave-sustained plasmas, electromagnetic SW discharges are known for their very broad range of discharge conditions (frequency, gas pressure, tube dimensions and shape) [6,7], a feature of interest when optimizing plasma processes. SW discharges are already being utilized or considered in various applications [6–8]; however, their use for diamond deposition is hindered by non-uniformity prob-

SSDI 0925-9635(94)00237-1

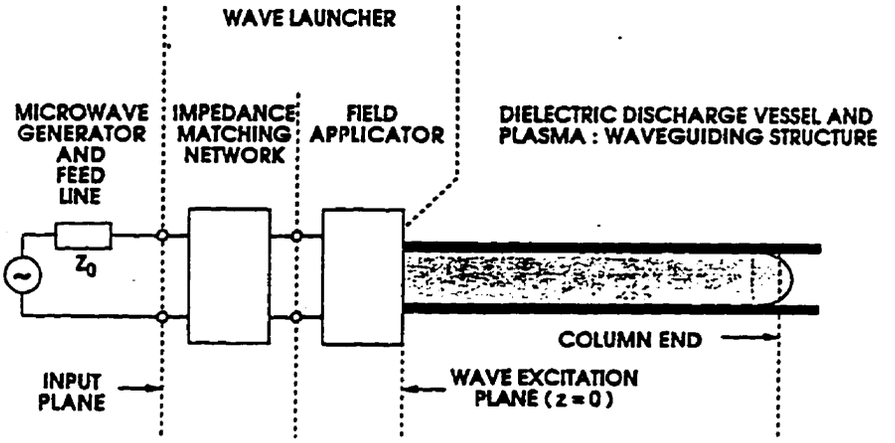

Fig. 1. Essential elements of a classical SW plasma source [8].

lems as discussed below. The usual configuration and set-up of an SW discharge is shown in Fig. 1 where a straight cylindrical discharge tube is used. The SW is excited by a localized wave launcher (comprising a field applicator and an impedance matching network) and uses both the sustained plasma and the discharge tube as its sole propagating structure [6–8]. The length of the plasma column increases with the microwave power supplied to the launcher; when the plasma reaches the end of the tube, the wave is reflected back, increasing the density of the plasma. SW can be used to fill tubes of different shapes with plasma, provided that changes in dimensions and configuration along the tube are not too abrupt so the wave can propagate across it with little reflection.

2.2. Previous surface wave systems used for diamond deposition

Until now, two configurations of SW discharges have been considered for thin diamond film deposition, as illustrated in Fig. 2. (1) The first is a cylindrical straight tube with the (independently heated) substrate located perpendicularly to the tube axis (Fig. 2(a)). Because the SW electric field intensity decreases radially toward the axis, the active species are mainly created close to the tube wall and their radial distribution of density n_s reflects this origin [6]; Fig. 2(a) shows a sketch of such a distribution at gas pressures typically exceeding 1 Torr. Using a 30 mm internal diameter tube, we found the deposit thickness d_f to be radially non-uniform, as sketched in Fig. 2(a): it decreases toward the axis and the film morphology also changes, starting from a dense coverage close to the wall to scarcely spread crystals on the axis. Clearly, such a method cannot provide uniform coating on large diameter surfaces. (2) The second is a mild transition tapered tube with the substrate located parallel to the tube wall in the transition section, as shown in Fig. 2(b) [9]. The susceptor cross-section is

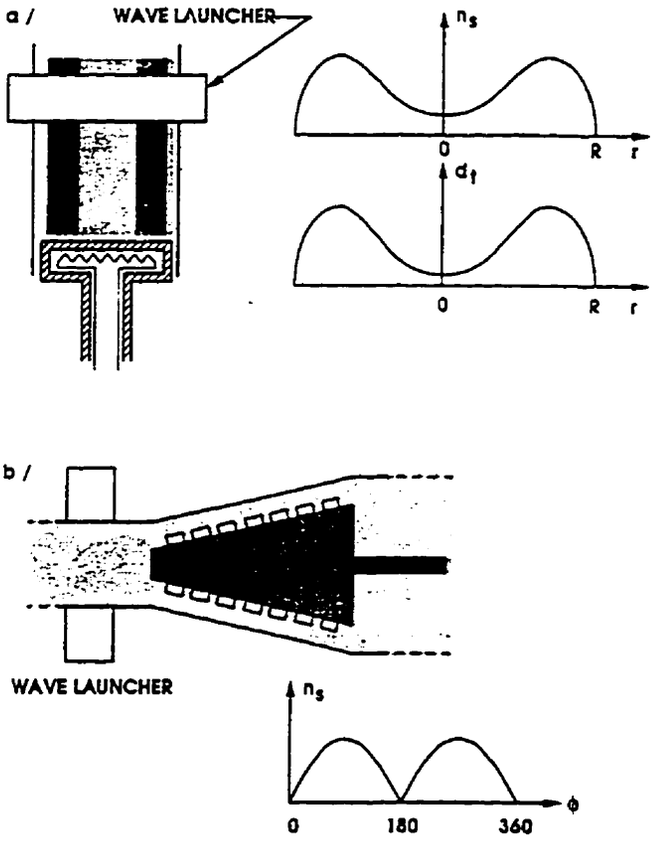

Fig. 2. Previous configurations of SW discharges used for thin diamond film deposition: (a) straight tube; (b) tapered tube with a mild transition in which the graphite susceptor rotates [9]. The radial and azimuthal distributions of the species concentrations are only approximate.

octagonal, providing flat deposition surfaces. The diameter of the tube inserted into the wave launcher is 75 mm and the 130 mm long transition ends on a 160 mm diameter tube. Recall that SWs can propagate in different modes which are characterized by an integer m yielding the dependence on the azimuthal angle ϕ of the wave

field intensity (proportional to $\exp(jm\phi)$) [10]. Since here the product of the radius R of the tube in the launcher and the wave frequency f is large, the wave propagates in an $m=1$ (dipolar) mode [10] and therefore n_s varies with ϕ as sketched in Fig. 2(b). To eliminate this non-uniformity, the susceptor is rotated around its axis. This tapered tube scheme is limited to flat deposition surfaces of narrow width.

2.3. New surface wave system for diamond deposition

The novel configuration is shown in Fig. 3. In contrast to the smoothly tapered tube in Fig. 2(b), the transition from the small to the large diameter tube is so abrupt that the surface wave cannot propagate across it. Instead, a hemispherical plasma appears slightly below the transition plane, as sketched in Fig. 3: the diameter of the hemisphere and its position with respect to the transition plane are determined by the configuration and dimensions of the transition, and very little by the absorbed power density: the exact shape of the hemisphere depends somehow on the position of the susceptor with respect to it. This contrasts with most bell jar systems where the plasma ball tends to move with the substrate, although there are exceptions depending on the way the susceptor is held with respect to the conducting plate below it [5]. In the arrangement described in the next section, the ratio between the diameters of the large and small tubes is only 1.5; however, the larger this ratio, the less chances there are that the SW propagates in the large diameter tube when power is pushed up.

The main advantage of the new system over the previous SW discharge schemes is that a uniform deposition can be achieved over a larger surface, namely the whole diameter of the plasma hemisphere. Compared with commercial plasma ball systems, its advantages are as follows: (1) a much higher flexibility of adjustment of

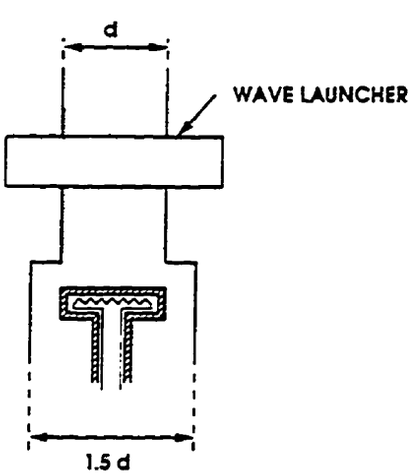

Fig. 3. Sketch of the novel SW configuration used to produce a hemispherical plasma tip for diamond deposition on an independently heated susceptor.

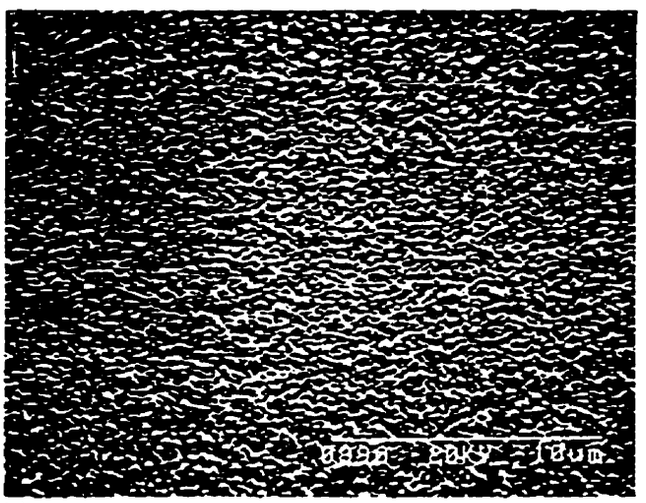

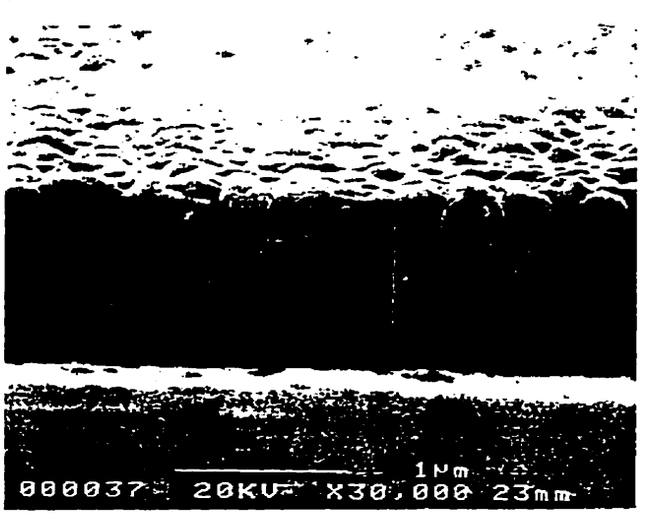

Fig. 4. Scanning electron microscopy micrographs at 0.75% CH_4, 15 Torr total pressure and 100 standard $cm^3\ min^{-1}$ gas flow, T_s = 900 °C, substrate dimensions 2.5 cm × 1.5 cm: (a) low magnification; (b) high magnification; (c) cleaved cross-section. (Original Magnifications: (a) 2000 ×; (b) 10 000 ×; (c) 30 000 ×.)

the plasma hemisphere position with respect to the substrate, which we found was crucial in obtaining high quality and fast growing diamond films; (2) a negligible heating of the substrate by microwave radiation, as discussed below. However, when operating at high microwave power densities, this arrangement requires cooling the discharge tube wall to avoid damaging it and contaminating the plasma with Si; cooling the tube also reduces drastically the wall recombination of atomic hydrogen, increasing its steady state concentration [11].

2.4. Arrangement and conditions of experiment

The arrangement tested consisted of a 26 mm inner diameter (30 mm outer diameter) cylindrical fused silica tube on the launcher side, connecting abruptly to a 47 mm inner diameter tube. A base pressure of 2×10^{-6} Torr was reached before admitting gases; the discharge was sustained in H_2 gas to which CH_4 was added and varied between 0.5% and 1.5% of the total gas content; the total gas flow was 100 standard cm^3 min^{-1} at pressures ranging from 1 to 60 Torr. The discharge tube is enclosed in a larger Pyrex tube providing a cooling jacket filled with dimethylpolysiloxane, which is circulated by a gear pump (about 18 l min^{-1}) through a heat exchanger with a refrigerating unit. The surface wave was launched with a waveguide surfatron [12] at 2.45 GHz with power up to 1.8 kW; the fR product here allowed us to propagate the surface wave in either the $m=0$ or the $m=1$ mode by proper adjustment of the launcher [10]. The substrate temperature T_s was controlled independently by external heating from approximately 500 to 1100 °C, as measured with an optical pyrometer. The position of the substrate with respect to the tube transition for which the film growth rate, uniformity and quality are optimum corresponds to the hemispherical plasma just fully covering the substrate surface; this occurs at a 15 mm distance in the present conditions. When the plasma barely touches the center of the substrate, there are only scarce diamond crystallites (with some grain boundaries) at the substrate edges. On the contrary, when the plasma hemisphere is crushed by the susceptor, the substrate is damaged and nucleation density is low. The results presented below were obtained at the optimum substrate position.

3. Results

Scanning electron micrographs from a typical sample are shown in Fig. 4. The diamond films showed dense nucleation (10^{10} cm^{-2}) on Si(100) surfaces. The deposited layer is quite uniform as can be seen at low magnification (Fig. 4(a)). A higher magnification (Fig. 4(b)) shows well-defined facets with a broad distribution in crystallite size. Fig. 4(c) is the cleaved cross-sectional micrograph of the same sample. It shows that growth is columnar, yielding a good quality film. Diamond film grows at approximately 1.5 μm h^{-1}. The deposited films were also analyzed by macro Raman spectroscopy using an Ar^- laser at 514.5 nm (100 mW). The Raman spectrum in Fig. 5 shows a clear 1332 cm^{-1} diamond longitudinal optical phonon line. The full width at half-maximum value of this line is typically 3.5 cm^{-1}.

We have examined the influence of gas pressure and

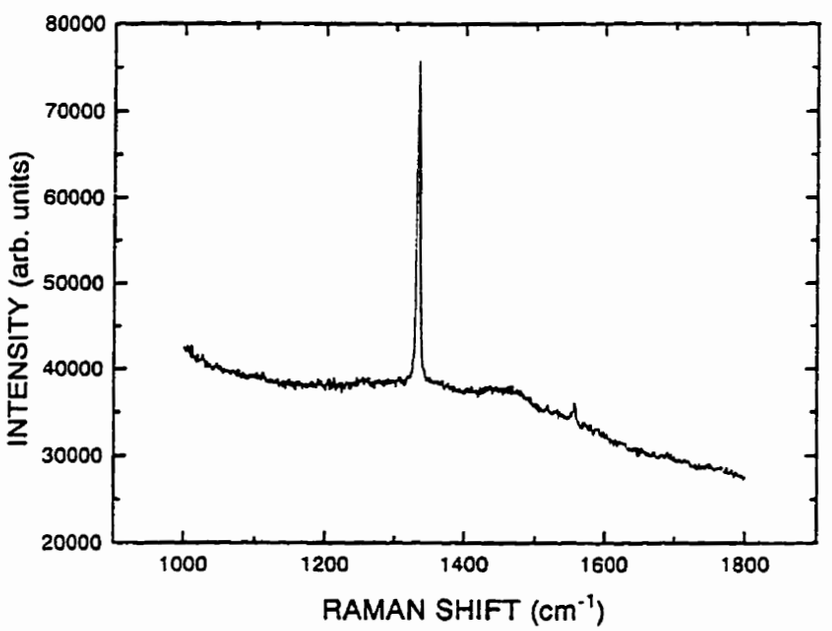

Fig. 5. Raman spectrum of a diamond film deposited at 0.75% CH_4 and $T_s = 900$°C; the sharp peak at about 1332 cm^{-1} represents the diamond phase.

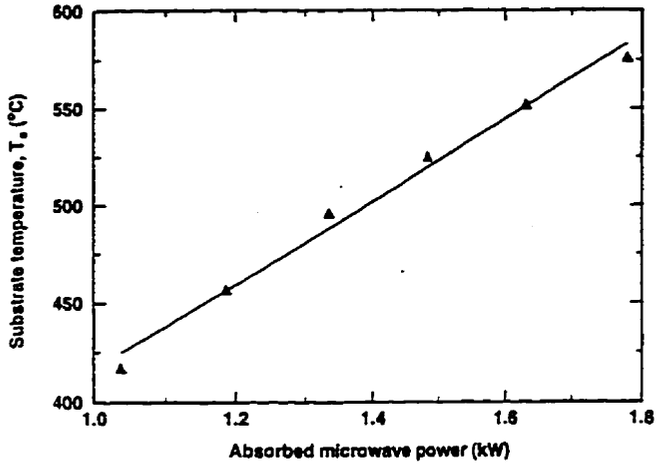

Fig. 6. Temperature of the substrate as measured in the absence of external heating at 15 mm from the transition plane as a function of microwave power absorbed in the plasma (1.8 kW corresponds to 97 W cm^{-3}), at 10 Torr in hydrogen with 0.5% CH_4.

power density on T_s with the substrate located at various positions with respect to the transition. At the optimum substrate position and at 10 Torr, Fig. 6 shows that, up to 1.8 kW (97 W cm^{-3}), T_s remains below 600 °C in the absence of external heating. At the same substrate position and for a fixed power of 1 kW, we see from Fig. 7 that T_s increases only from 415 to 425 °C when gas pressure is increased from 10 to 60 Torr. In contrast, in some bell jar systems, for example at 1 kW and 50 Torr, T_s was reported to be as high as 980 °C [13]. As far as temperature uniformity of the substrate surface is concerned, we have measured T_s over nine points evenly distributed on the sample; it is constant (± 1 °C) when sustaining plasma with an SW in the $m=0$ (symmetrical) mode while it varied by as much as 20 °C when using the $m=1$ (dipolar) mode. This is related to the fact that

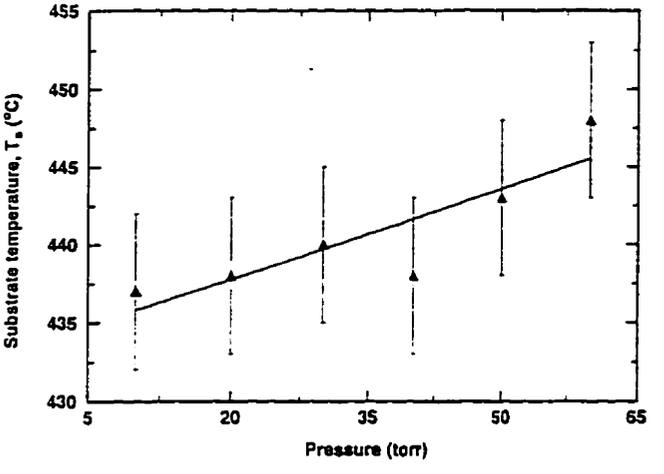

Fig. 7. Temperature of the substrate measured in the absence of external heating at 15 mm from the transition plane as a function of the total gas pressure in hydrogen with 0.5% CH_4, at 1.2 kW absorbed power.

the microwave power flux along an SW plasma is only incompletely absorbed at the end of the column when it is sustained in the $m=1$ mode (see Fig. 16 in Ref. [10]).

The roughness of the deposit was measured with an atomic force microscope, using a statistical program to determine its root mean square value. At 0.75% CH_4 and a power density of 60 W cm^{-3} (1.1 kW), it is 21 nm. Ravet et al. [14] have reported similar values in a bell jar configuration. We have found roughness to decrease with increasing power density in our system in contrast to observations with bell jar systems [15]; this could be due to the presence of energetic ions at the end of SW plasma columns [16].

4. Conclusion

The new system disclosed provides a microwave-sustained hemispherical plasma that yields high quality diamond films. Microwave power is fully absorbed in the plasma when using $m=0$ mode SWs. The power density in the plasma is higher than in resonant cavity (43 W cm^{-3} compared with 30 W cm^{-3} for 800 W absorbed power [17,18]) and bell jar (54 W cm^{-3} compared with 30 W cm^{-3} at 1000 W absorbed power [5]) systems; a higher power density yields a faster growth rate and, in our system, a lower roughness of the deposit. Finally, the fact that the susceptor is not heated by microwaves allows us to have an independent and uniform heating of this susceptor down to, for example, 450 °C at 1.2 kW (60 Torr) and 580 °C at 1.8 kW (10 Torr) in contrast to most other microwave-based systems which require cooling the susceptor to meet such conditions [19]. The deposition rate in our system is 350 μg cm^{-2} h^{-1} on Si substrates, approximately two times larger than in other microwave systems under similar operating conditions [5,19,20]. Our system thus appears as an interesting and flexible variant to existing plasma ball systems.

Acknowledgments

The authors would like to express their gratitude to F. Roy, R. Lemay, R. Martel and J.E. Samuel for technical assistance. The skilled assistance of G. Veilleux of INRS–Énergie et Matériaux with the electron microscope at Énergie et Mines Canada is gratefully acknowledged. Special thanks are due to P. Maubert who participated in the earlier stage of this project. Dr. C. Barbeau, Dr. L. Martinu, L. St-Onge, G. Sauvé and Professor Z. Zakrzewski also contributed to this project through discussions and support. This work was carried out thanks to the France–Québec scientific exchange agreement (Projet 02-58-02-91). One of the authors (C.E.M.B.) is grateful to CNPq (Brazil) for his fellowship.

References

[1] S. Matsumoto, Y. Sato, M. Kamo and N. Setaka, *Jpn. J. Appl. Phys., 21* (1985) L183.

[2] K. Suzuki, A. Sawabe, H. Yasuda and T. Inuzuka, *Appl. Phys. Lett., 50* (1987) 728.

[3] P.K. Bachmann, W. Drawl, D. Knight, R. Weimer and R. Messier, in G. Johnson, A. Badzian and M. Geis (eds.), *Extended Abstracts Diamond and Diamond-Like Materials Synthesis, 1988*, Materials Research Society, Pittsburgh, PA, 1988, p. 99.

[4] J.P. Dismukes and K.R. Walton, in J.P. Dismukes (ed.), *Proc. 1st Int. Symp. Diamond and Diamond Like Films*, Electrochemical Society, Pennington, NJ, 1989, p. 653.

[5] A. Gicquel, K. Hassouni, S. Farhat, Y. Breton, C.D. Scott, M. Lefebvre and M. Pealat, *Diamond Relat. Mater., 3* (1994) 581.

[6] M. Moisan, C.M. Ferreira, Y. Hajlaoui, D. Henry, J. Hubert, R. Pantel, A. Ricard and Z. Zakrzewski, *Rev. Phys. Appl., 17* (1982) 707.

[7] M. Moisan, J. Hubert, J. Margot, G. Sauvé and Z. Zakrzewski, in C.M. Ferreira and M. Moisan (eds.), *Microwave Discharges: Fundamentals and Applications*, NATO ASI Series, Vol. B 302, Plenum, New York, 1993, p. 1.

[8] M. Moisan and Z. Zakrzewski, *J. Phys. D, 24* (1991) 1025.

[9] P. Bou, L. Vandenbulcke, A. Quilgars, M. Coulon and M. Moisan, *Fr. Patent 2,678,956*, 1993; patents pending in other countries.

[10] J. Margot-Chaker, M. Moisan, M. Chaker, V.M.M. Glaude, P. Lauque, J. Paraszczak and G. Sauvé, *J. Appl. Phys., 66* (1939) 4134.

[11] L. St-Onge and M. Moisan, *Plasma Chem. Plasma Process., 14* (1994) 87.

[12] M. Moisan, M. Chaker, Z. Zakrzevski and J. Paraszczak, *J. Phys. E. 20* (1987) 1356.

[13] Y. Liou, A. Inspektor, R. Weimer and R. Messier, *Appl. Phys. Lett., 55* (1989) 631.

[14] M.F. Ravet, A. Gicquel, E. Anger, Z.Z. Wang, Y. Chen and F. Rousseaux, in M. Yoshikawa, Y. Tzeng and W.A. Yarbrough (eds.), *2nd Int. Conf. on Applications of Diamond Films and Related Materials*, MYU, Tokyo, 1993, p. 73.

[15] E. Angers, *Thèse de Doctorat*, Université Paris Nord, May 1994.

[16] L. Paquin, D. Masson, M.R. Wertheimer and M. Moisan, *Can. J. Phys., 6* (1985) 831.

[17] H. Rau and B. Trafford, *J. Phys. D, 23* (1990) 1637.

[18] K. Kobashi, K. Nishimura, Y. Kawate and T. Horiuchi, *Phys. Rev. B. 38* (1988) 4067.

[19] Y. Liou, R. Weimer, D. Knight and R. Messier, *Appl. Phys. Lett., 56* (1990) 437.

[20] D.J. Pickrell, W.Z. Zhu, A.R. Badzian, R. Messier and R.E. Newnham, *Appl. Phys. Lett., 56* (1990) 2010.

CHAPITRE 3

Influence of process parameters on diamond film CVD in a surface-wave driven microwave plasma reactor

C. F. M. Borges, L. St-Onge, M. Moisan, and A. Gicquel

Publié dans Thin Solid Films
Reçu: 4 janvier 1995; Accepté: 17 juillet 1995

ELSEVIER

Thin Solid Films 274 (1996) 03-17

thin solid films

Influence of process parameters on diamond film CVD in a surface-wave driven microwave plasma reactor

Carlos F.M. Borges [a], Louis St-Onge [a], Michel Moisan [a,*], Alix Gicquel [b]

[a] *Groupe de Physique des Plasmas, Université de Montréal, C.P. 6128, Succursale Centre-ville, Montréal, Qué. H3C 3J7, Canada*

[b] *Laboratoire d'Ingénierie des Matériaux et des Hautes Pressions, CNRS-UPR 1311, Avenue J.B. Clément, 93430 Villetaneuse, France*

Received 4 January 1995; accepted 17 July 1995

Abstract

The influence upon diamond film chemical vapour deposition of operator-set process parameters in a novel microwave plasma reactor is examined. The new reactor operates with a discharge sustained by an electromagnetic surface wave in a non-conventional configuration that yields a plasma hemisphere in the vicinity of the substrate. The basic advantages of this reactor compared with "plasma-ball" systems in resonant cavity and bell-jar arrangements have been reported in a previous paper. The present paper provides the results of a parametric study of the quality of diamond films as well as of the gas temperature and hydrogen atom concentration in the discharge as functions of methane and oxygen concentrations, substrate position and temperature, gas pressure, and microwave power density absorbed in the plasma. The conditions optimizing both maximum growth rate and film quality correspond to a total gas pressure of 15 Torr (2 kPa), with a 0.75% CH_4 content and a substrate temperature of 930 °C, although good quality films can be achieved over a broader range, at gas pressures between 10 and 60 Torr (1.33–8 kPa), with a 0.25–0.75% CH_4 content, and with substrate temperatures in the range 870–980 °C.

Keywords: Chemical vapour deposition; Diamond; Plasma processing and deposition

1. Introduction

Various techniques have been employed for diamond film chemical vapour deposition (CVD). The most common one at the moment calls for low-pressure microwave discharges. As far as we know, two companies, Astex and Denki Kogyo, are presently commercializing [1] such reactors. The 2.45 GHz Astex system produces a plasma ball over a plane surface, three or four inches in diameter; microwave power is generally limited to 1 kW because of microwave heating of the various parts of the system, including the substrate. In the Denki Kogyo reactor, the deposition chamber is situated inside the waveguide, enabling higher powers to be used. However, the plasma ball position ceases to be stable and reproducible with respect to the susceptor at powers exceeding 2 kW [2]. In the end, the limitation in the growth rate set by the maximum microwave power density achievable and the limitation in size imposed by the microwave structure dimensions restrict the use of these reactors as industrial tools for diamond deposition.

One method of circumventing these limitations is to utilize a discharge sustained with electromagnetic surface waves, but in a new, non-conventional configuration. It provides a plasma with a hemispherical shape facing the susceptor; it is used to deposit diamond films as with plasma balls in resonant cavity and bell-jar systems. The advantages of such a new plasma reactor compared with these well-known arrangements are: (i) a higher power density in the plasma for a given microwave power absorbed in the reactor, which reflects in a higher deposition rate and a lower surface roughness; (ii) no microwave heating of the susceptor, whose temperature due to the plasma alone does not exceed 600 °C at power densities as high as 100 W cm^{-3}; this provides the possibility of independently heating the substrate to the most adequate temperature from 600 °C upwards; (iii) a higher flexibility in adjusting the susceptor position relative to the plasma hemisphere, hence a better control on the quality of the deposit; (iv) this method enables one scaling up the system to achieve a hemispherical plasma with a diameter larger than the vacuum wavelength in contrast to present plasma-ball systems.

The aforementioned paper [3], the first one to deal with the novel surface-wave sustained reactor, was concerned with disclosing its configuration and specific characteristics. The present paper scrutinizes the influence of operating conditions on the properties of the deposited films. It also correlates the

* Corresponding author.

SSDI 0040-6090(95)06967-4

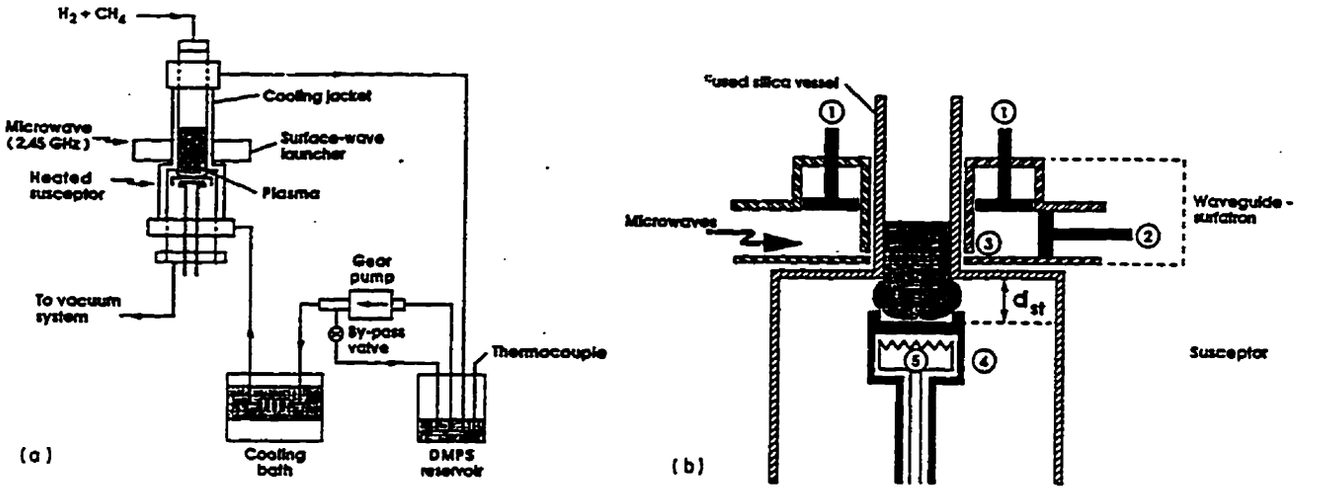

Fig. 1. Schematic drawing of the surface-wave driven microwave plasma reactor showing: (a) the plasma source, the susceptor, and the discharge tube cooling system. (b) details of the surface-wave plasma source and relative location of the susceptor (cooling jacket not represented). 1, coaxial tuning stub and 2, waveguide tuning stub in the waveguide-surfatron launcher; 3, launching gap [6]; 4, molybdenum casing; 5, tungsten filament.

gas temperature and hydrogen atom concentration with the properties of the diamond films, following Gicquel et al. [4]. Such a systematic characterization of the reactor is essential in demonstrating its specific properties with respect to conventional low-pressure microwave systems.

We thus examine the growth rate, morphology (as indicated by scanning electron microscopy (SEM)) and structure (as indicated by Raman spectroscopy) of the deposited films as functions of a number of so-called process parameters. These externally set parameters are: percentage of methane concentration (CH_4%), percentage of oxygen concentration (O_2%), substrate distance (d_{st}), substrate temperature (T_s), total gas pressure p, and microwave power P_{mw}. We use emission spectroscopy to determine the gas temperature (through the rotational emission spectrum of H_2), and the relative atomic hydrogen concentration (through actinometry) which we know is critical in the growth of diamond films [5]. It is indeed thought that, because H atoms help stabilize the diamond sp^3 hybridization, the net growth rate of diamond is proportional (at least up to a certain extent) to the atomic hydrogen concentration.

The paper is organized as follows. Section 2 describes the experimental arrangement and the methods used to characterize the diamond films and the plasma. Section 3 shows the individual influence of the process parameters upon the properties of the plasma and deposited films. Section 4 is the conclusion.

2. Experimental

The arrangement used to deposit the diamond films is described in Fig. 1. Fig. 1(a) is a schematic overview of this surface-wave based reactor [3]. It includes a plasma source sustained by microwaves at 2450 MHz, an independently heated susceptor and a dielectric liquid cooling arrangement [3]. The substrate position d_{st} is defined with respect to the plane at which the tube diameter changes abruptly, as shown in Fig. 1(b); this way of measuring the substrate distance is easy and valid because the shape and position of the plasma hemisphere are perfectly reproducible and depend little on the susceptor position. Details on the surface-wave launcher (waveguide-surfatron) can be found in Ref. [6]. Monocrystalline silicon wafers with (111) orientation were used as substrates. Samples of 2 cm in diameter were submitted for 60 min to ultrasonic impacts of 20–40 μm diamond powder immersed in ethanol. The substrate temperature T_s, controlled by a filament-heated molybdenum susceptor, could be varied from 500 to 1000 °C and was measured with an optical pyrometer. Gases were premixed before entering the plasma source. The sum of H_2 and CH_4 flow rates was kept constant at 100 sccm. The methane relative concentration in hydrogen (CH_4%), defined as the ratio of the CH_4 flow rate to the total flow rate, was in the range 0–2%. Likewise, the oxygen relative concentration (O_2%) was the ratio of the O_2 flow rate to the total ($H_2 + CH_4 + O_2$) flow rate, and varied between 0 and 0.7%. Finally, the gas pressure p was varied from 10 to 60 Torr (i.e. from 1.33 to 8 kPa, 1 Torr being equal to 133 Pa), as measured by a capacitance manometer. Other experimental details can be found in Ref. [3].

The growth rate of diamond films can be expressed in terms of either the film thickness or the weight of deposited carbon. This is because one measures it either: (i) by breaking the sample and determining the film thickness (in μm) directly under a scanning electron microscope, and the growth rate is then expressed in μm h^{-1}; or (ii) by weighing the sample before and after deposition, and calculating the average rate of weight gain per unit surface (expressed in μg $cm^{-2} h^{-1}$); we used an analytical balance with a 0.1 mg resolution for that purpose. Assuming the density to be that of monocrystalline diamond (3.52 g cm^{-3}), the correspondence of units between the two methods makes 32 μg $cm^{-2} h^{-1}$ equivalent to 0.1 μm h^{-1}. Clearly, one cannot fully rely on this conversion factor because of two possible sources of discrepancies:

(i) the assumption that the film density is that of monocrystalline diamond: diamond films deposited in non-optimal conditions actually contain some graphite and other non-diamond phases and, since such phases have a lower density than diamond, the films have in reality a density lower than 3.52 g cm^{-3}; (ii) the etching of the silicon substrate, which is temperature activated: this mechanism lowers the silicon substrate weight and leads to an underestimation of the diamond weight gain. In the end, the growth rate expressed in $\mu m\ h^{-1}$ can be lower by as much as 15% when determined from the weight method compared with the SEM thickness measurement. The values of the growth rate below are taken as the average of these two methods.

After a deposition time of 3 h, the samples were examined by SEM and the quality of the deposits was evaluated by macro-Raman spectroscopy with a double monochromator. The Raman measurements were performed in a backscattering configuration using an argon laser beam incident at 488 nm with a 100 mW laser power; the samples were characterized at their centre using a laser spot of 200 μm diameter. In a different set of experiments, we determined the density of nucleation and the size of the crystal particles; to this end, we set the deposition time at 1 h instead of 3 h, so that the individual diamond crystals did not coalesce to form a uniform film. The nucleation density was then obtained from SEM micrographs by counting the average number of crystallites per unit surface, and the particle size is simply the average particle diameter.

For the optical spectroscopy measurements, the light from the plasma was collected by an optical fibre (2 mm i.d.) pointing perpendicularly to the discharge tube axis without further collimation, and positioned 1–2 mm above the susceptor; the line intensity is thus some average over the plasma diameter. This optical fibre was connected either to a 34 cm or to a 1 m focal-length spectrophotometer, for actinometry or rotational band spectroscopy respectively, and the detected intensity was displayed on a recording chart. We have used argon as the actinometer at a fixed flow rate of 3 sccm and monitored the intensity of the Ar I 750.4 nm and 434.0 nm Balmer H_γ lines. Their intensity ratio I_H/I_{Ar} is a probe of the relative H-atom concentration. However, the dissociative excitation of H_2 contributing to H_γ is a major cause of departure from ideal actinometry conditions which assume electron impact excitation of H in its ground state [7]. This means that one should not apply actinometry to experiments in which the electron energy distribution function (EEDF) changes significantly, which is the case for example when pressure is varied [7].

To determine the gas temperature, we took advantage of the correspondence observed in H_2 discharges between the actual gas temperature and the rotational temperature deduced from the R branch of the $G^1\sum \rightarrow B^1\sum$ $(0--0)$ band of H_2 [8]. However, more recent observations [9] show that this rotational temperature can be considered as representative of the gas temperature variations only, not of its absolute value. This result was obtained by comparing the rotational temperature from the above G → B system with the rotational temperature of the molecule in its ground state (X) using coherent anti-Stokes Raman spectroscopy; the rotational temperature of the G state exceeds that of the ground state by approximately 400 K at 2100 K, although both temperatures vary in the same manner with changes in the discharge conditions. The wavelengths of the rotational structure lines of the G → B system and the G-state rotational level energies are taken from Ref. [10].

3. Results and discussion

We examine below the individual influence of a series of process parameters upon plasma (gas temperature and H-atom concentration) and deposited film characteristics. The characterization of the films, which was performed after that of the plasma, was also the occasion of optimizing the parameters investigated to yield the best quality film. This explains why the range of experimental conditions considered for film characterization is broader than for plasma characterization.

3.1. The influence of methane concentration

3.1.1. Film characterization

The deposition parameters are $p = 15$ Torr, $T_s = 950$ °C, $P_{mw} = 1.15$ kW (76 W cm^{-3}), and $d_{st} = 1.9$ cm (the tip of the hemispheric plasma is barely touching the substrate). The influence of methane concentration on the diamond content of the deposited films is evidenced by the Raman spectra in Fig. 2: when increasing the methane concentration from 0.25 to 1.5%, the 1332 cm^{-1} diamond peak decreases rapidly relatively to the 1550 cm^{-1} non-diamond carbon phase peak, indicating that the deposited films contain an increasing amount of non-sp^3 bonding. This influence of the methane concentration is well known in the literature [11–13].

The dependence of the film growth rate upon CH_4% is shown in Fig. 3 for the same deposition conditions as in Fig. 2. The growth rate increases markedly when increasing the CH_4% from 0.5 to 2%, essentially because of an increasing amount of carbonic reactive species in the plasma, hence a higher degree of carbon supersaturation [14].

The morphology of these films can be appraised from the SEM micrographs in Fig. 4. It evolves from faceted to non-faceted grains as CH_4% increases, because of the increased presence of non-diamond phases. The grain size increases with CH_4% until it reaches 2% (not shown), then decreases to submicron size, because of the renucleation process. We have also found that increasing the methane concentration increases the nucleation density, but at the expense of the quality of the film, as we have already seen from Raman spectra.

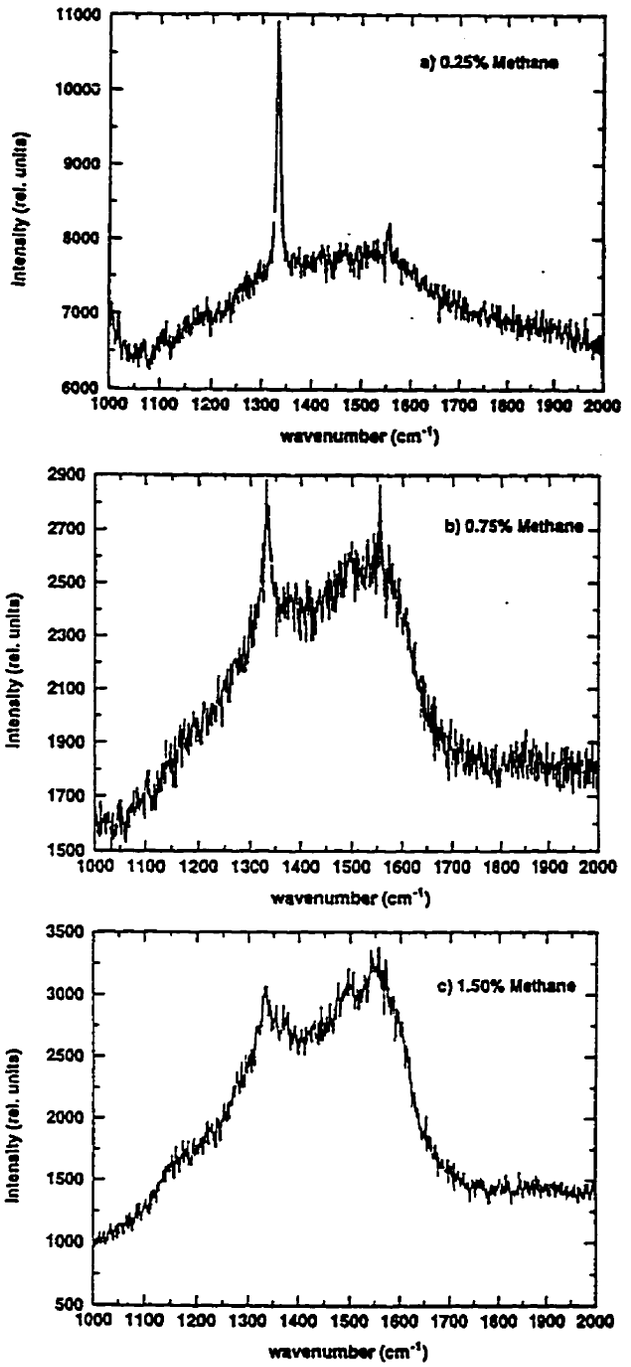

Fig. 2. Raman spectrum of the films deposited on a (111) silicon substrate at three different methane concentrations. Other deposition parameters: $p = 15$ Torr, $T_s = 950$ °C, $P_{mw} = 1.15$ kW (76 W cm^{-3}), and $d_{st} = 1.9$ cm.

3.1.2. Plasma characterization

The actinometry method cannot be applied confidently to the case of a varying CH_4 concentration, because of a possible related variation of the EEDF [7]. We nonetheless performed such measurements and found that the I_H/I_{Ar} ratio (hopefully proportional to the H-atom concentration) decreased with increasing CH_4 concentration; the decrease of atomic hydrogen concentration with CH_4% has been observed by many workers [4,15–18] and predicted by chemical kinetics models [19–21]. Such a decrease is thought to be due to increasing volume reactions of hydrogen atoms with methyl radicals and methane; it could also come from an increased etching of the carbon material by H atoms, since carbon increasingly deposits in non-diamond phases which are more susceptible to etching.

3.2. The influence of oxygen concentration

3.2.1. Film characterization

Two sets of deposition parameters are reported: one that shows the evolution toward the best quality diamond film and the other for comparison with the plasma characterization data. The first set corresponds to $p = 15$ Torr, $T_s = 950$ °C, $P_{mw} = 1.15$ kW, $d_{st} = 1.2$ cm, and 0.75% CH_4, while the second set, denoted P.C. (for plasma characterization), has been obtained with $p = 10$ Torr, $T_s = 950$ °C, $P_{mw} = 890$ W (59 W cm^{-3}), $d_{st} = 1.5$ cm, and 0.5% CH_4.

The surface morphology of the films grown is drastically influenced by the addition of oxygen to the gas mixture. SEM micrographs corresponding to different O_2% are displayed in Fig. 5. Under oxygen-free CVD with the same d_{st} and CH_4% (see also Fig. 22(b)), the individual diamond particles exhibit a rather rounded face while, in contrast, Fig. 5(a)–5(c) shows that a small addition of oxygen (0.25–0.7%) makes the diamond particles well faceted, as we already know from the literature (for example, see Ref. [22]). The evolution of the film morphology under P.C. conditions is similar, as shown in Fig. 5(d)–5(f).

We have examined the Raman spectrum of these films, observing that up to 0.3% O_2 the spectral contribution from non-diamond carbon phases is dominant. However, when the O_2 percentage is equal to or larger than 0.5%, the diamond peak at 1332 cm^{-1} is definitely the main feature of the spectrum, as can be seen in Fig. 6. The evolution of the non-diamond phase content with O_2 under P.C. conditions is similar, but this content is lower in absolute value.

The influence of oxygen is also manifest in the film growth rate v. Fig. 7 shows that v is almost constant as O_2% is

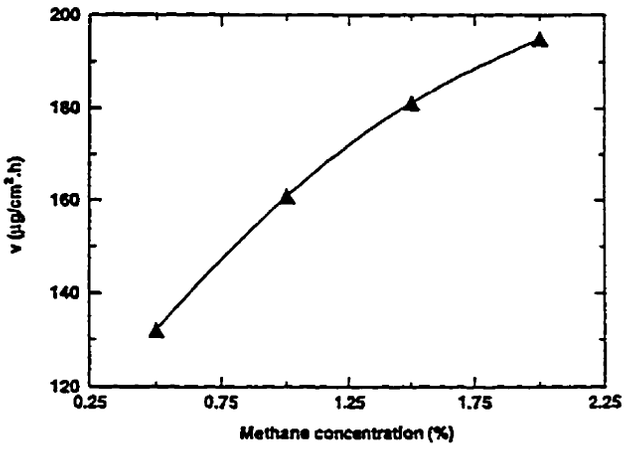

Fig. 3. Growth rate v of the film as a function of methane concentration. Other deposition parameters as in Fig. 2.

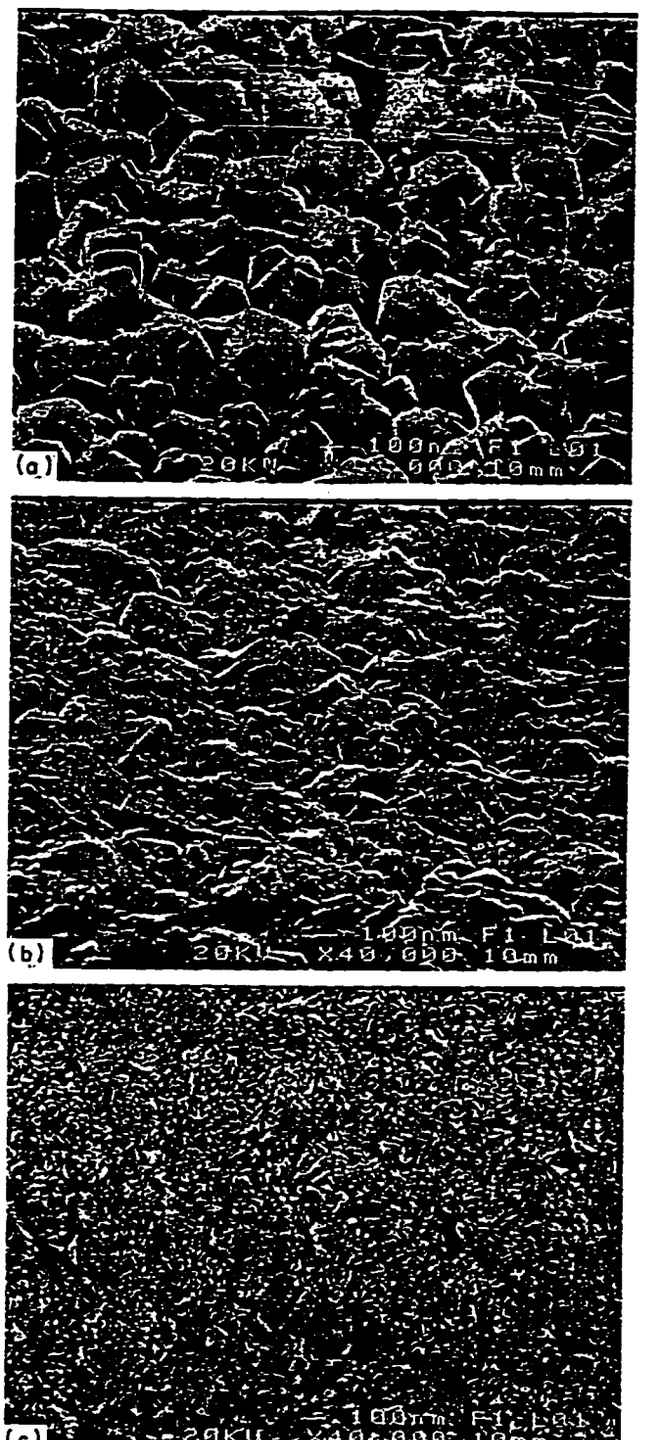

Fig. 4. SEM micrographs showing the film morphology at three different methane concentrations: (a) 0.25%, (b) 0.75%, and (c) 1.5%. Other deposition parameters as in Fig. 2.

increased from 0 to 0.3% but decreases afterwards with the oxygen content, under both sets of operating conditions. Further experiments made in this reactor have shown that when the O_2 to CH_4 concentration ratio exceeds unity, nucleation is markedly decreased; Gicquel et al. [22] had previously found that, in a hot filament reactor, nucleation density also decreases with the addition of O_2.

3.2.2. *Plasma characterization*

We have checked that the actinometry method that we were using to determine the hydrogen atom concentration in a pure H_2 discharge remained valid to a first approximation when a small amount of O_2 was added to it. Fig. 8 shows the relative H-atom concentration observed in this way at 1 mm above the susceptor, as a function of O_2%; the operating conditions are the P.C. values in Fig. 5–7 except for the fact that the susceptor is not heated externally and that there is no silicon substrate on it. We observe a rapid increase of the H-atom concentration with added O_2 up to 0.4%, followed by saturation.

Two, possibly complementary, mechanisms can be brought forward to explain the increase of H atoms when adding O_2 in small quantities (0–0.4%): (i) surface reactions: the oxygen atoms form a passivation layer on the reactor walls (fused silica), thereby reducing H-atom losses [15]; and (ii) volume reactions: oxygen atoms react in the plasma with methyl radicals (to form stable byproducts), preventing the methyl radicals to recombine with hydrogen atoms, hence increasing the steady-state concentration of the latter (a similar explanation has been given for the increase of the fluorine atom concentration when adding O_2 to CF_4 and SF_6 discharges [23,24]). It is noteworthy that this increase in H-atom concentration does not lead to an increase in film growth rate (recall Fig. 7), suggesting the existence of an additional factor controlling the growth process in the presence of O atoms.

Above 0.4% O_2, the H-atom concentration saturates while v decreases. To gain insight into this decrease of v, we refer to Howard et al. [25] who have demonstrated recently that atomic oxygen poisons the growing surface by forming strongly chemisorbed sites which become trapped in the growing film. The defective (non-diamond) carbon deposited above this trapped oxygen is thus etched more rapidly than diamond in subsequent cycles, slowing down the film growth process as O_2% is increased. An alternative interpretation calls on the fact that oxygen atoms are better etchants than hydrogen atoms not only for graphite but also for diamond, hence the observed decrease in the diamond growth rate. Clearly, both surface poisoning and diamond etching by oxygen atoms may combine to cause the observed decrease in the growth rate.

Another point is that this decrease of v occurs only above $\approx 0.4\%$ O_2, and not at lower percentages. We believe that, in going from 0 to $\approx 0.4\%$ O_2, the lowering of the growth rate by oxygen atoms is compensated by the favourable effect on film growth of increasing H-atom concentration. Above $\approx 0.4\%$ O_2, the mechanisms of poisoning and etching by oxygen atoms persist, while the H-atom concentration ceases to increase, giving the observed decrease of v.

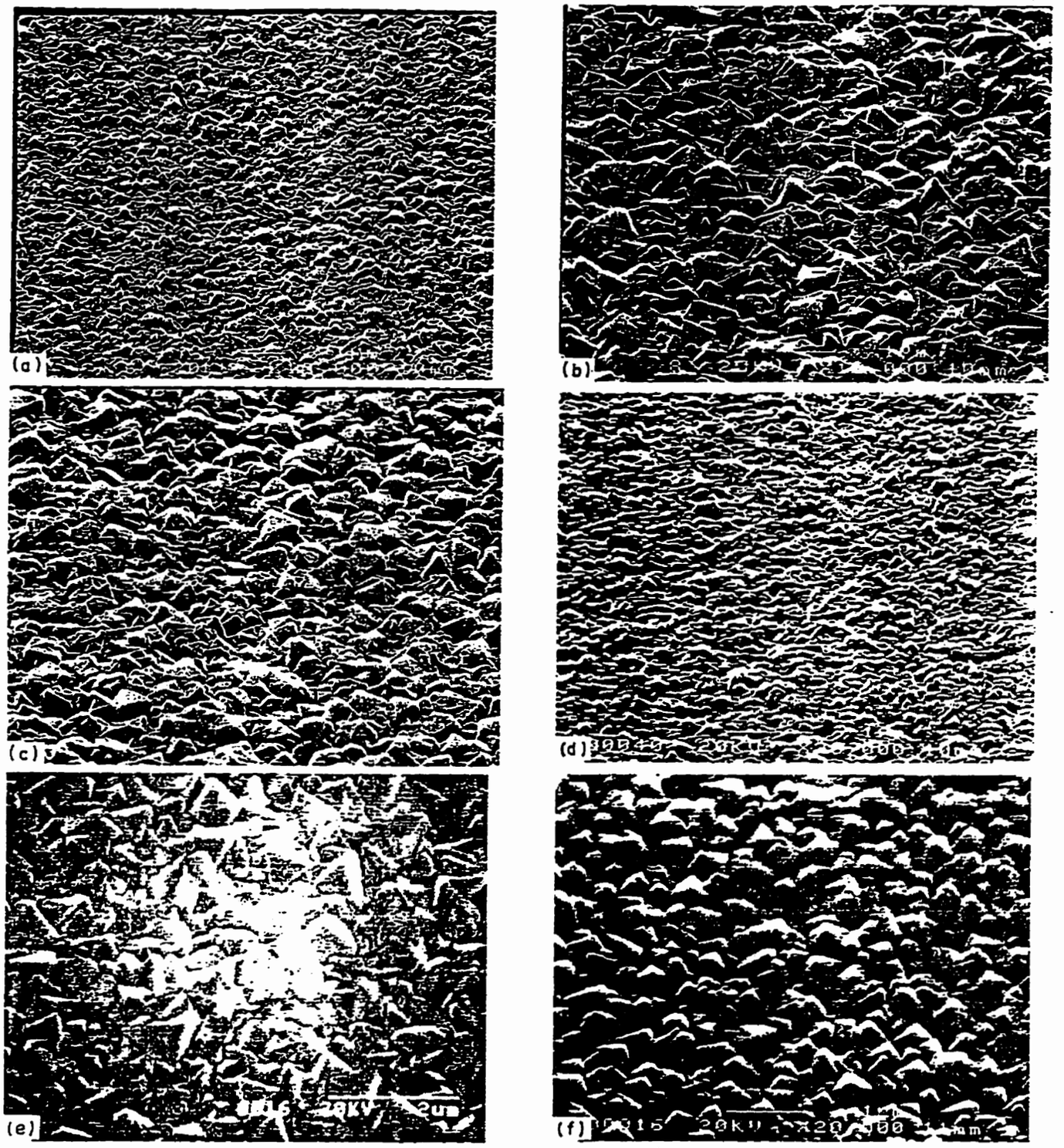

Fig. 5. SEM micrographs showing the film morphology at different O_2 concentrations. First set of data: deposition parameters as in Fig. 2 except for $d_{st} = 1.2$ cm, and with $CH_4\% = 0.75\%$: (a) 0.25% O_2, (b) 0.5%, and (c) 0.7%. Second set (P.C.) of deposition parameters: $p = 10$ Torr, $T_s = 950$ °C, $P_{mw} = 890$ W (59 W cm^{-3}), $d_{st} = 1.5$ cm, $CH_4\% = 0.5\%$: (d) 0.15%, (e) 0.5%, and (f) 0.7%.

3.3. The influence of substrate position

3.3.1. Film characterization

We have varied the position of the susceptor relatively to the plane where the discharge tube abruptly changes diameter (see Fig. 1(b)): at $d_{st} = 0$, the susceptor is well in the plasma source while at $d_{st} = 1.9$ cm, it barely touches the tip of the hemispherical plasma. Fig. 9 shows the dependence of the film growth rate upon d_{st}: the maximum growth rate occurs at a distance of approximately 1.2 cm from the transition under both operating conditions.

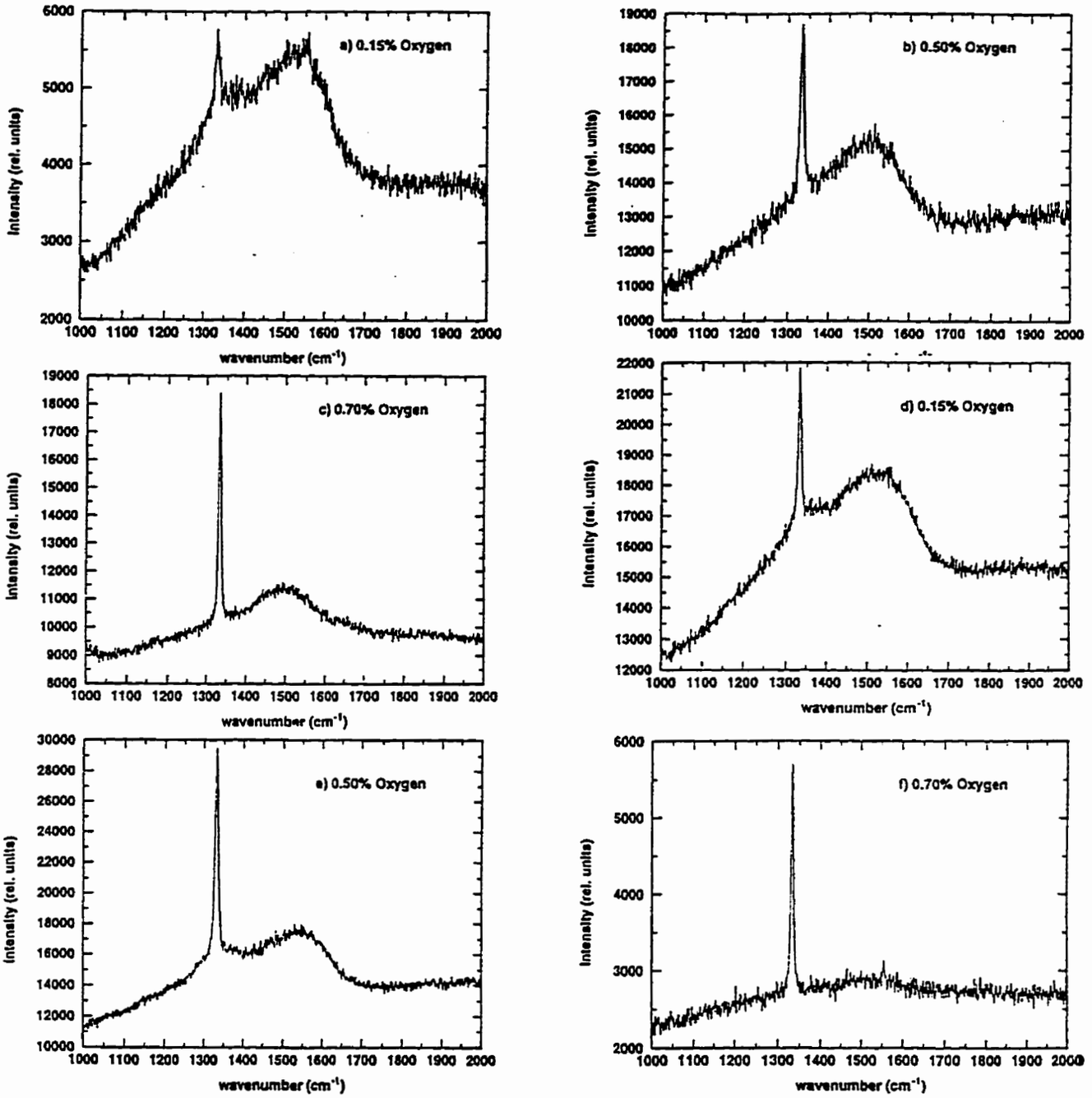

Fig. 6. Raman spectrum of the deposited films at different O_2 concentrations. First set of data ((a) 0.25%, (b) 0.5%, and (c) 0.7%) and second set (P.C.) of data ((d) 0.15%, (e) 0.5%, and (f) 0.7%) as in Fig. 5.

The substrate position also influences the diamond content of the film. The Raman spectra in Fig. 10 show that the position of the susceptor for the best film quality is slightly further away than for the optimum growth rate under both sets of operating conditions.

We have also observed that a susceptor too close to the tube transition, say $d_{st} = 0.4$ cm, leads to a poor film quality on the substrate edges; this could be related to the higher gas temperature on the substrate edges in this particular case[1], favouring non-diamond phases.. The micrograph in Fig. 11(a) ($d_{st} = 0.4$ cm) compared with Fig. 11(b) ($d_{st} = 1.9$ cm) shows larger grain sizes at $d_{st} = 0.4$ cm. Our investigations also show that Fig. 11(a) corresponds to a region of low nucleation density. In conclusion, moving the substrate from $d_{st} = 0.4$ cm to $d_{st} = 1.9$ cm improves both the

[1] When the susceptor is too close to the tube transition, $d_{st} \leq 0.4$ cm here, the plasma hemisphere cannot develop and the situation is akin to that of a classic surface-wave discharge, hence the radial non-uniformity [3].

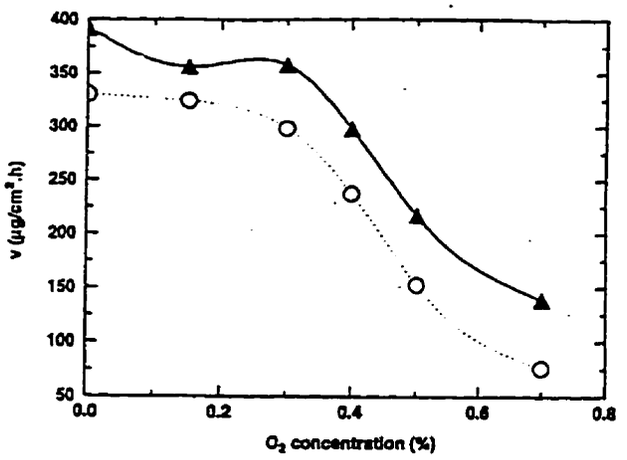

Fig. 7. Growth rate of the deposited film as a function of oxygen concentration. First set of data (full line) and second set (P.C.) of data (dotted line) as in Fig. 5.

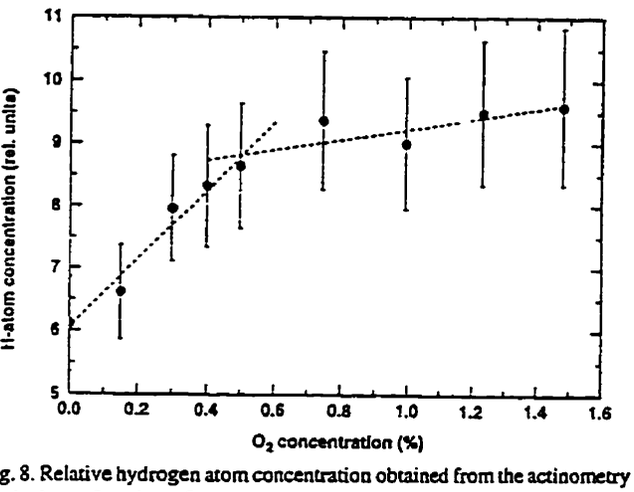

Fig. 8. Relative hydrogen atom concentration obtained from the actinometry method as a function of oxygen concentration, without external heating of the susceptor and in the absence of a Si substrate. The remaining operating parameters are the P.C. conditions in Figs. 5–7.

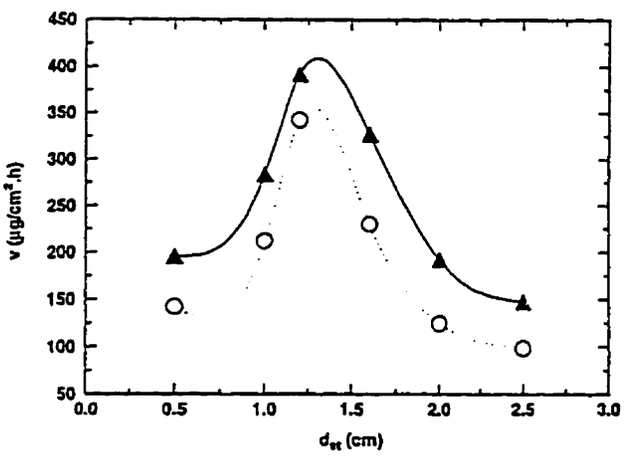

Fig. 9. Growth rate of the film as a function of the substrate position. Film characterization conditions (full line): $CH_4\% = 0.75\%$, $p = 15$ Torr, $T_s = 950$ °C, and $P_{mw} = 1.15$ kW (76 W cm^{-3}) and plasma characterization conditions (dotted line): $CH_4\% = 0.5\%$, $p = 10$ Torr, $T_s = 950$ °C, $P_{mw} = 930$ W (61 W cm^{-3}).

plasma and film uniformity, increases the diamond content in the film, increases the nucleation density, and reduces grain sizes. Further increasing d_{st} mainly results in a lower growth rate and lower diamond content.

3.3.2. Plasma characterization

Fig. 12 shows the diameter average H-atom concentration observed by actinometry, as a function of distance from the tube transition (i.e. by moving axially the optical fibre with respect to the tube transition) in the absence of a susceptor, for the same P.C. conditions as Fig. 9 and Fig. 10. The observed decrease of concentration when moving away from the transition is probably related to an axial decrease of electron density.

3.4. The influence of substrate temperature

3.4.1. Film characterization

These experiments were conducted at $p = 15$ Torr, $P_{mw} = 1.15$ kW (76 W cm^{-3}), and $d_{st} = 1.2$ cm for 0.5, 0.75, and 1.5% CH_4. We also considered P.C. conditions: $p = 10$ Torr, $P_{mw} = 890$ W, $d_{st} = 1.5$ cm, and 0.5% CH_4. In our reactor, in absence of external heating of the susceptor, the substrate is solely heated by the plasma and not by microwaves [3], in contrast with other types of reactor [26,27]. In practice, at power densities not exceeding 100 W cm^{-3} and for $p = 15$ Torr, filament heating of the susceptor enables us to vary the surface conditions independently from the plasma by setting T_s at any value from 600 to 1000 °C.

Fig. 13 shows that the growth rate reaches a maximum as a function of T_s at about 950 °C for CH_4 percentages ranging from 0.5% to 1.5%. This behaviour can be explained by the model proposed by Derjaguin and Fedoseev [28] in which diamond grows via chemisorbed hydrogen and by addition of carbon to the free surface. The pace of the data points in Fig. 13 actually reflects the competing effects of three mechanisms: the chemisorption of H, the desorption of H and H_2, and the incorporation of C in the lattice. The chemisorption of H decreases with T_s. Its desorption from the diamond surface is induced by a specific vibrational interaction between adsorbed hydrogen atoms and the diamond surface; it is predicted to be maximum between 900 °C and 1000 °C [28]; the net desorption rate results from a delicate balance between the chemisorption of H and the desorption of H and H_2. As for the incorporation of carbon in the lattice, the branching ratio between C and H incorporation is strongly temperature dependent because the thermal desorption of C (breaking a C–C bond) has a very much higher activation energy of about 83 kcal mol^{-1} than the incorporation reaction (H abstraction) of about 10 kcal mol^{-1}. Thus, at low substrate temperatures (< 900 °C), desorption of carbon is relatively slow and most of the carbon which adsorbs is eventually incorporated into the lattice, the drawback at low T_s being a low nucleation density, as shown later. At higher substrate temperatures (> 1000 °C), thermally activated desorption of carbon becomes increasingly important, reduc-

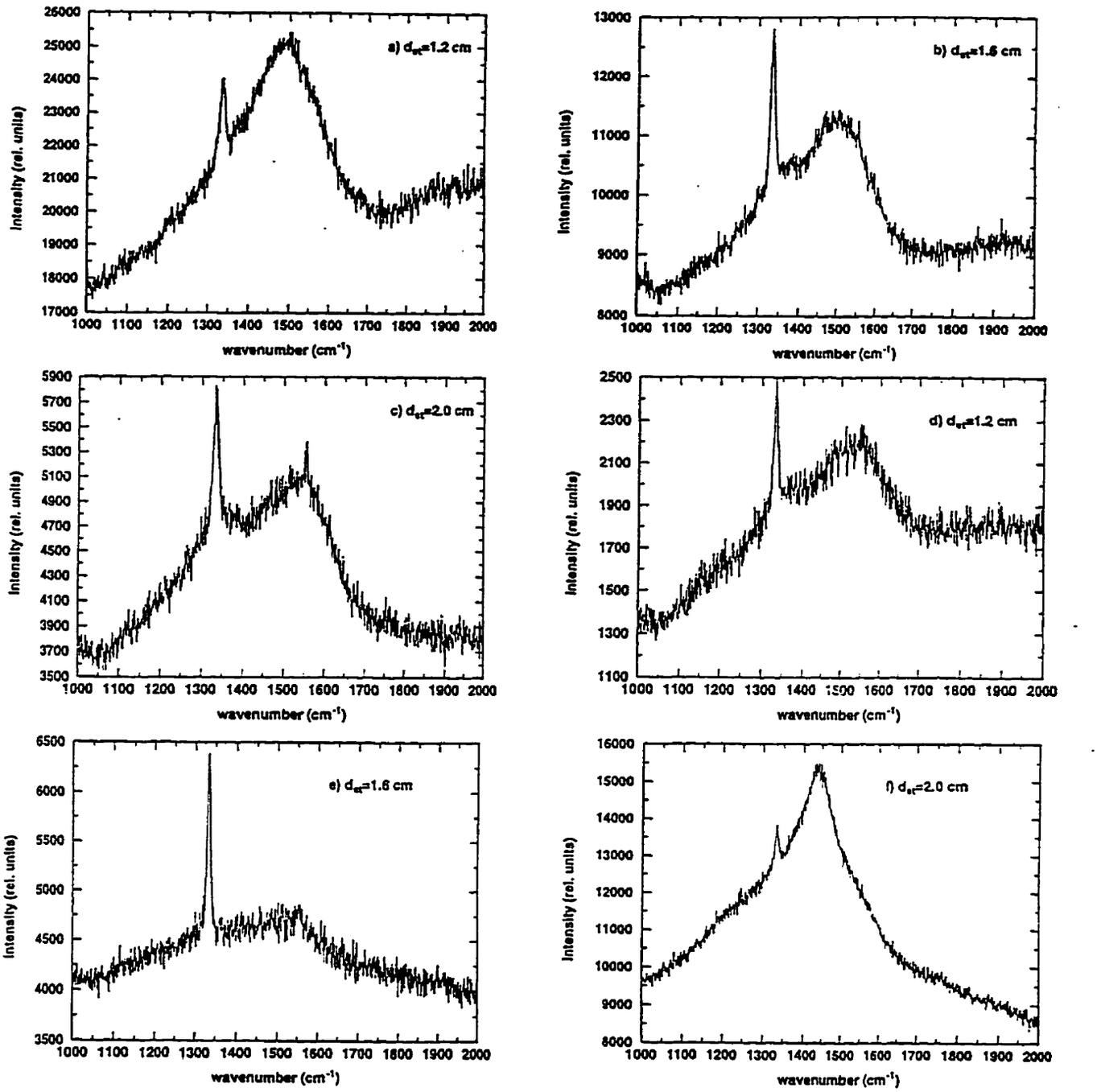

Fig. 10. Raman spectrum of the deposited films at various substrate positions; (a), (b) and (c): film characterization conditions, and (d), (e) and (f): plasma characterization conditions, as in Fig. 9.

ing the growth rate. Also, at temperatures above 1000 °C, the etch rate of diamond by atomic hydrogen increases while that of graphite decreases [29,30] thereby increasing the probability of graphite retention as a second phase component.

Besides growth rate, the nucleation density is also strongly related to the substrate temperature and local conditions of growth (e.g. substrate topography). Fig. 14 shows that the nucleation density goes through a maximum as a function of substrate temperature at approximately 900 °C for CH_4 percentages between 0.5 and 1.5% (same maximum under P.C. conditions). The existence of this maximum could result from a compromise between the thermodynamically favoured nucleation of crystals at temperatures higher than this maximum, and the increased desorption of precursors as T_s increases [31].

The particle size has also been measured at different substrate temperatures. Fig. 15 shows that the largest particle size is reached at 800 °C. The particle size is correlated with the film growth rate but also related to the critical radius for nucleation (the radius below which a crystal nucleus is not

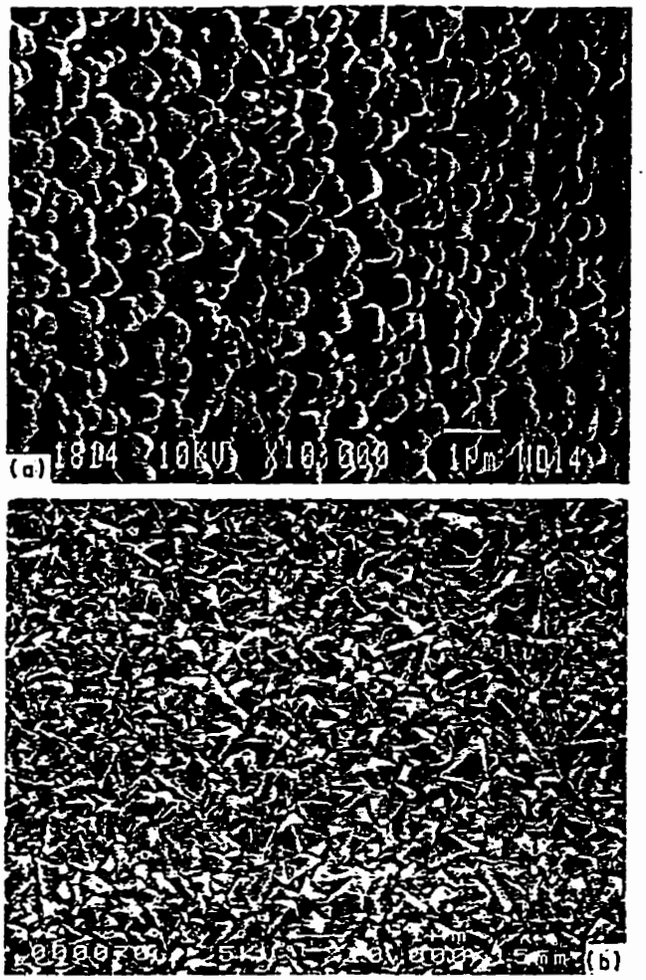

Fig. 11. SEM micrographs showing the film morphology for: (a) $d_{ss} = 0.4$ cm, and (b) $d_{ss} = 1.9$ cm. Remaining deposition parameters as in Fig. 9 (film characterization conditions).

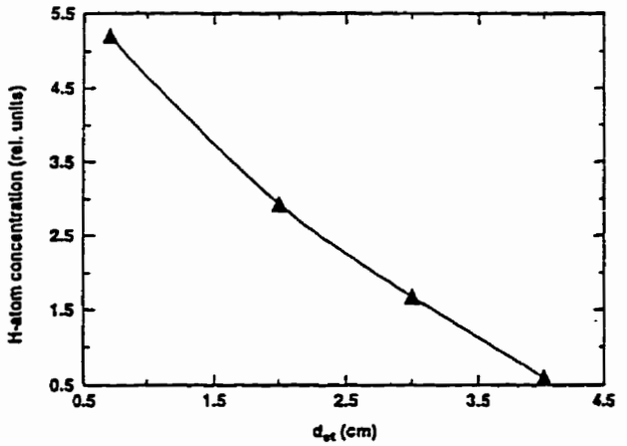

Fig. 12. Relative (diameter average) hydrogen atom concentration as a function of distance from the tube transition of the light-collecting fibre, in absence of susceptor. Remaining operating parameters as in Figs. 9 and 10 (plasma characterization conditions).

stable) [31]. This and possible differences in lateral and vertical growth rates could explain why T_s for the maximum

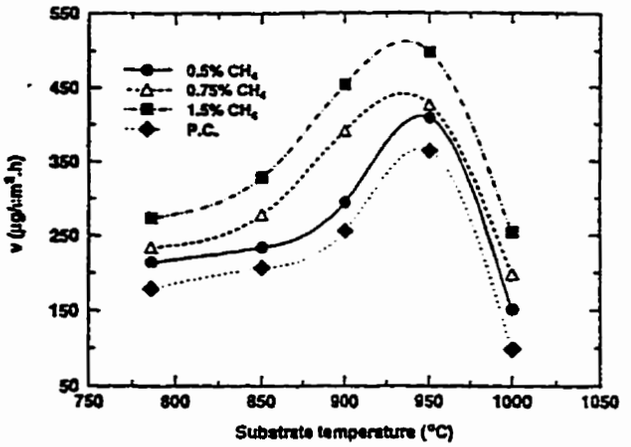

Fig. 13. Growth rate of the film as a function of substrate temperature at three CH_4 percentages. Remaining deposition parameters: $p = 15$ Torr, $P_{mw} = 1.15$ kW, and $d_{ss} = 1.2$ cm. The P.C. conditions (dotted line) are: $p = 10$ Torr, $P_{mw} = 890$ W, $d_{ss} = 1.5$ cm, and 0.5% CH_4.

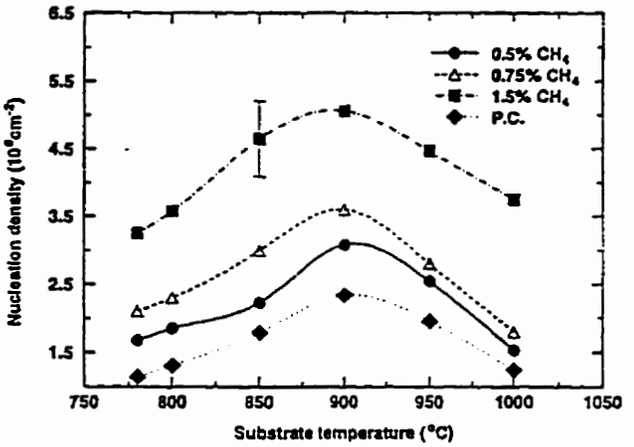

Fig. 14. Nucleation density of diamond crystals as a function of substrate temperature at three CH_4 percentages, with $p = 15$ Torr, $P_{mw} = 1.15$ kW, and $d_{ss} = 1.2$ cm. P.C. conditions: $p = 10$ Torr, $P_{mw} = 890$ W, $d_{ss} = 1.5$ cm, and 0.5% CH_4.

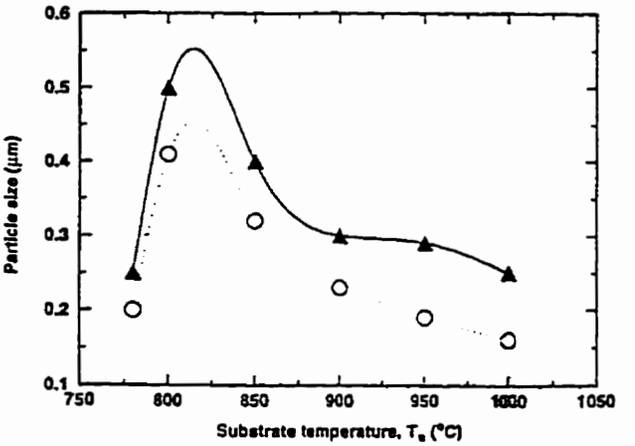

Fig. 15. Particle size of the diamond crystals as a function of the substrate temperature. Operating conditions as in Fig. 14.

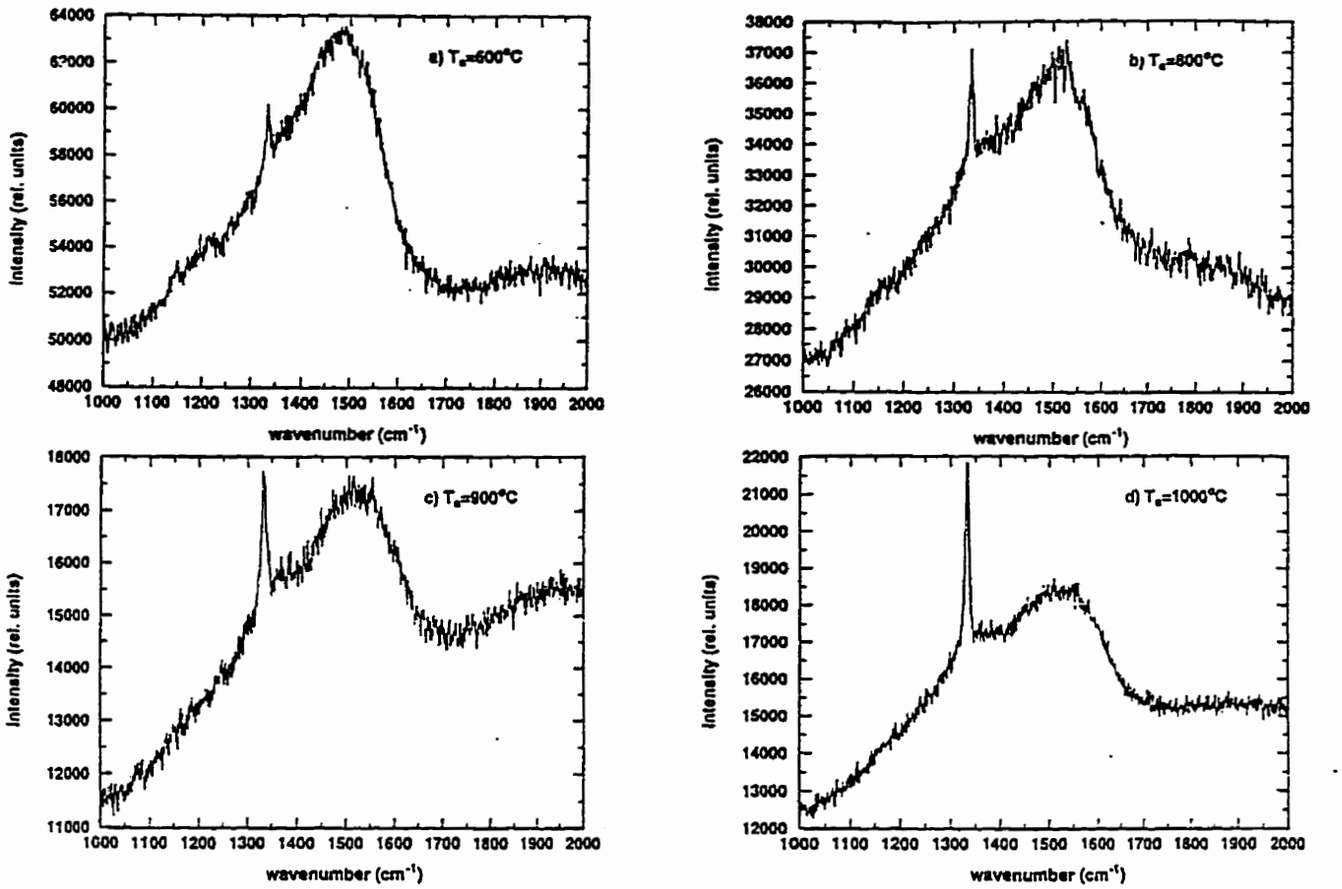

Fig. 16. Raman spectrum of the deposited films at various substrate temperatures. Remaining deposition parameters similar to those for film characterization in Fig. 14, with 0.75% CH_4.

particle size is lower than for the maximum growth rate (Fig. 13).

The Raman spectra in Fig. 16 show that the broad non-diamond Raman peak at 1500–1600 cm^{-1} as well as the luminescence background decrease relative to the diamond peak at 1332 cm^{-1} when increasing the substrate temperature, the deposition conditions being the same as above with 0.75% CH_4. This suggests an increasing degree of diamond content in the film with increasing substrate temperature.

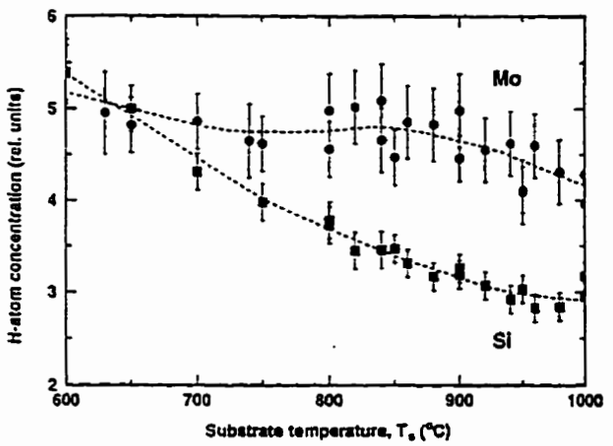

Fig. 17. Relative hydrogen atom concentration as a function of substrate temperature 1 mm above the susceptor, for two different substrate materials (Mo, Si). Remaining P.C. parameters: $CH_4\% = 0$, $p = 10$ Torr, $P_{mw} = 890$ W, and $d_{st} = 1.5$ cm.

3.4.2. *Plasma characterization*

It seems quite unlikely that varying the substrate temperature induces substantial changes in the EEDF, and thus the actinometry method is used confidently in this case. We have measured I_H/I_{Ar} as a function of the substrate temperature approximately 1 mm above the molybdenum susceptor, with and without the silicon substrate on it. The experimental conditions were the following: $CH_4\% = 0$, $p = 10$ Torr, $P_{mw} = 890$ W, and $d_{st} = 1.5$ cm. These values are close to typical deposition conditions, except for methane. The absence of methane prevents diamond deposition and thus enables one to study without interference the interaction between hydrogen atoms and a given surface material as a function of the surface temperature. Such conditions correspond to the very initial moments of diamond deposition, before any diamond is formed. Fig. 17 shows that, for both materials (Mo and Si), there is a decrease of H-atom concentration as T_s is increased, and that the hydrogen atom concentration is more strongly reduced in the presence of the Si surface.

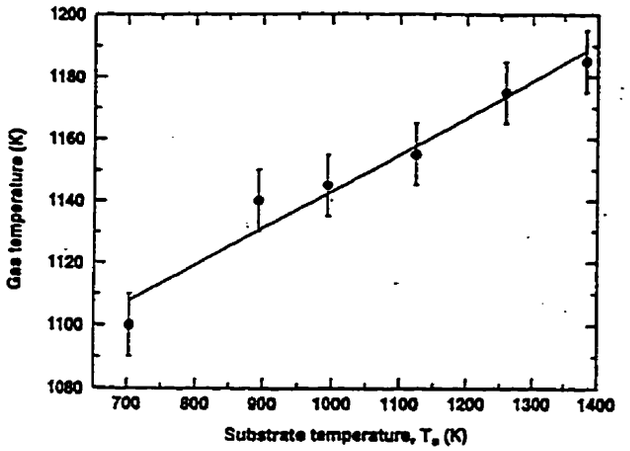

Fig. 18. Rotational temperature of H_2 G state (construed as the gas temperature) as a function of the susceptor temperature (as monitored 5 mm above the Mo susceptor). Other parameters: $CH_4\% = 0$, $p = 10$ Torr, $P_{mw} = 890$ W, and $d_{st} = 2$ cm.

The substrate temperature is believed to influence the lateral surface mobility of adsorbed hydrogen atoms in such a way as to favour their recombination into H_2 as T_s is increased, but it could also promote the formation and desorption of volatile etching products such as SiH_4; in general, the lateral surface mobility of atoms increases linearly with the surface temperature [31]. The results in Fig. 17 suggest that, prior to diamond nucleation, etching reactions take place on Si substrates which, on the one hand, decrease the volume concentration of H atoms and, on the other hand, alter the surface, creating surface defects as confirmed by our SEM observations. The general picture is thus that H recombination occurs on both Mo and Si, but perhaps faster on Si, and that etching reactions most probably take place on Si but not on Mo.

We have further measured the gas temperature 5 mm above the bare Mo susceptor, with $CH_4\% = 0$, $p = 10$ Torr, $P_{mw} = 890$ W, and $d_{st} = 2$ cm. The results are shown in Fig. 18. The rotational temperature (from the G → B system) of H_2, here construed as the gas temperature T_g, is seen to

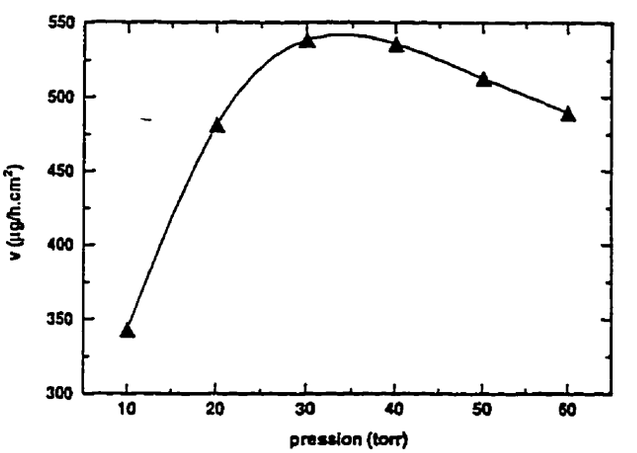

Fig. 19. Growth rate of the film as a function of gas pressure. Remaining deposition parameters: $CH_4\% = 0.75\%$, $T_s = 950$ °C and $P_{mw} = 1.15$ kW.

increase monotonically (in fact, almost linearly) with increasing T_s: the fact that the gas at approximately 5 mm above the substrate tends to be in thermal equilibrium with the surface is not a surprise. Gicquel et al. [4], using a bell-jar reactor, had shown before that there exists an approximately 15 mm thick boundary layer above the substrate across which a large gas temperature gradient prevails. Beyond this layer, T_g is that of the plasma "bulk" and approximately independent of T_s, actually depending on gas pressure and absorbed microwave power. The inverse action of heat transfer, i.e. from the plasma to the susceptor, had been examined earlier for the present reactor: T_s was seen to increase with increasing gas pressure and absorbed microwave power [3].

3.5. The influence of gas pressure

3.5.1. Film characterization

Fig. 19 shows that the growth rate of the deposited films depends strongly on the total gas pressure, going through a maximum near 30 Torr. Gas pressure also influences the diamond content of the film but, as indicated by the Raman spectra in Fig. 20, this is not as sensitive to pressure as to the other parameters examined above.

The influence of p as an external parameter is complex. For instance, although we know for sure that the electron temperature (or average electron energy) decreases with p, determining the concentration of the various species in the plasma is not straightforward. Nonetheless, relying on this decrease of electron temperature with p, one expects the electronic dissociation yield per molecule of the feed gas as well as the ionization rate to decrease with p. In other respects, at the same time, the reservoir of molecules (H_2 and CH_4) available for electron impact increases. In addition, thermal dissociation (as opposed to electron impact dissociation) increases with p because of an increasing gas temperature (see further on). Then considering all these mechanisms, one can conclude that there is a possibility for an optimal pressure for which the concentrations of atoms, radicals, and ions needed for diamond deposition yield a maximum growth rate (Fig. 19). A further problem with investigating p as an external parameter comes from the decrease of the plasma volume with p: the radius of the plasma hemisphere decreases and its tip retracts with respect to the susceptor as pressure is increased. Because of this, d_{st} has to be adjusted so that the plasma hemisphere always touches or covers the substrate in the same way.

3.5.2. Plasma characterization

Fig. 21 shows that the gas temperature T_g increases with pressure (recall that T_g is deduced from the rotational temperature of the G → B system of H_2). In this case, we set d_{st} at 2 cm in such a way that at the lowest pressure considered, the plasma was barely touching the susceptor, and then retracting away from it with increasing p. The optical fibre was positioned 5 mm below the tube transition, hence T_g represents here the gas temperature in the plasma bulk.

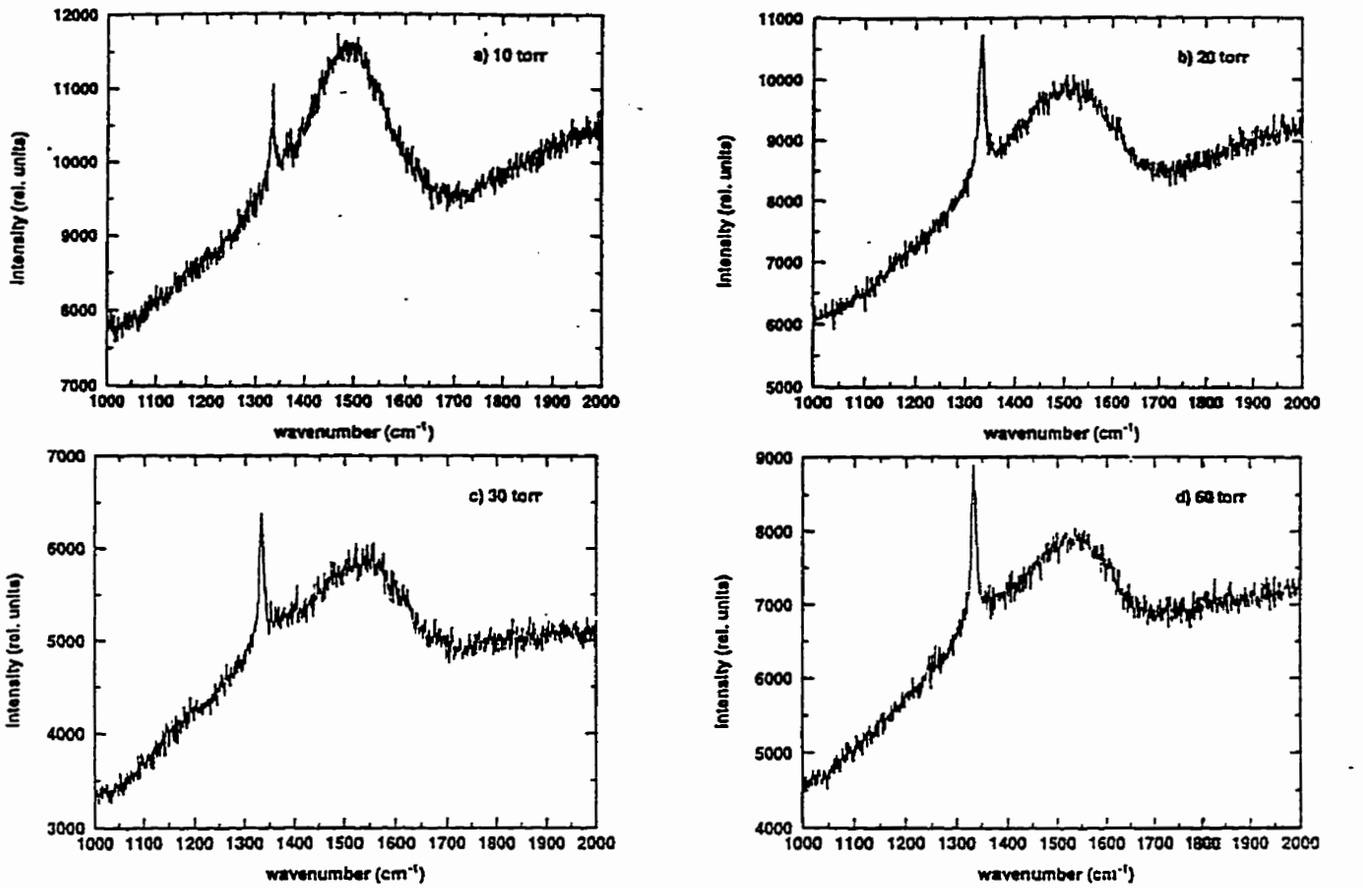

Fig. 20. Raman spectrum of the deposited films at various gas pressures. Remaining deposition parameters as in Fig. 19.

The increase in Fig. 21 can be traced back to an increase in electron density n_e, based on results from a tubular H_2 discharge sustained with surface waves. It was demonstrated in that case that T_g and n_e are related by the empirical relation

$$T_g = 7.4 \times 10^{-10} n_e + 420 \quad (1)$$

where n_e is expressed in cm^{-3} and T_g in K [7]. This expression holds irrespective of the way n_e is varied (pressure, microwave power or field frequency); it was validated for p between 0.4 and 2 Torr, and field frequencies between 40 and 2450 MHz [7]; we are assuming that it remains valid, at least qualitatively, up to 25 Torr. It means that increasing the power density in the plasma, which increases n_e, increases T_g (see Section 3.6).

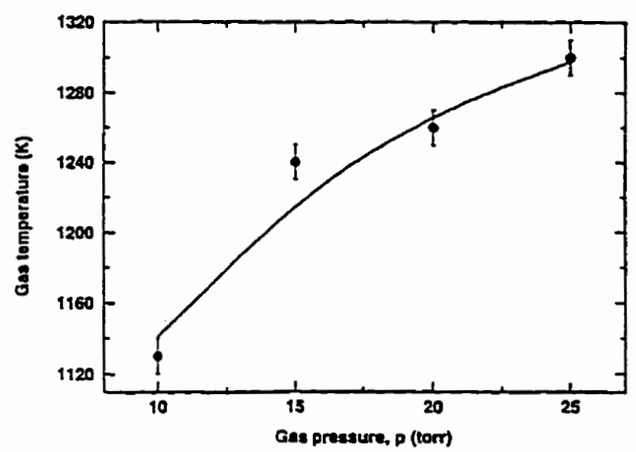

Fig. 21. Gas temperature at 15 mm above the susceptor (without external heating) as a function of gas pressure. Remaining P.C. parameters: $CH_4\% = 0$, $P_{mw} = 890$ W, and $d_g = 2$ cm.

We can extrapolate the results of Fig. 21 to higher pressures; one should thus expect $T_g > 1300$ K at $p > 25$ Torr: high gas temperatures (typically, $T_g > 1500$ K [7,32]) are required to obtain non-negligible thermal dissociation of the feed gas. The main impact from increasing T_g upon diamond deposition in this reactor should thus be an increase of the thermal dissociation rates in the plasma bulk, and an increased heating of the wall of the (fused silica) discharge tube. This latter effect leads to a greater loss of H atoms [7], since the efficiency of heterogeneous recombination of H atoms increases (almost exponentially) with the surface temperature [33]. The cooling system described in Fig. 1(a) considerably reduces these losses.

3.6. The influence of the microwave power

3.6.1. Film characterization

When the microwave power is raised from 600 W to 1200 W, the substrate temperature being maintained by external heating at a fixed value of 900 °C, the most important effect

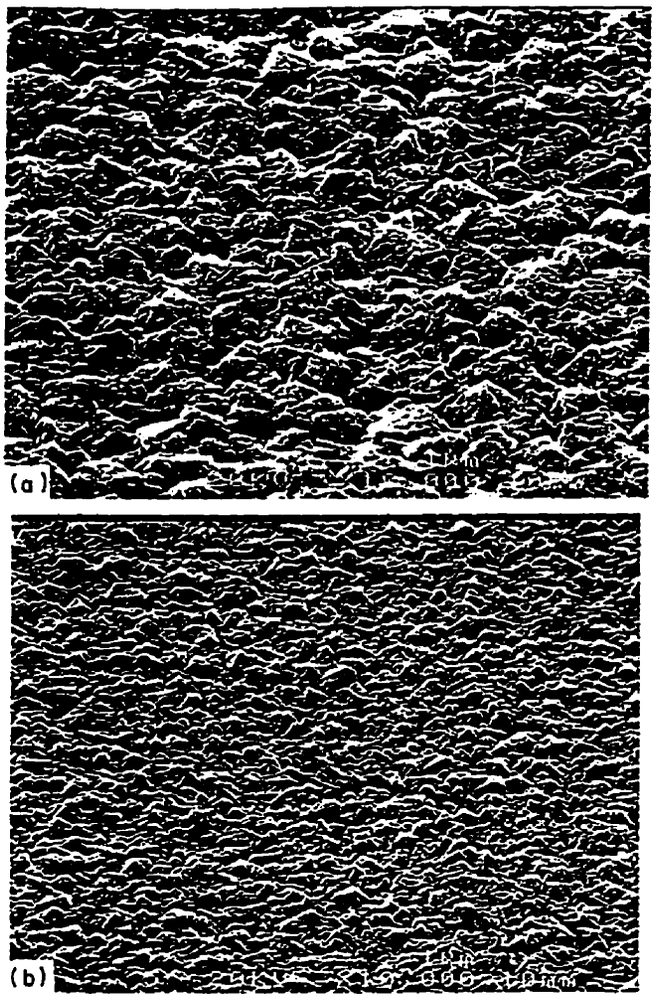

Fig. 22. SEM micrographs showing the film morphology for P_{mw} of: (a) 630 W (41 W cm^{-3}) and (b) 1.15 kW (76 W cm^{-3}). Remaining deposition parameters: $CH_4\% = 0.75\%$, $p = 15$ Torr, $T_s = 950$ °C, and $d_{st} = 1.2$ cm.

observed is the increase of the growth rate, attributable to an increase in electron density (recall Eq. (1)) and thus in the number of reactive radicals and ions. For instance, in a feed consisting of 0.75% CH_4, with $p = 15$ Torr, $T_s = 950$ °C, $d_{st} = 1.2$ cm and $P_{mw} = 630$ W (41 W cm^{-3}), the growth rate is ≈ 240 μg cm^{-2} h^{-1} while, with $P_{mw} = 1150$ W (76 W cm^{-3}), under the same conditions, it increases to ≈ 360 μg cm^{-2} h^{-1}. The fact that the growth rate does not increase linearly with P_{mw} implies that n_e does not grow linearly with P_{mw}. This could come from the volume recombination of charged particles: this recombination rate is proportional to n_e^2 (the diameter of the plasma hemisphere increases only very slightly with P_{mw} and we consider this effect on n_e to be negligible).

Fig. 22 shows the SEM micrographs at 630 and 1150 W. They show that, apart from increasing the film growth rate, increasing the microwave power density absorbed in the plasma reduces the film grain size and roughness. This may be explained by: (i) assuming a greater probability for the renucleation of diamond at higher power density, which results in a lower film roughness [34]; (ii) a higher ion flux on the substrate at higher P_{mw}; ions are accelerated through the boundary layer because of the very large gradient of electric field intensity across it [35].

3.7. The influence of wall temperature

As already pointed out, the heterogeneous losses of H atoms on the discharge tube walls depend strongly on the wall temperature [33]. Externally cooling the discharge tube with compressed air or using a cooling jacket of dimethyl polysiloxane (DMPS), a low-loss dielectric liquid, increases notably the concentration of H atoms in the plasma, as shown by St-Onge and Moisan [7] using actinometry. Rousseau et al. found similar results when cooling a surface-wave reactor with compressed air [36]. In the present reactor, much higher power densities are used and the cooling jacket is further required to prevent the fused silica tube from melting. DMPS was found to be efficient for that purpose. Varying the coolant flow rate varies the wall temperature; such an experiment provides a direct access to the role of H atoms in diamond deposition. We found that the main impact of cooling the discharge tube, and thus independently increasing the H-atom concentration, was to increase the film growth rate; the film quality was comparable in all cases.

4. Summary and conclusion

We have characterized a new type of microwave plasma reactor for diamond deposition. Based on a novel configuration of surface-wave discharges, it produces a hemispherical plasma facing the susceptor. Although this reactor has some similarities with plasma-ball reactors, its specific features required an independent characterization. This objective has been achieved through a parametric study of the main process parameters for diamond deposition, namely CH_4 concentration, addition of O_2, position of the substrate with respect to the plasma source, substrate temperature, gas pressure and microwave power. We have examined the influence of these parameters on the main film characteristics (quality of the film, growth rate, nucleation density and particle size), and on two plasma properties, the H-atom concentration and the gas temperature. We have found that the conditions optimizing both maximum growth rate and film quality correspond to a total gas pressure of 15 Torr, with a 0.75% CH_4 content and a substrate temperature of 930 °C. Diamond films with well-faceted crystals and with minimal defects have been obtained over broader operating conditions, at gas pressures between 10 and 60 Torr, with a 0.25–0.75% CH_4 content, and with substrate temperature in the range 870–980 °C. Finally, we anticipate that uniform films of larger area could be achieved with a larger tube diameter; this has already been verified with a reactor tube 1.5 times larger than the present one.

Acknowledgements

The authors would like to express their gratitude to Professor L. Martinu for commenting on the manuscript, and to F. Roy, R. Lemay, R. Martel and J.E. Samuel for their skilled technical assistance. We are endebted to Georges Villeneuve and EDRL-Énergie et mines du Canada for providing the SEM photos. One of the authors (CFMB) is grateful to CNPq (Brasil) for his fellowship. This work has been achieved thanks to the France–Québec scientific cooperation program (Projet 02-58-02-91).

References

[1] P. Bou, *Thèse de doctorat*, Université d'Orléans, 1991.
[2] D.M. Tung, W.L. Hsu and K.F. McCarty, in J.P. Dismukes (ed.), *Proc. 1st Int. Symp. on Diamond and Diamond Like Films*, Electrochem. Soc., 1989.
[3] C.F.M. Borges, M. Moisan and A. Gicquel, *Diamond Relat. Mater.*, *4* (1995) 149.
[4] A. Gicquel, C. Héau, D. Fabre and J. Perrière, *Diamond Relat. Mater.*, *1* (1992) 776.
[5] T. Anthony, in R. Freer (ed.), *The Physics and Chemistry of Carbides, Nitrides, and Borides*, Kluwer, Dordrecht, 1990, pp. 133–158.
[6] M. Moisan and Z. Zakrzewski, *J. Phys. D: Appl. Phys.*, *24* (1991) 1091.
[7] L. St-Onge and M. Moisan, *Plasma Chem. Plasma Process.*, *14* (1994) 87.
[8] H.N. Chu, E.A. Den Hartog, A.R. Lefkow, J. Jacobs, L.W., Anderson, M.G. Lagally and J.E. Lawler, *Phys. Rev. A*, *44* (1991) 3796.
[9] A. Gicquel, unpublished results.
[10] H.M. Crosswhite, *The Hydrogen Molecule Wavelength Tables of G.H. Dieke*, Wiley–Interscience, New York, 1972.
[11] R. Meilunas, M.S. Wong, K.C. Sheng and P.H. Chang, *Appl. Phys. Lett.*, *54* (1989) 2204.
[12] P. Bou, L. Vandelbulcke and R. Herbin, *Diamond Relat. Mater.*, *1* (1992) 933.
[13] K. Kobashi, K. Nishimura, Y. Kawate and T. Horiuchi, *Phys. Rev. B*, *38* (1988) 4067.
[14] A. Inspektor, Y. Liou, T. McKenna and R. Messier, *Surf. Coat. Technol.*, *39* (1989) 211.
[15] J.A. Mucha, D.L. Flamm and D.E. Ibbotson, *J. Appl. Phys.*, *65* (1989) 3448.
[16] W.L. Hsu, *Appl. Phys. Lett.*, *59* (1991) 1427.
[17] L. Schäfer, U. Bringmann, C.P. Klages, U. Meier and K. Kohse-Höinghaus, *NATO-ASI Ser. B: Phys.*, *266* (1991) 643–651.
[18] F.G. Celii, P. Pehrsson, H.T. Wang and J.E. Butler, *Appl. Phys. Lett.*, *52* (1988) 2043.
[19] P. Bou, J.C. Boettner and L. Vandelbulcke, *Jpn. J. Appl. Phys.*, *31* (1992) 1505.
[20] P. Bou, J.C. Boettner and L. Vandelbulcke, *Jpn. J. Appl. Phys.*, *31* (1992) 2931.
[21] D.G. Goodwin and G.G. Gavillet, *J. Appl. Phys.*, *68* (1990) 6393.
[22] A. Gicquel, C. Heau, D. Fabre and J. Perrière, *Diamond Relat. Mater.* *1* (1992) 776.
[23] C.J. Mogab, A.C. Adams and D.L. Flamm, *J. Appl. Phys.*, *49* (1978) 3796.
[24] R. d'Agostino, F. Cramarossa, S. De Benedictis, F. Fracassi, L. Láska and K. Mašek, *Plasma Chem. Plasma Process.*, *5* (1985) 239.
[25] W.N. Howard, K.E. Spear and M. Frenklach, *Appl. Phys. Lett.*, *63* (1993) 2641.
[26] P.K. Bachmann, W. Drawl, D. Knight, R. Weimer and R. Messier, in G. Johnson, A. Badzian and M. Geis (eds.), *Extended Abstracts*, Materials Research Society, Pittsburgh, PA, 1988, p. 99.
[27] J.P. Dismukes and K.R. Walton, in J.P. Dismukes (ed.), *Proc. 1st Int. Symp. on Diamond and Diamond Like Films*, Electrochem. Soc., 1989.
[28] B.V. Derjaguin and D.V. Fedoseev, *Growth of Diamond from the Gas Phase*, Nauka, Moskow, 1977 (in Russian).
[29] W.L. Hsu, *J. Vac. Sci. Technol. A*, *6* (1988) 1803.
[30] B.V. Spitsyn and L.L. Bouilov, in G. Johnson, A. Badzian and M. Geis (eds.), *Extended Abstracts*, Materials Research Society, Pittsburgh, PA, 1988, p. 12.
[31] M. Ohring, *The Materials Science of Thin Films*, Academic Press, New York, 1992.
[32] A. Gicquel, K. Hassouni, S. Farhat, Y. Breton, C.D. Scott, M. Lefebvre and M. Pealat, *Diamond Relat. Mater.*, *3* (1994) 581.
[33] B.J. Wood and H. Wise, *J. Chem. Phys.*, *66* (1962) 1049.
[34] E. Anger, *Thèse de doctorat*, Université Paris-XIII, 1994.
[35] L. Paquin, D. Masson, M.R. Wertheimer and M. Moisan, *Can. J. Phys.*, *6* (1985) 831.
[36] A. Rousseau, A. Granier, G. Gousset and P. Leprince, *J. Phys. D: Appl. Phys.*, *27* (1994) 1412.

CHAPITRE 4

Silicon contamination of diamond films deposited on Si substrates in silica based reactor

C. F. M. Borges, S. Schelz, L. St-Onge, M. Moisan, and L. Martinu

Publié dans J. Appl. Phys.
Reçu: 15 septembre 1995; Accepté: 3 december 1995

Silicon contamination of diamond films deposited on silicon substrates in fused silica based reactors

C. F. M. Borges
Groupe de physique des plasmas, Université de Montréal, C.P. 6128, Succursale Centre-ville, Montréal H3C 3J7, Québec, Canada

S. Schelz
Département de génie physique, École Polytechnique, Montréal H3C 3A7, Québec, Canada

L. St.-Onge and M. Moisan[a)]
Groupe de physique des plasmas, Université de Montréal, C.P. 6128, Succursale Centre-ville, Montréal H3C 3J7, Québec, Canada

L. Martinu
Département de génie physique, École Polytechnique, Montréal H3C 3A7, Québec, Canada

(Received 15 September 1995; accepted for publication 3 December 1995)

Deposition of thin diamond films on silicon (Si) substrates and in a reactor with fused silica walls can lead to the incorporation of Si impurities. In the present work, impurities in the bulk of the films were analyzed quantitatively using complementary diagnostic techniques (elastic recoil detection, electron microprobe analysis and secondary ion mass spectrometry), while surface analysis was achieved with x-ray photoelectron spectroscopy. The Si contamination level in the bulk reaches up to 0.16 at. %. We show that the presence of Si impurities correlates with the fluorescence background that accompanies the 1332 cm^{-1} diamond peak in the Raman spectra. Experiments were performed to distinguish between the Si originating from the wall and from the Si substrate. The effect of O_2 added to the process gases is also investigated. The diamond films were prepared in a recently developed plasma reactor using a novel configuration of surface-wave-sustained discharge: the reactor operation is akin to that of the well-known plasma-ball systems. © *1996 American Institute of Physics.* [S0021-8979(96)09205-1]

I. INTRODUCTION

The interest in diamond films is spreading to various scientific and industrial fields because of their excellent intrinsic properties:[1–3] diamond is the hardest known material[3] and it combines broadband optical transparency, high thermal conductivity and chemical inertness; when *n* or *p* doped, it is a good candidate as a wide band-gap semiconductor material.[1,2]

The nucleation and growth processes involved in chemical vapor deposition (CVD) of diamond films are strongly affected by the initial surface characteristics of the substrate. It is well known that pretreatment of the substrate is required to enhance diamond nucleation necessary to obtain a continuous film of high quality. This aspect of diamond CVD has already received much attention because of its influence on the morphology and crystal quality of the films.

Crystalline silicon is an ideal substrate for fundamental studies of polycrystalline diamond film CVD. In particular, its lattice constant is similar to that of diamond, which favors heteroepitaxial growth. However, diamond nucleation occurs readily on these surfaces only along scratches or sharp fracture edges. Furthermore, long exposure times are required before the bare silicon (Si) surface transforms into SiC, which seems to be a necessary step before diamond crystals start growing.[4,5] This suggests that depositing a SiC layer directly onto Si should enhance the formation of diamond nuclei. It appears that the surface condition of the substrate is qualitatively changed provided the deposited SiC film is at least 200 nm thick.[6]

In all deposition systems, the growing diamond films can be contaminated by species originating from the reactor walls or from the gas phase, which may adversely affect the materials characteristics. In the present work, we systematically investigate the level and origin of silicon impurity in diamond films deposited on Si substrates under various operating conditions, and we correlate it with broadband luminescence observed in the Raman spectra.

II. EXPERIMENT

We have examined diamond films grown following two different surface modifications of the (100) silicon substrate:

(i) deposition of a 200-nm-thick SiC film prepared by laser ablation[6] and
(ii) pretreatment by an abrasive powder (about 20–40 μm in diameter) in an ultrasonic methanol bath for 60 min, followed by cleaning with methanol.

Diamond deposition was carried out using a novel configuration of surface-wave-sustained discharge,[7] operated at 2450 MHz, as shown in Fig. 1(a). Details concerning this experimental arrangement were described elsewhere.[7] After introducing the substrate into the reactor, the system was pumped down to a base pressure of 2×10^{-6} Torr (2.7×10^{-4} Pa). The substrate temperature, monitored by an optical pyrometer, was raised to 950 °C using external heating

a)Electronic mail: moisan@ere.umontreal.ca

 0021-8979/96/79(6)/3290/9/$10.00

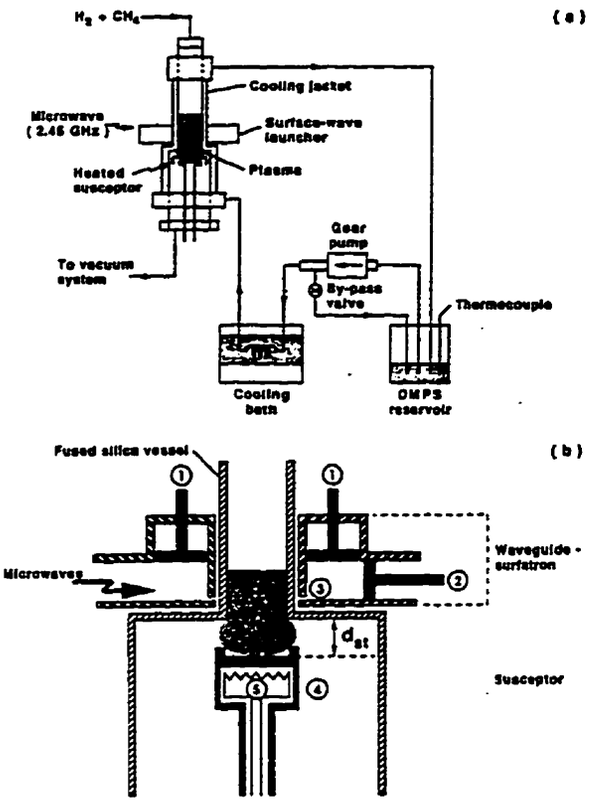

FIG. 1. (a) Schematic illustration of the surface-wave microwave plasma reactor including the discharge tube cooling system using dimethyl polysiloxane (DMPS); (b) details of the surface-wave plasma source and relative location of the susceptor (cooling jacket not represented). The numbers refer to: 1-coaxial tuning stub and 2-waveguide tuning stub in the waveguide-surfatron launcher;[7] 3-launching gap; 4-molybdenum casing; 5-tungsten filament. The distance d_{st} is adjustable (Ref. 12).

of the molybdenum susceptor [Fig. 1(b)]. The gases were premixed before entering the discharge tube, and the total flow rate was fixed at 100 standard cubic centimeters per minute (sccm); in most experiments, the methane concentration (CH_4%) in hydrogen was constant at 0.5%. The working gas pressure p, determined by a capacitance manometer, was 10 Torr (1.33 kPa).

After a deposition time of 2 h, which yields an approximately 1-μm-thick film, the samples are examined with a scanning electron microscope (SEM), Jeol model JSM-6300F, and the quality of the deposits was evaluated by Raman spectroscopy. Raman measurements were performed in a backscattering configuration, using a double beam-monochromator and the 488 nm line from an argon laser (100 mW power).

Optical emission spectroscopy (OES) was used to diagnose the plasma. The emitted light was collected by an optical fiber (2 mm i.d.), pointing perpendicularly to the discharge tube axis without further collimation and positioned about 1 mm above the sample susceptor. The optical fiber was connected to a 1 m focal-length spectrometer. For actinometry measurements, argon was introduced at a fixed flow rate of 3 sccm. We monitored the intensity of the Ar I 750.4 nm line and of the 434.0 nm Balmer H_γ line. Their intensity ratio I_H/I_{Ar} is a probe of the relative H-atom concentration. The specific limitations of the actinometry method when applied to atomic hydrogen in a H_2 discharge are discussed, for example, in Ref. 8.

The elemental composition of the films was analyzed by several methods. The elastic recoil detection (ERD) used at Université de Montréal has already been described in Refs. 9 and 10. In this technique, atoms of the constituent elements are ejected from the sample in the forward direction by an energetic heavy ion beam (30 MeV, $^{35}Cl^{5+}$). Silicon surface-barrier detectors record the number of recoiled atoms and their energy spectra, which are related to the atomic concentration and to the depth respectively. A time-of-flight detection system is used for mass discrimination of the recoil atoms.

Secondary ion mass spectrometry (SIMS) depth profiles of the elemental (atomic) composition of the diamond films were obtained using a 10 keV Cs^+-ion sputtering beam and detecting negative secondary ions. In this technique, molecular ions may share the same nominal mass with elemental ions; for example, $^{12}C^{18}O$ can interfere with the ^{30}Si signal. Therefore, the molecular contributions were preferentially removed by analyzing secondary ion populations of higher energy, extrapolating the data to infinite sputtering velocity (infinite velocity method).[11]

The electron microprobe analyses (EMA) were carried out in a Jeol JSM 840 SEM. In this technique, an electron beam (10 keV, 60 mA in source) impinges on the surface of the sample at glancing angle, below the critical angle for total external reflection, and it induces fluorescence from atoms in the top several monolayers of the sample. The fluorescence x-rays are then analyzed by an energy dispersive spectrometer.

The x-ray photoelectron spectra (XPS) were recorded with a VG ESCALAB MkII spectrometer. The deposited films were exposed to air before being placed in the ultrahigh vacuum system. The XPS measurements were performed with a non-monochromatized MgK_α source ($h\nu$=1253.6 eV) and with a spectrometer pass energy of 20 eV resulting in an energy resolution of about 0.8 eV. The energy calibration of the core levels was performed with a gold reference sample, setting the Au $4f_{7/2}$ binding energy at 84.0 eV. Some of the recorded spectra were energy-shifted in order to compensate for the charging effects.

III. RESULTS AND DISCUSSION

A. Concentration of atomic hydrogen

Prior to the film characterization, we have determined the gas-phase hydrogen concentration as it is the most pertinent plasma property in the present case.

The (relative) H-atom concentration [H] was measured as a function of the substrate temperature T_s approximately 1 mm above the silicon sample, which was either bare or covered with a SiC layer. For comparison, we have also made these measurements in the absence of any substrate on the molybdenum susceptor. The experimental conditions were the following: pure hydrogen (no CH_4 added) at p=10 Torr, microwave power P_{mw}=890 W, and distance from the susceptor to the transition in tube diameter [see Fig. 1(b)]

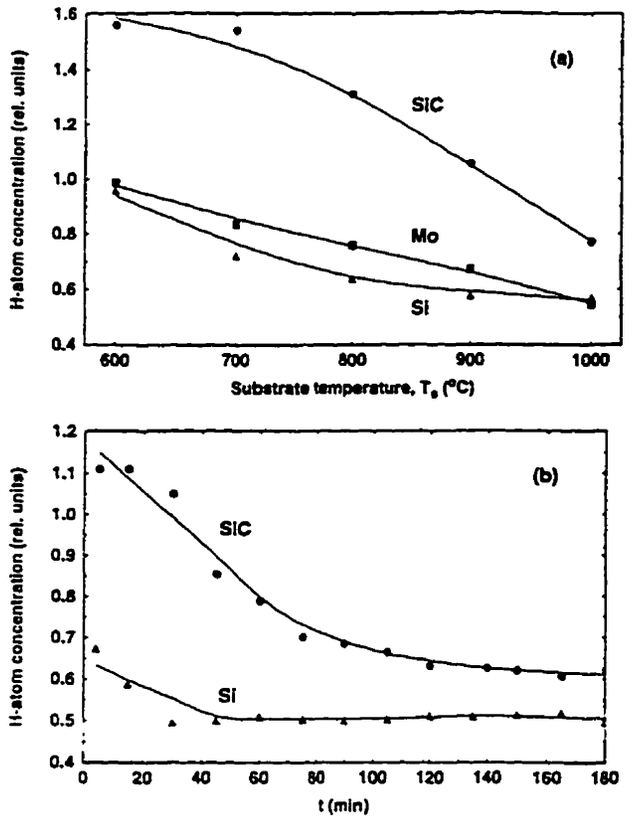

FIG. 2. Relative H-atom concentration at approximately one mm above the susceptor: (a) as a function of substrate temperature (Si, SiC, and Mo) in the absence of CH_4; (b) as a function of time during diamond deposition onto bare or SiC-coated Si substrate. Deposition conditions: T_s=800 °C, p=10 Torr, CH_4% =0.75%, P_{mw}=890 W, and d_{st}=1.5 cm.

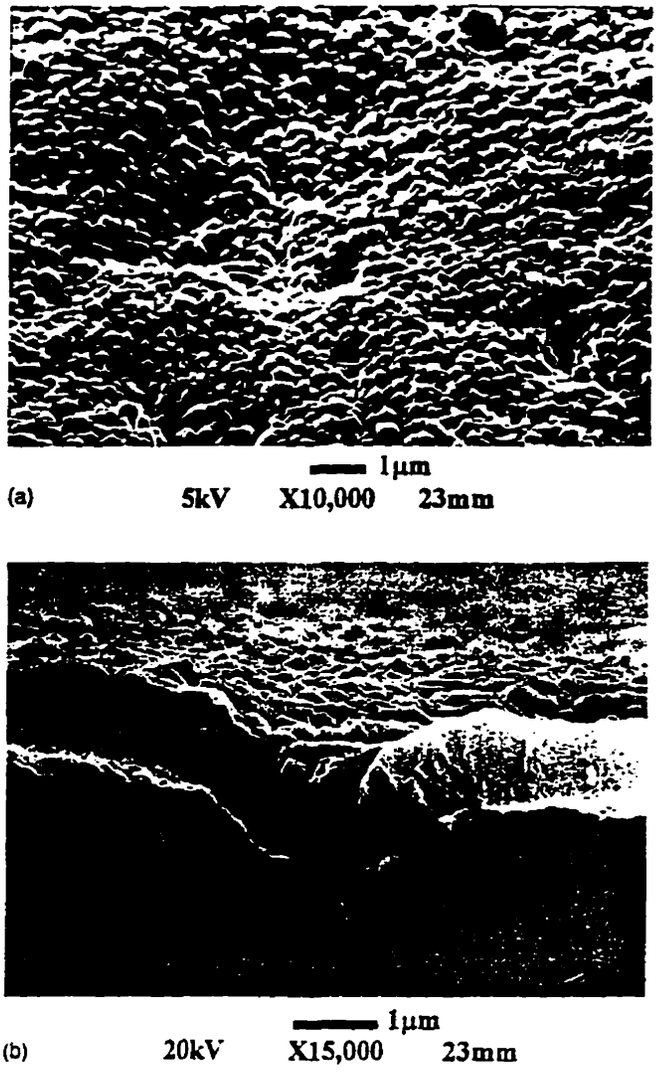

FIG. 3. SEM micrographs showing the presence of surface defects on a diamond-covered Si substrate: (a) top view of the surface; (b) cross-section view.

d_{st}=1.5 cm. This represents typical diamond film deposition conditions, except for the absence of methane. It enables one to study, without the interference of diamond growth, the interaction between hydrogen atoms and a given material as a function of its surface temperature. Such conditions correspond in reality to the initial moments before any diamond is deposited.

Figure 2(a) shows that the [H] values systematically decrease with rising T_s for all materials (Si, SiC, or Mo). This general behavior has been pointed out in our previous publication,[12] and was explained in terms of an increase in the lateral surface mobility of adsorbed H atoms which favors their recombination into H_2. The results in Fig. 2(a) also suggest that the probability of H-atom surface recombination varies with the material; this effect can also be interpreted as H atoms reacting with a surface to form volatile products at a rate that depends on the nature of the surface.

It has been suggested earlier[13] that H atoms are responsible for surface defects on diamond-covered Si substrates due to their etching action on such substrates in the instants preceding diamond nucleation. Figure 3 is a SEM micrograph showing clearly that such defects reflect in the film topography. Therefore, etching reactions may at least in part account for the increased H-atom depletion occurring when T_s is increased, as shown in Fig. 2(a).

Figure 2(b) shows the concentration of H atoms during the whole deposition process (3 h). The deposition conditions were: T_s=800 °C, p=10 Torr, CH_4% =0.75%, P_{mw}=890 W, and d_{st}=1.5 cm. In the first instants, the [H] values are significantly higher above the SiC surface compared to bare Si, as already shown in Fig. 2(a), but this difference reduces considerably as the diamond film grows and eventually covers the surface. Assuming that [H] stabilizes only after a complete coverage of the substrate by diamond, one can infer from Fig. 2(b) that a continuous film forms faster (≈30 min) on bare Si than on a SiC layer (≈90 min). This interpretation contradicts the idea[4,5] that predepositing SiC on Si substrates facilitates diamond growth as mentioned in the introduction. The fact that the growth rate v of diamond on SiC-coated Si substrates (v=0.53 $\mu g\,h^{-1}$) is lower than for bare Si (v=0.74 μgh^{-1}) confirms our interpretation of Fig. 2(b).

B. Film characterization

The elemental composition and the impurity levels of four different diamond films about 1 μm thick were investi-

TABLE I. Pretreatment and deposition conditions for samples 1, 2, 3, and 4 (CH_4%=0.50%, p=10 Torr, T_s=950 °C).

Sample	Pretreatment	$\%O_2$	$\%H_2$
1	powder	0	99.50
2	powder	0.4	99.10
3	SiC film	0	99.50
4	SiC film	0.25	99.25

TABLE II. ERD-TOF atomic concentration in the bulk of diamond films from Table I.

Sample	Carbon (at. %)	Hydrogen (at. %)	Oxygen (at. %)	Silicon (at. %)
1	98.61	1.22	0.01	0.16
2	99.53	0.44	0.01	0.01
3	97.82	2.11	0.01	0.06
4	99.18	0.57	0.239	0.02

gated by ERD-TOF, SIMS and EMA. Two of the layers were deposited on prescratched Si and two on SiC-coated Si. The deposition conditions of these samples are listed in Table I. The following are the results of the elemental analysis and compositions of these films.

1. ERD-TOF depth profile analysis

Figures 4(a)–4(d) display depth profiles of the atomic concentrations of all elements detected by this method. The profiles are different from each other, and the concentration values in the film bulk are summarized in Table II.

For sample 1 (silicon substrate pretreated with diamond powder), the silicon impurity level is approximately constant over the probed depth [Fig. 4(a)]. The oxygen impurities in this film are at the detection limit of this technique. In sample 2 (prescratched Si as for sample 1, but with O_2 added throughout the growth), very low amounts of both silicon and oxygen impurities were detected [Fig. 4(b)]. For sample 3 (Si with 200 nm SiC), the silicon concentration in the bulk [Fig. 4(c)] is lower than in sample 1, but notably higher than in sample 2. Finally, sample 4 [Fig. 4(d)] shows that for a SiC-coated Si substrate the addition of oxygen to the process gases results in a strong increase of Si impurities in the interfacial region, at a depth of approximately 0.3 μm.

2. Secondary ion mass spectrometry

Figures 5(a)–5(d) show the SIMS depth profiles of samples 1 to 4 from Table I, respectively. These results agree with those obtained by ERD-TOF (Sec. III B 1). In sample 1, we observe a contamination by Si impurities over the whole probed depth, whereas in sample 2 such contamination is absent. Again, as with the ERD method, the concentration of

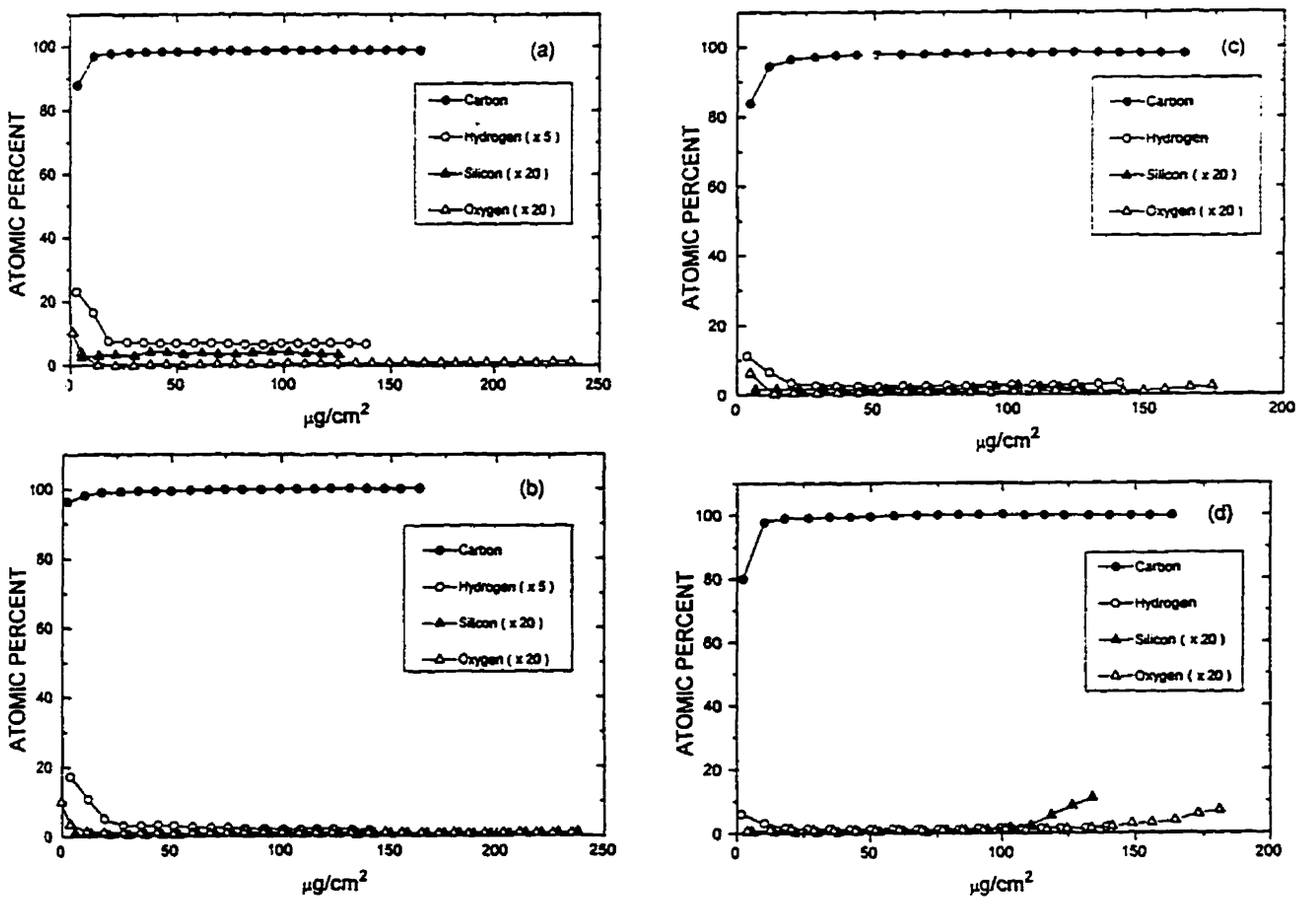

FIG. 4. Atomic concentration depth profiles measured by the ERD-TOF method for the samples from Table I. The profile starts from the surface (left), and reaches down to about 0.6 μm for oxygen.

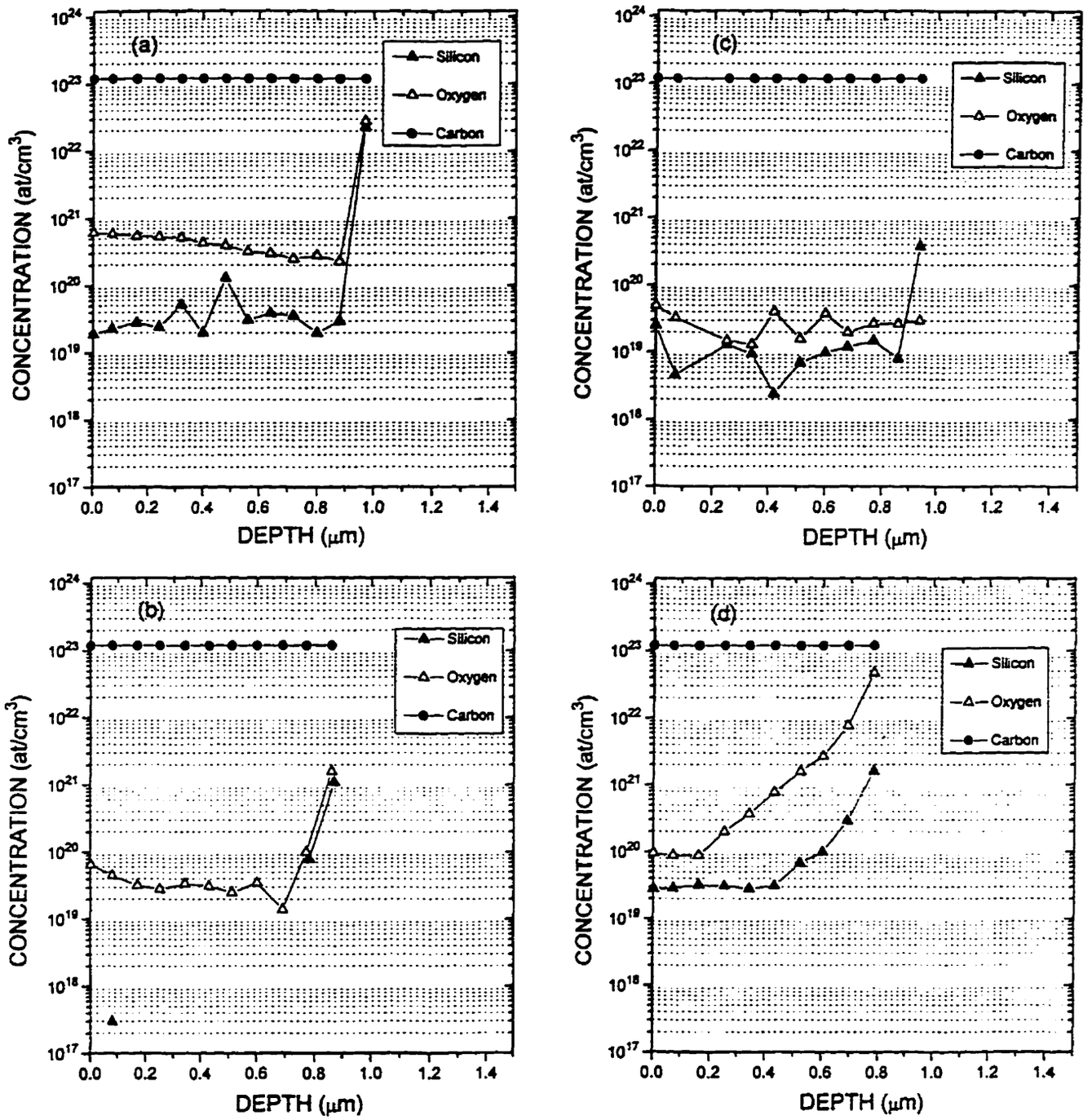

FIG. 5. SIMS depth profiles of samples 1–4 from Table I.

Si impurities in sample 3 is lower than in sample 1. The Si concentration is approximately constant throughout samples 1, 2, and 3, but it strongly increases with depth for sample 4.

3. Electron microprobe analysis

Figures 6(a)–6(d) show the results of EMA analysis of samples 1 to 4 from Table I, respectively. This analysis correlates well with the SIMS and ERD-TOF results described above. For example, no Si was identified in sample 2 by any of these three methods while Si is present in the case of samples 1, 3, and 4. It should be mentioned, however, that the EMA technique is comparatively more surface-sensitive, and it rather provides an average composition close to the surface.

4. General discussion

The results obtained from the above three diagnostic techniques can be explained by considering the origin and inclusion mechanisms of Si into the diamond films. The Si impurities arise partly from the walls of the reactor and partly from the Si substrate. Si originating from the substrate is believed to be incorporated into the diamond film first as a

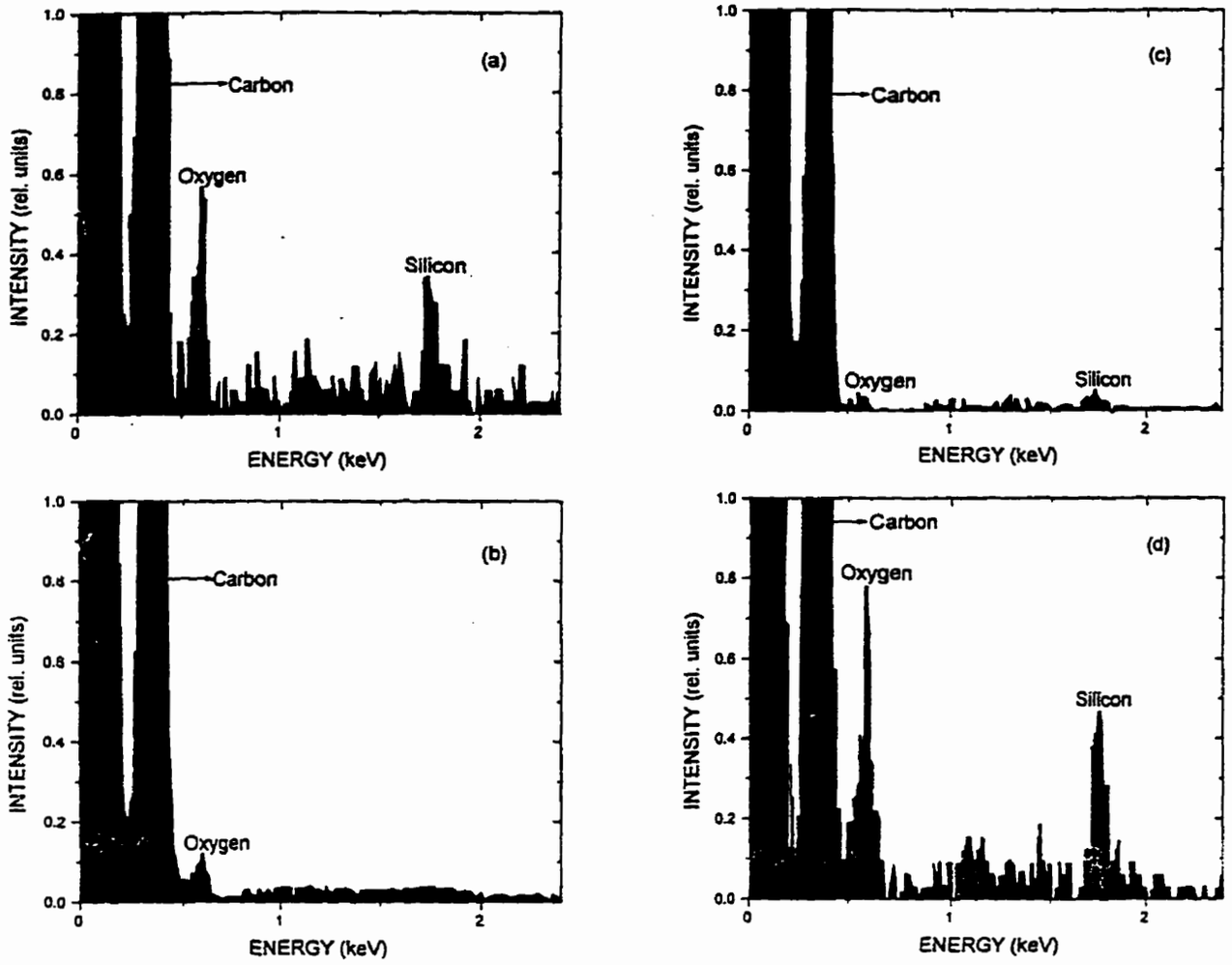

FIG. 6. EMA analysis of samples 1–4 from Table I. The lowest energy peak is the peak calibration of the detector.

result of H-atom etching reactions with the exposed substrate, and then by diffusion through the growing film. The former mechanism is well established; it is responsible for the surface topographic irregularities revealed in Fig. 3: the bumps on the film surface reflect a strong initial etching effect of Si by the hydrogen/methane plasma.

When comparing the four samples from Table I, the Si impurity level in sample 1 can be inferred to originate both from the reactor wall and etching of the substrate. Because of the high T_s value, the Si atoms can diffuse through the film during the deposition process.[13]

The beneficial effect of adding oxygen to the H_2/CH_4 gas mixture is clearly demonstrated in sample 2. Oxygen is believed to passivate the fused silica wall with respect to its etching by H atoms, thus decreasing the formation of SiH_x ($0 \leq x \leq 4$) species which can transport Si toward the substrate surface.[14,15] OES recording of Si lines in $H_2/CH_4/O_2$ plasmas confirms a total quenching of this emission when 0.5% O_2 is added.[14] Oxygen can also be considered as a diamond nucleation activator for the following two reasons:

(i) it enhances the concentration of H atoms in the gas phase by suppressing heterogeneous recombination to H_2 on the silica walls; this enables one to raise the methane concentration and hence the deposition rate while maintaining the same diamond quality as that obtained at a lower methane concentration in the absence of O_2[15] and

(ii) it suppresses Si superficial contamination (because of wall passivation) which could introduce a delay in the nucleation process.[15]

The effect of SiC intermediate layers on the Si impurity level in the diamond films is clarified by studying samples 3 and 4. The silicon concentration in sample 3 is low, because it originates only from the reactor wall; the possible diffusion effect from the substrate itself into the diamond film is efficiently suppressed by SiC which acts as a diffusion barrier. Adding oxygen to the process gas (sample 4) in this case prevents Si contribution from the discharge tube wall (recall sample 2), but it also results in a strong reaction of O atoms with the SiC layer, producing CO or CO_2 gases.[16–18] The Si atoms liberated from the SiC surface can react with H atoms to form SiH_x ($0 \leq x \leq 4$) species. These species may be responsible for the transport of silicon into the growing diamond film.

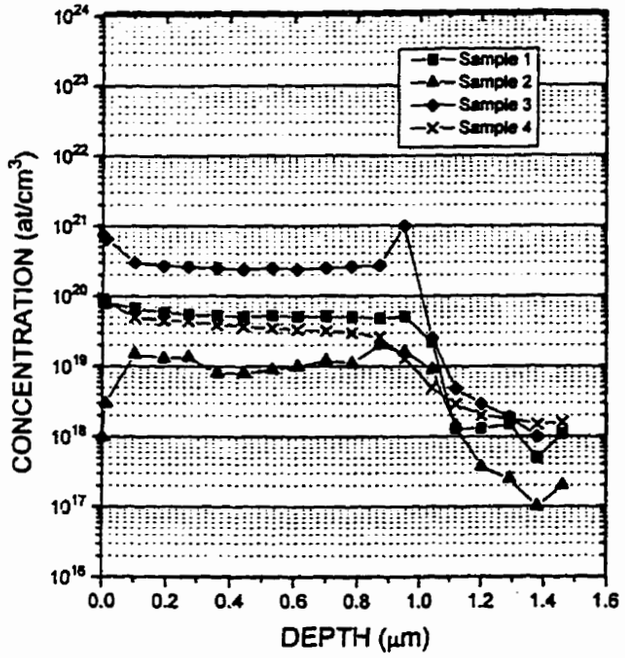

FIG. 7. SIMS depth profile of hydrogen for samples 1–4 from Table I.

Figure 7 shows the SIMS depth profile of the hydrogen atom signal for samples 1 to 4. The intensity of the carbon signal is 1000 times larger than that of hydrogen, but the shape of its depth profile is nearly the same as that of H atoms, in agreement with the ERD data. This result supports the idea that hydrogen is predominantly bonded to carbon. Similar results have also been observed by Terranova *et al.*[19]

Figures 8(a)–8(d) show Raman spectra for samples 1 to 4, respectively. We observe the presence of a broadband luminescence background signal in samples 1, 3 and 4, which contain a relatively high amount of Si impurities. These spectra contrast with the spectrum of sample 2 where the background intensity around the diamond peak is negligible and flat; in this case, the diamond film was deposited directly on the prescratched Si with the contribution of oxygen in the process gases. Since the level of Si impurities is the lowest in sample 2 and is the largest in sample 4, we conclude that the higher the concentration of Si impurities, the higher the observed broadband luminescence. Considering Table II, we see that the variations of the other impurity contents do not correlate with the variation in the background fluorescence.

We have observed that the density of secondary nucleation and the presence of ball-like structures are higher in the

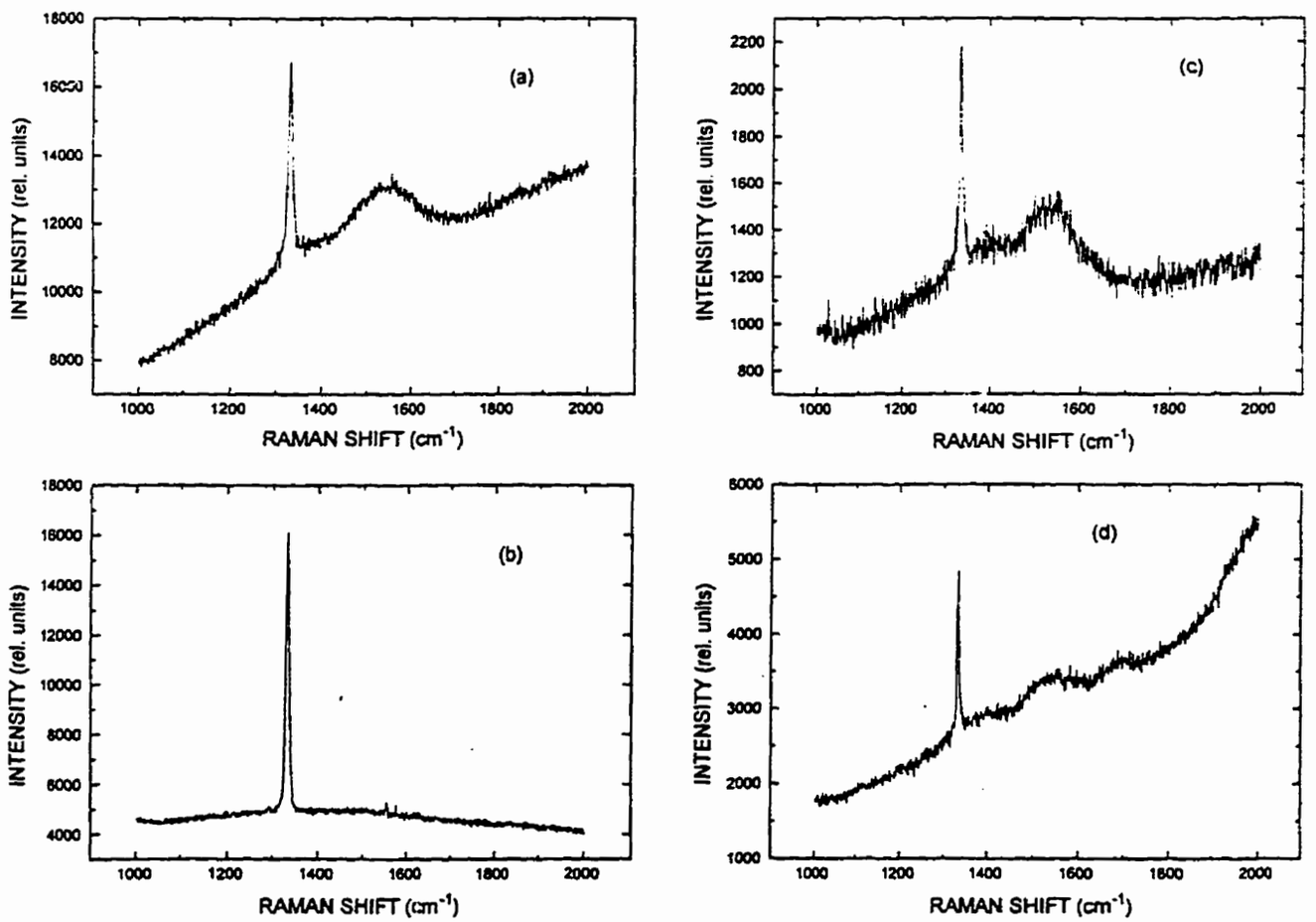

FIG. 8. Raman spectra for samples 1–4 from Table I.

TABLE III. Surface elemental composition, as obtained by XPS, of diamond samples deposited with O_2 concentration in the working gas of 0, 0.2, 0.3, 0.4, and 0.5% (from A to E).

Sample	Carbon (at. %)	Oxygen (at. %)	Silicon (at. %)	Oxygen/Silicon
A	90.4	6.5	3.1	2.1
B	89.9	6.3	3.8	1.7
C	89.0	7.0	4.0	1.7
D	88.6	7.2	4.2	1.7
E	87.9	8.4	3.7	2.3

samples that contain a high concentration of Si impurities. Koichi *et al.*[20] have noted similar results when adding a small concentration of silane during the diamond deposition, showing that increasing the silane concentration increases the density of secondary nucleation.

5. XPS analysis and further discussion

In addition to the depth profile analysis presented above, we have performed XPS measurements to determine Si and oxygen impurities at the film surface (~5 nm probing depth). Table III shows the surface elemental composition for five samples which were deposited at O_2 concentrations in the gas phase of 0, 0.2, 0.3, 0.4, and 0.5%. These samples were obtained in the same deposition conditions as for the depth profile analysis, with the powder pretreatment. The oxygen contamination on the various deposited film surfaces ranges from 6.3 to 8.4 at.%, while the silicon concentration lies between 3.2 and 4.2 at. %. Measurements at different locations on the same sample, say 1 cm apart from each other, show that these impurities are not homogeneously distributed (±2 at. %) over the film surface. Nevertheless, the oxygen to silicon concentration ratio does remain approximately constant.

Determination of the energy positions of chemical bonds can be affected by electron emission from the insulating diamond films due to electrostatic charging. Resulting energy shifts of approximately 0.1 to 0.6 eV have been observed and compensated for by shifting the whole spectrum, setting the reference energy of the C1*s* peak at 284.7 eV, a characteristic value for diamond.[21,22] The corresponding binding energies of the observed Si2*p* and O1s core levels amount to 102.3±0.1 eV and 532.3±0.1 eV, respectively.

Comparing the binding energy values observed above with data from the literature, we cannot distinguish confidently between pure silicon and some SiO phase.[23–25] The full width at half maximum (FWHM) of the recorded energy for Si2*p* and O1*s* core levels is found to be 1.7±0.1 eV and 1.9±0.1 eV, respectively. These rather low FWHM values and the fact that the core level shapes are quite symmetric lead us to believe that the observed silicon and oxygen elements are bound in one single phase. There are then at least two possibilities:

(i) a SiO phase; this would lead to a Si2*p* binding energy close to 102.1 eV with a corresponding O1*s* binding energy of 532.1 eV, and a binding energy difference between these two core levels of 430.0 eV, and

(ii) a silicon oxycarbide phase.

To discriminate between these two phases, we have prepared $Si_xO_yC_z$ phases with different Si:O:C ratios by sputtering a SiC target with an oxygen-argon gas mixture under a variable oxygen content.[26] Nonetheless, the predicted C1*s* contribution of the silicon oxycarbide phase could not be distinguished from the main C1*s* diamond peak contribution.

The concentration ratio of the oxygen and silicon impurities in Table III shows that the stoichiometry ratio of O to Si is closer to 2 than to unity, favoring assumption (ii). However these values may have been affected by the fact that the samples were exposed to air prior to their measurement in the photoelectron spectrometer, allowing oxygen adsorption to occur on the diamond sample surface. The obtained oxygen to silicon concentration ratios are then upper limits of the stoichiometry of the impurity phase. Thus, comparing the binding energies and the oxygen to silicon concentration ratios, and making provision for oxygen adsorption when transferring samples, we finally conclude that the impurity phase observed on the diamond film surface can be associated either with a SiO phase or a silicon oxycarbide phase.

We have observed a significantly higher concentration of silicon and oxygen on the diamond film surface compared to the bulk (compare Tables II and III). This supplement of impurities most probably stems from the wall of the reactor tube, as a result of the way we end the deposition process. High values of impurity concentrations have already been found by Bou *et al.*[15] Their procedure for turning off the discharge was to decrease the methane gas flow before turning off the H_2 flow, as we did with our samples from Table III. We believe that the SiO or $Si_xO_yC_z$ impurity phase observed at the surface of the diamond film most likely also exists in the bulk of the diamond film, the oxygen impurities originating from the fused silica tube (SiO_2) when no O_2 is added to the discharge. It is possible that this contaminated, modified surface layer moves with the growing diamond film during the deposition process.

IV. CONCLUSION

We have deposited crystalline diamond films in a newly developed microwave plasma reactor based on surface-wave-sustained discharges, using H_2/CH_4 mixtures. We have systematically evaluated the concentrations of impurities in the bulk and at the surface of the films using various methods (ERD-TOF, SIMS, EMA, and XPS), and compared these results with the corresponding film quality (Raman spectroscopy, SEM) and H-atom gas-phase concentration (OES). We have found that the recombination and reaction probability of H atoms on surfaces decreases in the following sequence for the materials examined: Si > Mo > SiC. This result correlates with a high etch rate by hydrogen of the Si(100) surface.

We have shown that the main impurity in the films is silicon (typically between 0.01 and 0.2 at. %) which originates from the fused silica discharge tube and from the silicon substrate, and it is most probably bonded in the SiO or $Si_xO_yC_z$ form. Its concentration could be suppressed below the instrument's detection limit by adding oxygen to the

working gas. Addition of O_2 during the deposition process passivates the reactor wall. However, the situation is totally opposite with a substrate initially coated with SiC where, in the presence of O_2, we have observed an enhancement of Si in the bulk. This could be due to the formation of CO and CO_2 volatile compounds which liberates Si atoms.

The presence of silicon in the films is found to be responsible for the background fluorescence accompanying the Raman diamond peak. Raman spectroscopy measurements can therefore provide a practical method for the determination of the Si contamination level.

ACKNOWLEDGMENTS

The authors are grateful to Dr. S. G. Gujrathi (Université de Montréal) for the ERD-TOF analysis, to Dr. P. Van der Heide (University of Western Ontario) for the SIMS measurements, and to F. Roy, R. Lemay and R. Martel for their skilled technical assistance. This work was supported by the Natural Sciences and Engineering Research Council (NSERC) of Canada. We acknowledge the fellowships from the Ministère des Affaires Internationales du Québec (bourse d'excellence) for C.F.M.B., and from the Swiss Science Foundation and the Swiss Freie Akademische Geselschaft for S.S.

[1] J. C. Angus and C. C. Hayman, Science **241**, 913 (1988).
[2] K. E. Spear, J. Am. Chem. Soc. **2**, 171 (1989).
[3] X. Jiang, J. V. Harzerand, B. Hillebrands, Ch. Wild, and P. Koidl, Appl. Phys. Lett. **59**, 1055 (1991).
[4] B. E. Williams and J. T. Glass, J. Mater. Res. **4**, 373 (1989).
[5] B. E. Williams, B. R. Stoner, D. A. Asbury, and J. T. Glass, in *NATO-ASI Series B: Physics*, edited by R. E. Clausing, L. L. Horton, J. C. Angus, and P. Koidl (Plenum, New York, 1991), Vol. 266, pp. 737–744.
[6] S. Boily, M. Chaker, H. Pépin, T. Kerdja, J. Voyer, A. Jean, J. C. Kieffer, P. Leung, F. Cerrina, and G. Wells, J. Vac. Sci. Technol. B **9**, 3254 (1991).
[7] C. F. M. Borges, M. Moisan, and A. Gicquel, Diamond Relat. Mater. **4**, 149 (1995).
[8] L. St.-Onge and M. Moisan, Plasma Chem. Plasma Process. **14**, 87 (1994).
[9] J. L'Ecuyer, C. Brassard, C. Cardinal, J. Chabbal, L. Deschênes, J. P. Labrie, B. Terreault, J. G. Martel, and J. P. Martin, J. Appl. Phys. **47**, 881 (1976).
[10] R. Groleau, S. C. Gujrathi, and J. P. Martin, Nucl. Instrum. Methods **218**, 11 (1983).
[11] M. Ohring, *The Materials Science of Thin Films* (Academic, New York, 1992).
[12] C. F. M. Borges, L. St.-Onge, M. Moisan, and A. Gicquel, Thin Solid Films (in press).
[13] E. Anger, Ph.D. thesis, LIMHP, Université Paris-XIII, 1994.
[14] J. A. Mucha, D. L. Flamm, and D. E. Ibbotson, J. Appl. Phys. **65**, 3448 (1989).
[15] P. Bou, J. C. Boettner, and L. Vandenbulcke, Jpn. J. Appl. Phys. **31**, 1505 (1992).
[16] S. Dohmae, K. Shibahara, S. Nishima, and H. Matsunami, Jpn. J. Appl. Phys. **24**, L873 (1985).
[17] J. Sugiura, W. J. Lu, K. C. Cadien, and A. J. Steckl, J. Vac. Sci. Technol. B **4**, 349 (1986).
[18] W. S. Pan and A. J. Steckl, J. Electrochem. Soc. **137**, 212 (1990).
[19] M. L. Terranova, V. Sessa, V. Rigato, and F. Cacavale, Diamond Relat. Mater. **2**, 1365 (1993).
[20] K. Miyata, K. Kumagai, K. Nishimura, and K. Kobashi, Diamond Relat. Mater. **1**, 392 (1992).
[21] J. F. Morar, F. J. Himpsel, G. Hollinger, J. L. Jordan, G. Hughes, and F. R. McFeely, Phys. Rev. B **33**, 1340 (1986).
[22] A. Mansour, G. Indlekofes, and P. Oelhafen, Appl. Surf. Sci. **48–49**, 312 (1991).
[23] F. J. Himpsel, F. R. Feely, A. Taleb-Ibrahimi, and J. A. Yarmoff, Phys. Rev. B **38**, 6084 (1988).
[24] F. G. Bell and L. Ley, Phys. Rev. B **37**, 8383 (1988).
[25] S. Schelz and P. Oelhafen, Surf. Sci. **279**, 137 (1992).
[26] P. Gantenbein, S. Schelz, and P. Oelhafen, unpublished results.
[27] M. Moisan and Z. Zakrzewski, J. Phys. D **24**, 1025 (1991).

CHAPITRE 5

Adhesion of CVD diamond films on silicon substrates of different crystallographic orientations

C. F. M. Borges, S. Schelz, L. Martinu, and M. Moisan

Accepté pour publication dans Diamond and Related Materials; 04 juin 1996

Adhesion of CVD diamond films on silicon substrates of different crystallographic orientations

C. F. M. Borges, S. Schelz, L. Martinu [†], and M. Moisan

Groupe de physique des plasmas, Université de Montréal, C.P. 6128, Succursale Centre-ville, Montréal H3C 3J7, Québec

[†]Département de Génie physique, École Polytechnique de Montréal, Montréal H3C 3A7, Québec

Abstract

In order to gain insight into the adhesion mechanisms of diamond films, we examine Si substrates with three different crystallographic orientations at the various stages of the deposition process. This allows one to distinguish the surface phenomena involved in diamond deposition from those due to gaseous plasma processes. We find that the initial ultrasonic scratching treatment produces partial graphitization of the diamond powder and it controls the crystallite size through the carbon residues. On the other hand, an increased surface roughness due to H-atom etching correlates with increased adhesion. The deposited film adhesion is found to increase in the sequence Si(111) < Si(110) < Si(100), and it increases in the same order with nucleation density.

1. Introduction

Adhesion of CVD diamond films is an essential feature for future applications of these coatings. Many works have been devoted to it but, nonetheless, it is still an incompletely resolved issue. The term adhesion refers to the interaction between the closely contiguous surfaces of adjacent bodies, i.e. a film and a substrate in our case. It is defined as the condition in which two surfaces are held together by valence forces or by mechanical anchoring, or by both together [1]. In this paper, we bring insight into this phenomenon by analysing the results obtained when depositing diamond films simultaneously on Si substrates with different crystallographic orientations. In particular, we examine how adhesion correlates with the substrate pretreatment and with the hydrogen etching of Si in the first moments of nucleation. The results presented were obtained thanks to the advantageous and unique features of our novel plasma reactor.

Microwave plasma chemical vapour deposition (CVD) is one of several techniques developed over the past decade to produce high quality crystalline diamond films. In this paper, the diamond films were prepared in a non-conventional surface-wave sustained discharge yielding a plasma with a hemispherical shape in front of the substrate [2]. Compared to conventional microwave plasma systems, this newly designed plasma reactor has some unique features. These stem essentially from the fact that microwave power is totally absorbed in the plasma. Two important consequences of this are: 1) There is no residual microwave power that would heat the substrate. The substrate temperature can be adjusted indepen-

dently of the microwave power in the range from 650 to 1000° C up to 2.5 kW (165 W/cm^3) into the system. The substrate heating is uniform within ± 10 °C over a 2.5 cm diameter. 2) There is a strong gradient of microwave electric field, $\nabla \mid E \mid^2$, across the plasma boundary. This creates a ponderomotive force that accelerates both ions and electrons toward the substrate [2].

Table I summarizes the properties of silicon crystals according to their plane orientations [3]. We note that the entries for a given parameter vary monotonically in the sequence Si(100), Si(110) and Si(111). Si(111) provides the highest mechanical resistance; the atomic density per unit surface of the plane considered is also the largest with Si(111), a factor 2.3 larger than for Si(100).

2. Experimental

The system was operated at 2.45 GHz with a microwave power of 900 W (60 W/cm^3). Design and operating details concerning the experimental apparatus are described elsewhere [2]. The base pressure of the deposition chamber was 2×10^{-6} torr (3×10^{-4} Pa). The substrate temperature, measured with an optical pyrometer, was set at 900°C, and the total flow rate of hydrogen and methane was kept constant at 100 standard cubic centimeters per minute (sccm). These gases were premixed before entering the reaction tube, using a 0.5% methane concentration in hydrogen. The pressure during diamond deposition was kept at 15 torr (2 kPa).

Silicon substrates with (100), (110) and (111) orientations were pretreated

with a diamond powder suspension (grain size 20–40 μm) in methanol in an ultrasonic bath. This mechanical pretreatment was kept identical for all substrates.

The substrate surface mophology and surface chemical reactions in the early stages of the film growth are the key factors affecting the diamond nucleation process [4, 5]. This in turn controls the initial deposition rate, crystal quality and diamond to substrate adhesion. Using a Nanoscope IIIA atomic force microscope (AFM), we have successively examined the topography and surface roughness of: 1) as-received Si substrates; 2) Si substrates treated only in the ultrasonic bath; 3) as-received substrates submitted to H-atom etching (no CH_4); 4) Si substrates pretreated in the ultrasonic bath and submitted for 30 minutes to diamond deposition conditions. In this last case, scanning electron microscopy (SEM) was additionally used to determine the nucleation density and crystallite size using an image analyser. Finally, following a 3 hours deposition time leading to $3\mu m$ thick films, the crystal quality was investigated by Raman spectroscopy using a 488 nm argon ion laser beam. Adhesion of the films was evaluated using a Micro Scratch-Tester, equipped with a Rockwell C hemispherical diamond stylus (200 μm radius). The acoustic signal originating from the scratching of the stylus over the diamond surface was monitored: an abrupt increase of this signal occurring at a critical load F_c corresponds to the diamond film rupture and delamination. Such a test was repeated five times on each substrate, and an average critical load was calculated. The values obtained should be considered as relative indications, only an indentation method providing accurate absolute values.

3. Results

Table II shows the AFM results for the various cases described above. We note that with as-received substrates, the average roughness R_a is the lowest for Si(111) and the highest for Si(110). However, once these substrates have been either simply mechanically pretreated or etched, or pretreated and exposed to diamond deposition conditions for 5 minutes, R_a is the highest for Si(100) and the lowest for Si(111). It is noteworthy that the mechanically pretreated substrates examined under AFM show the most uniformly distributed holes for the Si(100) orientation; the biggest holes are found on Si(110) substrates and are unevenly distributed. In contrast, Si substrates submitted to H-atom etching, show the biggest holes for Si(100) and the smallest on Si(111); the uniformity of the hole distribution is comparable for the three Si orientations considered.

Besides topographical modifications, the ultrasonic treatment also provides graphitic sites on the Si substrate surfaces. These result from graphitization of the diamond powder upon impact on the Si surface because of the high translational energy transferred to the diamond powder grains by the ultrasonic bath [6]. This can be seen by Raman spectroscopy measurements on the pretreated, but yet uncoated silicon substrates. The Raman spectra (not shown here) reveal a peak at $520\,cm^{-1}$ corresponding to the Si crystalline structure of the silicon substrate, and an additional peak at $1575\,cm^{-1}$ originating from the graphitic phase present at the substrate surface as a result of the pretreatment [7, 8]. The ratio between the graphitic and the Si peak intensities (I^{1575}/I^{520}) is reported in Table III for the three crystallographic orientations considered. It is the highest for Si(100)

and the lowest for Si(110).

To get more information on the etching of the Si substrates by hydrogen atoms in the first moments of diamond deposition, we examined the role of the substrate temperature T_s. Table IV shows that for a fixed exposure time to a pure H_2 discharge, the higher T_s, the higher R_a. Table V shows to what extent increasing exposure time increases R_a; the first set of experiments was carried out on virgin Si substrates, while the second set concerned ultrasonically pretreated Si substrates. In both cases, R_a increases faster with time past a 10 minutes exposure.

Table III also shows the mean values of crystallite size d and nucleation density N_D corresponding to the three different silicon orientations. The deposition on these three differently oriented substrates was performed simultaneously in the same plasma. This complete procedure was repeated four times and the error bar is estimated from the standard deviation for the four cycles. The highest N_D and d values are observed for the Si(100) substrate. On the Si(110) substrate, the N_D value is intermediate but d is the smallest, while the Si(111) substrate exhibits the lowest N_D and an intermediate d value.

Results of the film adhesion tests on $3\,\mu m$ thick diamond films are reported in Table III [9]. It shows that the normal force applied to the scratching stylus leading to the diamond film rupture and delamination (critical load F_c) was the lowest for the Si(111) orientation and the highest for Si(100) substrates. To have a closer look at the influence of H-atom etching on the adhesion, we have used a large CH_4 concentration for the first three minutes of the deposition process:

the substrate is "saturated" with 5% methane in hydrogen before resetting the regular 0.5% methane concentration. Table VI shows that in all cases R_a is lower with this method, but F_c is also lower. Differences are the largest with Si(100) substrates and the smallest with Si(111) ones.

Figure 1 presents the Raman spectra of 3 μm thick diamond films deposited onto Si(100), Si(110) and Si(111) substrates. All three types of samples have been deposited simultaneously in the same plasma. They exhibit a sharp peak at 1332 cm^{-1} originating from the high quality diamond phase. The full width at half maximum (FWHM) of the diamond peak slightly varies with the silicon orientation. The lowest FWHM value is observed for the Si(100) substrate (6.80 cm^{-1}), the highest one for Si(110) (15.12 cm^{-1}), with an intermediate value (8.32 cm^{-1}) for the Si(111) surface. Clearly, this line width increases with decreasing crystallite size, as noted earlier by Bou and Vandenbulcke [10].

4. Discussion

We first examine the influence of the ultrasonic scratching treatment of Si substrates. The number and dimensions of holes and bumps, which are expressed through R_a, vary as a function of the crystallographic orientation (Table II) inversely as the Si surface hardness (Table I): Si(100), the softest surface, is the one most damaged by the ultrasonic impacts of the diamond powder grains. The presence of carbon residues on the substrate surface as a result of the pretreatment is known to be the driving force for the growth of diamond crystallites at the beginning of the deposition process. Comparing the relative density of graphitic

sites with d (Table III), we conclude that the crystallite size increases with the concentration of graphite.

From the literature, we know that the etching of silicon in a H_2 discharge leads to the formation of volatile SiH_4 as a result of surface reactions with adsorbed H-atoms [11]; the other main product of desorption is H_2 due to H-atom recombination, this reaction increasing with surface temperature [12, 13]. A plot of $\log R_a$ (related to the etch rate) as a function of $1/T_s$ displays an Arrhenius-like behavior, at least up to 900 °C; this tends to prove that the process is chemistry driven as opposed to ion assisted. The slope is negative, implying the existence of an activation energy. Turning to the influence of the Si crystallographic orientations, we have observed that the etch rate (as reflected from the R_a values) obtained in a pure H_2 discharge (Table II) increases in the following sequence: (111) < (110)< (100). Similar results have been observed with wet chemical etching: for the same orientations, Finne and Klein, for example, found an etch rate ratio of 1:10:17 [14]. However, the rate ratios and the sequence of anisotropy can be different depending on the chemical solution used [15]. In general, the etch rate anisotropy depends on the chemical process involved, on the activation energy and on the backbond geometry of the given surface [15]. The latter characteristic refers to the number of neighboring atoms [16]. During the etching process, in the case of (100) planes, only two bonds have to be broken (two are already free) in order to remove a Si atom. For (110) and (111) planes, three bonds have to be broken to remove an atom from the surface. However, for the (110) plane, two of the neighboring atoms are in the etch front and are thus more easily attacked

by the etchant [16], hence the etching sequence that we observe. This analysis in terms of the backbond configuration can be completed by considering the atomic lattice packing density; for the same three orientations, the surface density trends coincide with the etch rate (see Tables I and VI). We therefore believe that at lower surface density, the H atoms can penetrate more deeply into the lattice and benefit from a longer residence time to react with Si.

The diamond peak background in the Raman spectrum of films deposited on Si(100) substrates is significantly different from that of the other two configurations, showing an increase in the background signal towards higher wavenumbers. In a previous paper [17], we showed that this background signal originated from a broadband luminescence due to silicon impurities in the diamond film and that these impurities came from both the fused silica wall of the reactor and H-atom etching of the substrate during the initial stage of deposition (with subsequent diffusion of these impurities through the film as deposition went on). Since the three samples were exposed simultaneously to the same plasma and that luminescence is relatively small for films deposited on Si(110) and Si(111) substrates, we conclude that the main contribution to Si impurities in diamond films deposited on Si(100) arises from etching the substrate. This conclusion is supported by our AFM measurements (Table II) which show that etching is most pronounced on Si(100) substrates surfaces.

The results of the micro-scratch analysis correlate in Table III with the nucleation densities observed for the various silicon orientations, and not with the crystal size, suggesting that the larger N_D, the better the adhesion. Similarly

from Table II, we find that the higher R_a, the higher N_D. Adhesion thus seems to increase with the number of defects on the Si substrate that are created by the mechanical pretreatment and initial H-atom etching. A further experiment was carried out to determine the relative importance, as far as film adhesion is concerned, of topographical modifications due to the mechanical treatment as compared to the H-atom interaction with the surface. For that purpose, we used for the ultrasonic treatment a very fine diamond powder ($0.25\,\mu m$ grain size) which is 100 times smaller than the previous one, thereby reducing the pretreatment contribution on the substrate surface roughness. It showed that creating smaller defects with the ultrasonic bath did not significantly modify the degree of adhesion. It thus looks like the defects created by H-atom etching are those that act as anchoring points which ensure adhesion.

4. Conclusion

We have observed marked differences in the adhesion of diamond films deposited on Si substrates with various crystallographic orientations. Care had been taken to process the differently oriented substrates simultaneously in the plasma reactor. We have shown that adhesion increases with nucleation density (not with crystallite size) which, in turn, mainly depends on H-atom etching during the first moments of diamond deposition. It is indeed the defects caused by etching rather than those resulting from the initial mechanical treatment that ensure the anchoring of the diamond crystallites on the substrate surface. Hy-

drogen atom etching of Si in the present experiment is believed to be chemically driven.

The crystallite size has been shown to increase with the graphitic content on the substrate surface following ultrasonic treament, whereby diamond powder grains are graphitized upon impacting on the Si surface.

Acknowledgements

This work was supported by the Natural Sciences and Engineering Research Council (NSERC) of Canada. The fellowships provided by the Swiss National Foundation and the Swiss Freie Akademische Gesellschaft for S. S. and by the Programme Québécois de Bourses d'Excellence for C.F.M.B. are gratefully acknowledged. The authors are grateful to Prof. D. Guay at INRS-Énergie et Matériaux for his assistance with AFM measurements and to Profs. M. Wertheimer and J. Pelletier, and to Mr. R. Antaki for stimulating discussions.

References

[1] M. Ohring. *The Materials Science of Thin Films*, Academic Press, New York, 1992.

[2] C. F. M. Borges, M. Moisan, and A. Gicquel. *Diamond Relat. Mater.* 4, 149 (1995).

[3] Fumio Shimura. *Semicondutor Silicon Crystal Technology*, Academic Press, Inc., New York, 1989.

[4] B. Lux and R. Haubner, *Diamond Materials*, Vol. **91-8**, A. J. Purdes, J. C. Angus, R. F. Davis, K. E. Spear, and B. S. Mayerson, eds., NJ, 1991, p. 314.

[5] J. C. Angus, Z. Li, M. Sunkara, R. Gat, A. B. Anderson, S. P. Mehandru, and M. W. Geis, *p.125 in ref.1.*

[6] Kenneth S. Suslick, *MRS Bulletin* p. 29 (1995).

[7] R. J. Nemanich and S. A. Solin, *Phys. Rev. B* **20**, 392 (1979).

[8] D. S. Knight and W. B. White, *J. Mater. Res.* 4, 385 (1989).

[9] C. F. M. Borges, S. Schelz, L. Martinu, and M. Moisan, *Diamond Materials IV*, Vol. 95-4, K. V. Ravi and J. P. Dismukes, eds., The Electrochemical Society, Inc., New Jersey, 1995, pp. 136–141.

[10] P. Bou, , and L. Vandelbulcke, *J. Electrochem. Soc.* **138**, 2991 (1991).

[11] S. Veprek and F. A. Sarott, *Plasma Chemistry and Plasma Processing.* **2**, 233 (1982).

[12] J. Abrefah and D. R. Olander, *Surface Science* **209**, 291 (1989).

[13] L. St-Onge and M. Moisan, *Plasma Chem. Plasma Process.* **14**, 87 (1994).

[14] R. M. Finne and D. L. Klein, *J. Electrochem. Soc.* **114**, 965 (1967).

[15] H. Seidel, L. Csepregi, A. Heuberger, and H. Baumgartel, *J. Electrochem. Soc.* **137**, 3612 (1990).

[16] O. Than and S. Buttgenbach, *Sensors and Actuators* **A 45**, 85 (1994).

[17] C. F. M. Borges, S. Schelz, L. St-Onge, M. Moisan, and L. Martinu, *J. Appl. Phys.* **79**, 3290 (1996).

Figures captions

FIG. 1. Raman spectra of diamond films deposited on differently oriented silicon substrates.

Table I: Properties of silicon crystal planes [3].

Orientation	Young's modulus (10^{10} dyn/cm^2)	Surface atomic density (10^{14}/cm^2)
Si(100)	1.3	6.78
Si(110)	1.7	9.59
Si(111)	1.9	15.66

Table II: Average roughness R_a (nm) as determined with an atomic force microscope on Si substrates of different crystallographic orientations.

Orientation	Virgin Si	5 min. H-atom etching of virgin Si (T_s=900°C)	1 hour ultrasonic scratching on virgin Si	Ultrasonically treated substrates submitted 5 min. to deposition conditions (T_s=900°C)
Si(100)	0.8 ± 0.02	4.9 ± 0.2	5.0 ± 0.3	9.9 ± 0.2
Si(110)	1.1	1.7	3.5	4.9
Si(111)	0.2	1.0	1.0	2.8

Table III: Relative graphite to Si surface content of mechanically pretreated substrates of different orientations as compared to diamond film characteristics.

Orientation	Relative graphite content of pretreated substrates	N_D (10^9/ cm^2)	d (nm)	F_c (N)
Si(100)	0.24 ± 0.02	10.2 ± 0.2	220 ± 3	15 ± 0.9
Si(110)	0.08	9.1	100	7.3
Si(111)	0.11	8.3	130	4.6

Table IV : Influence of the substrate temperature T_s on the average roughness R_a of mechanically pretreated Si(100) substrates submitted for 5 min. to etching by H-atoms (no CH_4)

T_s (°C)	R_a (nm)
450 ± 5	6.7 ± 0.2
700	8.4
900	9.8
1000	13.3

Table V : Influence of H-atom etching time on the average roughness of Si(100) substrates (T_s=900°C, pure H_2 discharge)

t (min.)	Virgin substrates, R_a (nm)	Ultrasonically pretreated substrates, R_a (nm)
5	4.9 ● 0.2	9.7 ● 0.2
10	5.2	10.4
15	6.3	13.2

Table VI : Roughness and critical load when using a 5% CH_4 concentration in H_2 during the first three minutes of deposition as compared to a constant 0.5% CH_4 in H_2 throughout deposition time.

Orientation	**Constant 0.5% CH_4 concentration**		**Initial 3 min. at 5% CH_4, then 0.5% CH_4**	
	R_a (nm)	F_c (N)	R_a (nm)	F_c (N)
Si(100)	9.0 ± 0.2	15 ± 0.9	6.3 ± 0.2	9 ± 0.9
Si(110)	4.7	7.3	3.4	5.5
Si(111)	2.6	4.6	2.1	4.5

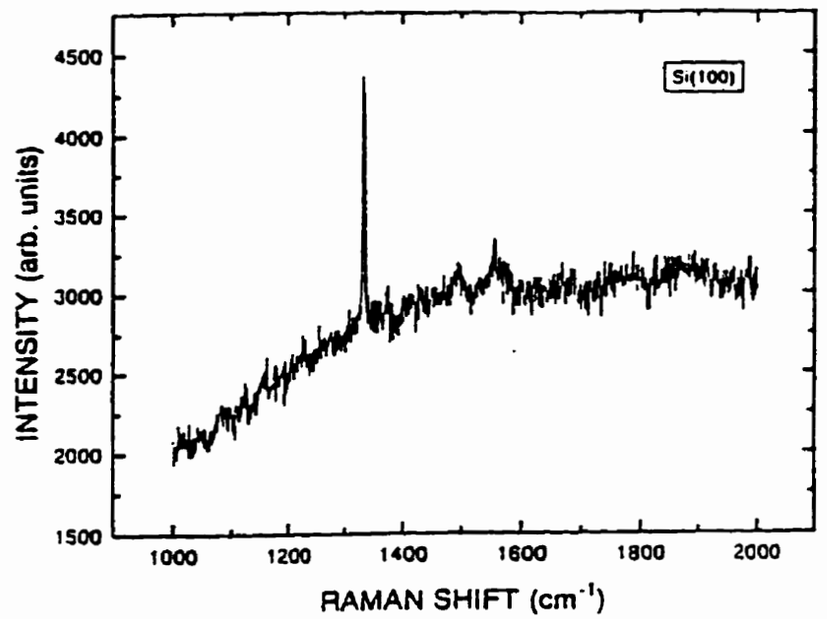
Si(100)
INTENSITY (arb. units)
4500
4000
3500
3000
2500
2000
1500
1000
1200
1400
1600
1800
2000
RAMAN SHIFT (cm-1)

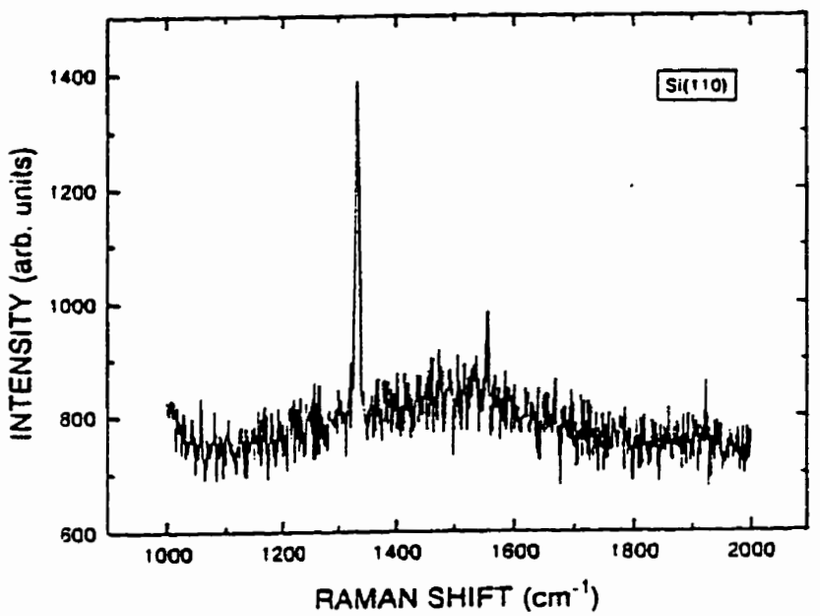
Si(110)
INTENSITY (arb. units)
1400
1200
1000
800
600
1000
1200
1400
1600
1800
2000
RAMAN SHIFT (cm-1)

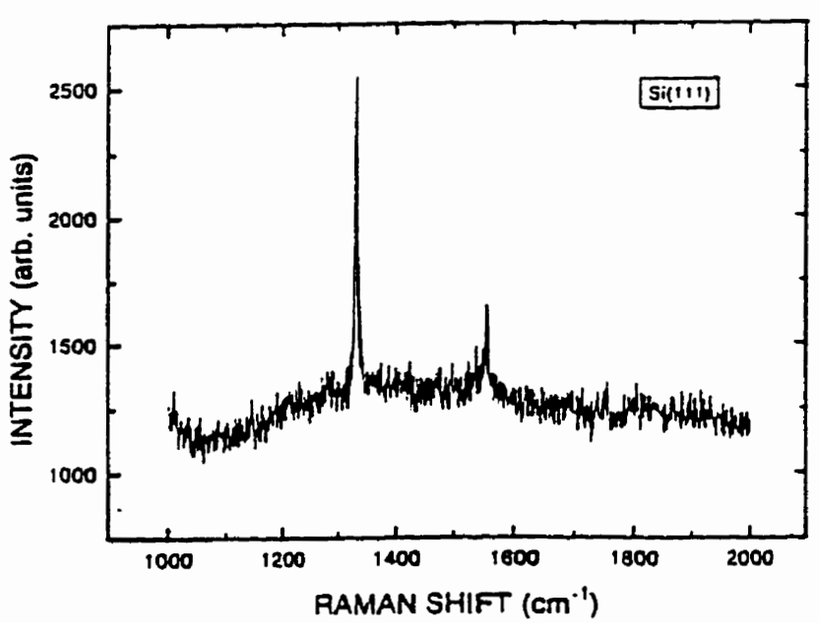
Si(111)
INTENSITY (arb. units)
2500
2000
1500
1000
1000
1200
1400
1600
1800
2000
RAMAN SHIFT (cm-1)

CHAPITRE 6

Achieving very low roughness diamond film deposition on Si substrates using a surface-wave sustained plasma

C. F. M. Borges, V. T.-Airoldi, E. J. Corat, M. Moisan, S. Schelz and D. Guay

Soumis pour publication à J. Appl. Phys.
Reçu: 28 mai 1996.

Achieving very low roughness diamond film deposition on Si substrates using a surface-wave sustained plasma

C. F. M. Borges, V. T. Airoldi [†], E. J. Corat [†], M. Moisan, S. Schelz, and D. Guay [‡]

Groupe de physique des plasmas, Université de Montréal, C.P. 6128, Succursale Centre-ville, Montréal H3C 3J7, Québec

[†]Instituto Nacional de Pesquisas Espaciais (INPE), 12227-010 - São José dos Campos - SP - Brasil

[‡]INRS-Énergie et matériaux, 1650 boul. Lionel-Boulet, Varennes J3X 1S2, Québec

ABSTRACT

We have investigated the operating parameters influencing the average roughness R_a of diamond films obtained through chemical vapour deposition (CVD) using microwave sustained plasmas. The plasma was provided by a surface-wave discharge in the form of a convex hemisphere facing the substrate and the films were deposited on Si(100) substrates. The procedure leading to very low R_a values called for high microwave power density absorbed in the plasma and very small grain size powder for substrate pretreatment in an ultrasonic bath. Pretreating with ≤ 0.25 μm diamond grit and operating, for example, with a microwave power density of 25 W/cm^3 (1.2 kW total absorbed power) and 0.75% CH_4 in a CH_4-H_2 mixture, we got $R_a = 6$ nm for a 1 μm thick film with an average crystallite size of 50 nm. The corresponding nucleation density was remarkably high, at 7.5×10^{10}

cm^{-2}: diamond film isoquality was good and adhesion to the substrate strong.

Classification: 81.15Gh, 81.20, 52.50Dg

1. Introduction

Diamond films can be deposited at reduced gas pressure through various chemical vapor deposition (CVD) schemes. The method to be used generally depends on the intended application. Diamond films are utilized, for example, as protective coatings for optical components [1], as membrane for x-ray lithography in microelectronics [2, 3] as well as low friction surfaces in mechanical devices [4]. A common requirement for these applications is a low average roughness; strong adhesion is also an essential feature for many of these coatings. In this article, we show how the microwave plasma reactor that we have developed, based on surface-wave discharges, can be employed to deposit high quality diamond films with, to our knowledge, the lowest average roughness ($R_a \approx 4$ nm) yet reported for conventional microwave plasma systems with comparable diamond isoquality. Such low R_a values are currently achieved only through smoothing of the surface by, for example, mechanical polishing [5], ion beam erosion [6] or laser ablation [7] of the CVD films. We obtain these low R_a values directly on deposited films of good diamond isoquality and that adhere strongly to the substrate.

The new type of microwave plasma reactor that we have introduced last year [8] uses the propagation of an electromagnetic surface wave in a non-conventional discharge configuration to yield a plasma with a hemispherical convex tip facing the substrate; the deposition technique is thus akin to that of the so-called plasma ball reactors. Compared to these conventional microwave systems, a unique feature of our reactor is that all microwave power is absorbed in the plasma. The advantages are then: 1) no residual microwave power to heat the substrate holder;

as a result, the substrate surface temperature can be set independently and uniformly with an external heater at temperatures as low as 650°C with as much as 165 W/cm^3 absorbed in the plasma ($\approx$ 2.5 kW in the system); 2) a strong gradient of microwave electric field intensity across the plasma boundary, $\nabla |E|^2$, which creates a ponderomotive force [9]. This force accelerates outwardly both electrons and ions; 3) the possibility of achieving higher density of absorbed microwave power in the plasma, a few times more than in conventional systems, which leads to higher densities of "active" species; 4) a finer and more easily reproducible tuning of the deposition conditions, namely the plasma to substrate distance, the degree of coverage of the substrate by the plasma and the level of microwave power absorbed in the plasma. Details concerning the operation and characterization of this new plasma reactor can be found elsewhere [8, 10, 11].

In a more recent paper [12], we have investigated the respective influence upon adhesion, of the substrate pretreatment with diamond powder and of the hydrogen atom etching of the Si substrate (in the first moments of diamond deposition). We showed that adhesion relies mostly on the defects caused by H-atom etching while the crystallites grow from the non-diamond phase carbon residues resulting from graphitization of the diamond powder during the ultrasonic pretreatment. In the present paper, our goal is to identify the operating parameters acting on R_a and determine their best values to achieve the lowest R_a value while, at the same time, ensuring good isoquality of the films and strong adhesion of them to the substrate.

2. Experimental

The diamond films were prepared in a microwave plasma using a surface-wave sustained discharge at 2.45 GHz with a microwave power density in the range of 25 to 130 W/cm^3. Note that we state power density, not total absorbed power, to characterize the CVD process; power density, for a given absorbed microwave power from the generator, depends on the diameter of the plasma hemisphere, which can be adjusted according to the area of the substrate to be processed. This possibility is illustrated in Fig. 1 which shows two configurations of the reactor chamber. In both cases, the tube on which the field applicator launches the surface wave is small enough (25 mm i.d. at 2.45 GHz) to ensure excitation of the wave in the azimuthally symmetric mode [13]. Such a symmetry with respect to the tube axis is required to obtain azimuthal uniformity of the plasma hemisphere, hence of the deposited films. The transition to the larger diameter tube, which encloses the substrate holder, must be abrupt enough so the surface wave does not propagate into this larger tube to fill it radially with plasma; the wave field in this tube past the transition is then evanescent, yielding the plasma hemisphere shown in the figure. The distance of the plasma hemisphere tip to the substrate is critical: when it is too small, i.e. when the plasma hemisphere is flatten by the substrate, we get a low nucleation density, mediocre uniformity, large crystallites (high R_a) and poor diamond isoquality whereas, when too far away, the nucleation density is again low, uniformity is good, crystallites are small (low R_a) but diamond isoquality is poor. The best distance is approximately 1 mm from the tip [10]. The plasma volume estimation used in determining power

density is accurate within ± 20%. Further details concerning the experimental apparatus can be found in Ref. [8, 10].

The substrate temperature T_s, measured by an optical pyrometer, was set between 850 and 950 °C, and the methane concentration was varied between 0.5 and 1.5 % of the H_2-CH_4 gas mixture, with a flow of 100 standard cubic centimeters per minute; the gases were premixed before entering the reaction tube and the pressure set at 10 torr. Si(100) samples of 1 cm^2 were submitted, prior to deposition: for i) 60 minutes to ultrasonic impacts from, alternatively, $20-40\mu$m, $8-16\mu$m and $\leq 0.25\mu$m diameter diamond particles immersed in hexane and ii) afterwards ultrasonically cleaned in methanol for 15 minutes. In all experiments, deposition time was 2 hours.

The morphology of the samples was examined with a 4.5 nm resolution scanning electron microscope (SEM). Atomic force microscope (AFM) pictures were taken with a Nanoscope IIIA (Digital Instruments); surface morphology of these films was visualized at a constant force (10^{-8}N) with microfabricated monocrystalline Si tips. The AFM pictures obtained were representative of a number of images taken for each sample with different tips. The nucleation density and the crystallite size were estimated from a 1 μm by 1 μm region on AFM images and confirmed through SEM pictures, both these quantities referring to a substrate submitted for 30 minutes to deposition conditions. The diamond isoquality of 1 μm thick films was evaluated by macro-Raman spectroscopy in a backscattering configuration using an argon laser at 488 nm.

The X-ray photoelectron spectra (XPS) were recorded with a VG ESCALAB

MkII spectrometer. The XPS measurements were performed with a non-monochromatized MgK_α source ($h\nu$=1253.6 eV) and with a spectrometer pass energy of 20 eV resulting in an energy resolution of about 0.8 eV. The energy calibration of the core levels was performed with a gold reference sample, setting the Au $4f_{\frac{7}{2}}$ binding energy at 84.0 eV. Some of the recorded spectra were energy-shifted in order to compensate for the charging effects.

3. Results

3.1 Influence of the diamond powder grain size

It is well known that the substrate on which diamond films are to be deposited requires some preparation to enhance diamond nucleation and to obtain a continuous film of high quality; abrasive diamond powders are used in various ways for this purpose [1, 14]. Recent reports [15] have indicated that the nucleation density enhancement following substrate pretreatment with micron size powder in an ultrasonic bath could be related to three specific mechanisms: i) the creation of topological defects (pits) in the surface; ii) the added presence of hybridated (sp^2) carbon seeds: in an ultrasonic bath, this follows from graphitization of the diamond powder and decomposition of the suspension liquid, which liberates carbon compounds; iii) the added presence of diamond particle seeds. Our substrate preparation technique excludes the existence of mechanism (iii): any loose diamond powder remaining on the substrate after the first ultrasonic bath is removed from it by a subsequent ultrasonic pure mathanol bath. In this article, we consider the influence of the grit size used in the substrate preparation,

employing the three sizes of powder grain mentioned above.

AFM analysis of the substrate immediately after the surface pretreatment (including rinsing) shows that the $\leq 0.25\ \mu m$ powder yields a dense distribution of smaller defects, on the average approximately 17 nm in size, while the 20 - 40 μm powder leads to defects 330 nm in size; both these sets of defects are nonuniformly distributed over the surface, as illustrated in Fig. 2. Table I shows that the grit size used for the ultrasonic pretreatment strongly affects the nucleation density. crystallite size and film roughness: for given deposition conditions, decreasing the pretreatment grit size increases nucleation density N_d, while it decreases crystallite size d and roughness, a previously known result [1]. Raman analysis of the samples obtained with these three sets of diamond grains indicates good quality of all these films, as shown in Fig. 3. We find the diamond peak to be at $1332 \pm 1\ cm^{-1}$, which means that the shift, if any, is small, implying a low stress film.

We also observed that adhesion does not vary significantly with the grit size used for pretreatment, hence with the size of the defects created by it. This result was obtained using a micro-scratch tester and determining the critical load F_c leading to the film rupture and delamination. The corresponding data is shown in Table I. These results agree with our previous analysis which suggested that H-atom etching in the first moments of deposition conditions, not ultrasonic scratching, is responsible for adhesion on Si substrates [12].

3.2 Influence of the ultrasonic bath liquids

-Hexane vs. methanol in the first bath

The above results have been obtained with hexane as the diamond powder suspension liquid in the first ultrasonic bath; methanol was subsequently used to rinse ultrasonically the substrate surface and remove any "loose" grit. When methanol is used instead in the first bath, the defects caused on the Si substrates by ultrasonic impact of a given size grit are not sensibly different, as can be seen in Table II by comparing the R_a values of ultrasonically treated (2 baths) substrates prior to deposition. However, for a given grain size with methanol in the first bath, the value of N_d is systematically lower but, most importantly. d is larger, which implies larger R_a values on deposited films.

Photoelectron spectroscopy was performed on ultrasonically treated but yet uncoated substrates in order to obtain information about the chemical bondings on the silicon surface after the pretreatment procedure. Figure 4 shows the Si2p core levels of two samples respectively pretreated using methanol and hexane as the diamond powder suspension liquid ($20-40\mu$m diamond powder). The curves are normalized to the same peak height. The peak at 99.4 eV binding energy (peak a) is related to Si while the second peak (peak b) at 103.4 eV originates from the native SiO_2 layer. The intensity built-up between peak a and b indicates the existence of distinct reactions with the substrate surface (for example the formation of a Si_w-O_x-$C_y$$H_z$ phase [16]) depending on the suspension liquid used. Figure 5 displays C1s core level spectra of silicon substrates pretreated with different powder grain sizes using either methanol or hexane as suspension liquid, and subsequently ultrasonically rinsed in methanol. The intensity ratio of peak B to peak A ($r_{B/A}$) strongly depends on the diamond powder size when

using methanol as suspension liquid ($r_{B/A} = 0.4$ and 0.2 for powder grain size of $20 - 40\mu$m and $\leq 0.25\mu$m, respectively), while pretreating in hexane does not significantly influence the intensity ratio of these peaks ($r_{B/A} = 0.2$).

The C1s core levels consist of three peaks located at 285.4 ± 1 eV (peak A), 287.0 ± 1 eV (peak B) and 289.4 ± 1 eV (peak C). The binding energy of peak C is close to the value obtained from CH_3COOH [17]. Such a phase is formed at the Si surface during exposure to methanol in the ultrasonic bath. The binding energy of peak A is significantly higher than the value typical for C-C or C-H bondings (284.6 eV) [18, 19] and lower than the binding energy of methanol (H_3-C-OH) (286.6 eV) [20]; recalling that the C1s core level of ethanol (H_3-C-CH_2-OH) is located at 286.3 eV [17], we conclude that increasing the number of carbon atoms in H-$(CH_2)_x$-OH molecules decreases the binding energy. Therefore, we attribute peak A (285.4 eV) to a partially oxidized carbon phase (C_x-OH) resulting from the use of methanol as the powder suspension liquid. The assignment of peak B is not straightforward. The strong dependence of the intensity ratio upon grit size when the diamond powder is dispersed in methanol suggests that this alcohol reacts with the silicon surface, forming a Si_w-O_x-C_yH_z phase at the substrate surface. The reaction seems to be activated by diamond powder particle impacts [21]: the larger the diamond grains, the more energy is transmitted to the silicon surface and the higher the ratio between peaks B and A. The formation of such a Si based phase is supported by the fact that the intensity built-up between 100 and 102 eV in the Si2p core line spectra (Fig. 4) is indeed larger with methanol as the suspension bath [16].

- Ultrasonic removal of diamond powder left from the first bath

Note that in contrast to Anger et al. [15] scheme, our preparation method includes a subsequent ultrasonic cleaning which removes most diamond particles from the substrate surface, as shown by SEM and AFM (we cannot however exclude the possibility that some pits be filled with diamond particles) [22]. Without the cleaning procedure, the diamond grains remain on the substrate surface and are expected to lead to larger R_a values on the deposited films.

3.3 Influence of the CH_4 content

It is well known that the roughness of deposited films decreases with increasing CH_4 percentage in the H_2-CH_4 gas mixture, as shown in Table III. We note that the grit size influence is more important than the variation of the CH_4 concentration: whatever the CH_4 percentage, the lowest R_a value is always obtained with the smallest size grain. Recall that increasing the methane concentration reduces the diamond film isoquality.

3.4 Influence of microwave power density in the plasma

In previous experiments [8, 10], we have reported that R_a decreases significantly when increasing the density of microwave power absorbed in the plasma. Table IV shows such kind of data for the smaller and larger grit sizes. It is noteworthy that with 59 W/cm^3 absorbed power (2.8 kW in configuration I) and for ≤ 0.25 μm powder, we have $R_a = 4$ nm. As far as we know, this is the smallest R_a value yet reported for films with good diamond isoquality.

A further series of experiments were conducted with the reactor in configuration II (Fig. 1b) which, for a given absorbed microwave power, yields a higher power density Π than configuration I: to achieve 25 W/cm^3, we only need 380 W while configuration I required 1.2 kW absorbed power. The rest of the operating conditions were somehow different from those of Table IV above: T_s = 950°C instead of 850° and $CH_4\%$ = 0.5 instead of 0.75. We have used 20 - 40 μm diamond powder and methanol as the powder suspension liquid for the pretreatment. Figure 6 shows crystallite size d as a function of Π. It decreases relatively slowly with increasing Π at low power densities, but rapidly past approximately 100 W/cm^3. Figure 7 shows that the decrease of R_a with Π is also higher at large Π values, reflecting the decrease of the crystalleite size in Fig. 6. We get R_a = 6 nm at Π = 131 W/cm^3 (20 - 40 μm powder). The observed decrease of R_a and d with Π leads us to believe that still smaller d and R_a values could be obtained by going to higher power densities.

3.5 Influence of the crystallographic orientation of Si substrates

In a previous publication [12], we have shown that the crystallographic orientation of silicon substrates strongly influences the deposition process. In particular, the R_a value of deposited films increases in the sequence Si(111) < Si(110) < Si(100), as shown in Table V. Thus one can turn to Si(111) substrates to reduce roughness, but at the expense of a lower adhesion, as also shown in Table V.

4. Discussion

The defects created by impact of the diamond particles on the substrate sur-

face during the pretreatment phase result from cavitation phenomena in the bath liquid. Small bubbles are formed that expand and suddenly collapse under the effect of the ultrasonic oscillations; the energy released from the collapse is enough to accelerate diamond particles [21]. Smaller particles create smaller defects of higher density. Also, this collapse process may induce a local heating to temperatures as high as 5000 K [21]. Such high temperatures are sufficient to graphitize diamond and dissociate the hexane or methanol molecules and generate disordered carbon seeds in the impact induced defects on the surface [23, 24]. These disordered carbon seeds may later transform into sp^3 carbon entities on the surface during the first stages of deposition [25, 26]. Thus, during the ultrasonic treatment with diamond powder, both amorphous and crystallized carbon seeds can be incorporated into surface defects.

The increase of N_D and the correlative decrease of R_a with decreasing grit size has already been reported. For example, Erz et al. [1] used 3 μm to 10 nm diamond powders to pretreat fused silica surfaces, subsequently cleaned in an ultrasonic acetone bath. The largest N_D value, 3 x 10^{10} nuclei/cm^2, and the lowest R_a value, 20 nm, were obtained with the smallest grit size. This was achieved with a remote plasma from a resonant cavity system: 550 W absorbed in the system, p = 38 torr, 2% CH_4 and 1% O_2 in an H_2-CH_4-O_2 mixture. The diamond film isoquality (T_s = 830°C) was low. Makita et al. [27] turned to 5 nm grit size for Si substrate pretreatment, removing "loose" diamond grit by centrifugation. Operating conditions were: p = 38 torr, T_s = 950 - 980°C and absorbed microwave power 275 W with CO as the source gas. They claim N_D

values of more than 5 x 10^{11} cm^{-2} and a continuous diamond film. There is no indication about R_a and diamond isoquality are given.

The formation of a Si_w-O_x-$C_y$$H_z$ phase on the pretreated Si substrates, which is more important when pretreating with methanol (Fig. 4), seems to slightly hinder the initial diamond nucleation process since lower N_D values are obtained in this case compared to the case of an hexane bath. The presence of oxygen in this phase during the first moments of deposition could be responsible for the lower N_D values and the larger d values found with methanol.

Besides the pretreatment grit size, the level of microwave power density in the plasma is the other decisive parameter to achieve low R_a values. For a given absorbed microwave power in the plasma, our reactor enables one to work at higher power densities than people using conventional microwave plasma reactors: in reactor configuration II, we get 52 W/cm^3 compared with 30 W/cm^3 for 800 W absorbed power in a resonant cavity [28, 29] while we can get 66 W/cm^3 compared to 15 W/cm^3 at 1000 W absorbed power in a bell jar system [30, 3]. In addition, we can operate at higher absolute values of microwave power density (165 W/cm^3 demonstrated) than with conventional microwave plasma systems (without affecting the substrate holder temperature with residual microwave heating). The maximum microwave power that we used was 3 kW, the maximum power of our generator. We see no reasons in principle why we could not operate at higher power levels.

To illustrate the influence of microwave power density, we compare with published results. For example, Anger et al. [15], using 45 μm diamond grit, T_s =

850°C, 1% CH_4 in a CH_4-H_2 mixture, p = 19 torr, and 9 W/cm^3 (600 W), find R_q = 30 nm (R_q and R_a are slightly different methods of evaluating the average surface roughness; as a rule, R_q is slighty larger than R_a) while we get R_q = 13 nm at 25 W/cm^3 using 20 - 40 μm diamond grit under comparable (except p = 10 torr in our case) operating conditions.

The advantage of using high power densities seems to stem from a higher electron density, hence a higher density of reactive species (mainly formed through electron collisions), such as hydrogen atoms. Two points should be underlined: i) In the presence of hydrogen atoms, diamond crystals nucleate copiously. Atomic hydrogen reacts with and covers the surface of small diamond nuclei and drastically reduces their surface energy. This reduction in surface energy, in turn, decreases the critical nucleus size to only a few atoms [31]. The number of sites where deposition occurs should thus increase with hydrogen atom concentration, hence with microwave power density. This results in small crystallites and high nucleation densities; ii) an increased concentration of hydrogen atoms reduces the presence of graphite precursors [31]. This might explain why we obtain good diamond isoquality even though the number of grain boundaries increases significantly with the decrease of the crystallite size. It seems that in conventional microwave plasma deposition systems, reducing crystallite size generally increases the presence of graphitic sites at the grain boundaries, thus reducing diamond isoquality, in contrast to what we observe.

There are experimental reports of nucleation density enhancement due to energetic ions bombarding the substrate surface; these ions are accelerated by

biasing negatively the susceptor with respect to plasma [32]. In our experiments, we have no external biasing but ions could be accelerated by the ponderomotive force existing at the plasma hemisphere boundary. However, we have not made any measurement of the ion energy distribution function; the beneficial effect of ion bombardment due to the ponderomotive force from surface-wave plasmas has been demonstrated in experiments on polymer deposition [33], but at much lower pressures (0.1 - 0.4 torr). In the present case, at 10 torrs, the ion mean free path between collisions is much lower. Considering collisions of the dominant hydrogen ions, H_3^+ [34] with H_2 molecules in a gas at 1500 K, we estimate the mean free path for thermal ions to be 0.05 mm; however, in the same conditions but with energetic ions, say of 10 eV energy, we find a mean free path of approximately 0.4 mm. This short mean free path (before the ion loses its energy) could possibly explain the critical positioning of the plasma hemisphere with respect to the substrate as far as achieving good diamond isoquality is concerned. We find this postion to be 1 ± 0.5 mm above the substrate.

5. Conclusion

We have investigated a series of parameters influencing the average roughness R_a of 1 μm thick diamond films deposited through CVD in a microwave plasma reactor. We have obtained R_a values as low as 4 nm by using ≤ 0.25 μm diamond grit and opreating at 59 W/cm^3 microwave absorbed power. These values appear to be the lowest ever reported with resonant cavity and bell jar systems that

yield good diamond isoquality of the deposited films; still lower R_a values are expected at higher power densities, because of larger densities of active species. These films also show little mechanical stress and adhere well to Si substrates.

We believe that these novel results are to be attributed to the peculiar characteristics of our surface-wave based plasma reactor, namely that: i) no residual microwave power goes into heating the substrate and the growing film; uniform heating of the substrate is achieved by external means; ii) precise and highly reproducible positioning of the substrate with respect to the plasma hemisphere convex boundary, but most importantly, iii) high microwave power density realized by reducing the diameter of the plasma hemisphere, which faces the substrate, and increasing the total absorbed microwave power (demonstrated up to 3 kW).

Acknowledgements

The fellowships provided by the Programme Québécois de Bourses d'Excellence and by the Swiss Janggen-Poehn-Stiftung for C.F.M.B. and S. S., respectively, are gratefully acknowledged. The authors are endebted to Professor L. Martinu at École Polytechnique and to L. St-Onge for discussions.

References

[1] R. Erz, W. Dotter, K. Jung, and H. Ehrhardt, *Diamond and Related Materials* **2**, 449 (1993).

[2] J. R. Maldonado, *J. Electronic Materials* **19**, 699 (1990).

[3] M. F. Ravet, A. Gicquel, E. Anger, Z. Z. Wang, Y. Chen, and F. Rousseaux, *X-Ray Lithography Mask based on Diamond Membranes Potentiality and Realization*, M. Yoshikawa, M. Murakawa, Y. Tzeng, and W. A. Yarbro, eds., 2nd International Conference on the Applications of Diamond Films and Related Materials, Tokyo, Japan, 1993, p. 77.

[4] R. F. Davis. *Diamond Films and Coatings*. Noyes Publications, Park Ridge NY, 1993.

[5] H. Tokura, Cheng-Feng Yang, and Masonori Yoshikawa, *Thin Solid Films* **212**, 49 (1993).

[6] A. Hirata, H. Tokura, and M. Yoshikawa, *Thin Solid Films* **212**, 43 (1993).

[7] S. Jamil, M. H. Gordon, G. J. Salamo, H. A. Naseem, W. D. Brown, and A. P. Malshe, *Applications of Diamond Films and Related Materials*, Vol. NIST Special Publication 885, National Institute of Standards and Technology, Gaithersburg, MD, 1995, p. 283.

[8] C. F. M. Borges, M. Moisan, and A. Gicquel, *Diamond Relat. Mater.* **4**, 149 (1995).

[9] F. F. Chen. *Introduction to plasma physics*, Plenum press. New York, 1974.

[10] C. F. M. Borges, L. St-Onge, M. Moisan, and A. Gicquel, *Thin Solid Films* **274**, 3 (1996).

[11] C. F. M. Borges, S. Schelz, L. St-Onge, M. Moisan, and L. Martinu. *J. Appl. Phys.* **79**, 3290 (1996).

[12] C. F. M. Borges, S. Schelz, L. Martinu, and M. Moisan, *submitted to Diamond and Related Materials* (1996).

[13] J. Margot-Chaker, M. Moisan, M. Chaker, V. M. M. Glaude, P. Lauque, J. Paraszczak, and G. Sauvé, *J. Appl. Phys.* 66, 4134 (1989).

[14] A. Gicquel, K. Hassouni, S. Farhat, Y. Breton, C. D. Scott, M. Lefebvre, and M. Pealat, *Diamond Relat. Mater.* **3**, 581 (1994).

[15] E. Anger, A. Gicquel, Z. Z. Wang, and M. F. Ravet, *Diamond and Related Materials* **4**, 759 (1995).

[16] S. Schelz and P. Oelhafen, *Surf. Sci.* **279**, 137 (1992).

[17] U. Gelius, P.F. Heden, J. Hedmann, B. J. Lindberg, R. Manne, R. Nordberg, C. Nordling, and K. Siegbahn, *Phys Ser.* **2**, 70 (1970).

[18] F. R. McFeely, S. P. Kowalczyk, L. Ley, R. G. Cavell, R. A. Pollak, and D. A. Shirley, *Phys. Rev. B* **9**, 5268 (1974).

[19] P. Oelhafen, D. Ugolini, S. Schelz, and J. Eitle, *Diamond and Diamond-Like Films and Coatings*, R. E. Clausing et al., ed., Plenum Press, New York, 1991, p. 377.

[20] D. T. Clark and H. R. Thomas, *Journal of Polymer Science: Polymer Chemistry Edition* **16**, 791 (1978).

[21] Kenneth S. Suslick, *MRS Bulletin* **April**. 29 (1995).

[22] S. Iijima and K. Baba, *Appl. Phys. Letters* **57**, 2146 (1990).

[23] B. Goss Levi, *Phys. Today* p. 18 (November 1991).

[24] G. J. Exardos, M. S. Donley, and R. H. Geiss, *Proceedings of the 22nd Annual Conference of the Microbeam Analysis*, San Franscisco Press. 1987.

[25] P. Koidl, *Brite/Euram Workshop on European Diamond Technology for the '90s*. Diamond Relat. Mater. 1992, p. 1065.

[26] J. J. Dubray, G. G. Pantano, M. Meloncelli, and E. Bertran, *J. Vac. Sci. Technol. A* **9**, 3012 (1991).

[27] H. Makita, T. Yara, N. Jang, K. Nishimura, A. Hatta, T. Ito, and A. Hiraki, *Applications of Diamond Films and Related Material: Third International Conference*, Gaithersburg, 1995, p. 333.

[28] H. Rau and B. Trafford, *J. Phys. D* **23**, 1637 (1990).

[29] K. Kobashi, K. Nishimura, Y. Kawate, and T. Horiuchi, *Phys. Rev. B* **38**, 4067 (1988).

[30] E. Anger. Ph.D. thesis, LIMHP, Université Paris-XIII, 1994.

[31] T. R. Anthony, *Material Research Society Symposium Proceedings vol. 162*, J. T. Glass, R. Messier, and N. Fujimori, eds., Boston, MA, 1990, p. 61.

[32] S. P. McGinnis, M. A. Kelly, and S. B. Hagstrom, *Appl. Phys. Lett.* **66**, 3117 (1995).

[33] L. Paquin, D. Masson, M. R. Wertheimer, and M. Moisan, *Can. J. Phys.* **6**, 831 (1985).

[34] L. St-Onge and M. Moisan, *Plasma Chem. Plasma Process.* **14**, 87 (1994).

[35] M. Moisan and Z. Zakrzewski, *J. Phys. D* **24**, 1025 (1991).

Figure captions

Fig. 1. Sketch of the reactor tube configuration showing how the diameter of the plasma hemisphere facing the substrate can be adapted to cover the substrate area: configuration I (a) and configuration II (b). For a given total absorbed microwave power, power density is higher with configuration II. The field applicator represented is a waveguide-surfatron wave launcher [35].

Fig. 2. Atomic force microscope recording showing that the smaller the grain size, the narrower and the deeper the holes created by ultrasonic impacts. Diamond grit sizes $\leq 0.25\mu$m (a), 8 - 16 μm (b) and 20 - 40 μm (c).

Fig. 3. Raman spectra of the diamond films deposited on substrates pretreated with diamond powders of three different sizes ($\leq 0.25\mu$m (a), 8 - 26 μm (b) and 20 - 40 μm (c)), followed by ultrasonic "cleaning" in methanol.

Fig. 4. XPS Si2p core level spectra of silicon substrates ultrasonically pretreated in either methanol or hexane as the powder suspension liquid ($20-40\,\mu$m diamond powder).

Fig. 5. XPS C1s core level spectra of silicon samples pretreated with different powder grain sizes using either methanol or hexane as the powder suspension liquid.

Fig. 6. Average crystallite size of a 1 μm thick film as a function of power density absorbed in the plasma. The data points can be fitted with two straight lines. Operating conditions: reactor in configuration II, T_s = 950 °C, $\%CH_4$ = 0.5, p = 10 torr, 20 - 40 μm diamond powder using methanol as the suspension liquid.

Fig. 7. Average roughness over a 1 μm thick film as a function of power density in the plasma. The data points have been fitted with two straight lines to try matching with the behavior of crystallite size with power density in Fig. 6. Same operating conditions as in Fig. 6.

Table I : Influence of diamond grit size on the silicon substrate surface defects after ultrasonic pretreatment ; on nucleation density and crystallite size ; on average roughness and critical load for rupture and delamination of a 1 μm thick deposit. Operating conditions : 25 W/cm^3 (1.2 kW), 0.75% CH_4, T_s = 850 °C, p =10 torr, hexane as diamond grit suspension liquid.

Powder grain size (μm)	Defect average size (nm)	N_D (cm^{-2})	d (nm)	R_a (nm)	F_c (N)
≤ 0.25	17 ± 1.6	7.5×10^{10} ± 10%	50 ± 3	6.2 ± 0.2	13.1 ± 0.9
8-16	140	1.6×10^{10}	140	11	12.1
20-40	330	8.6×10^{9}	250	12.1	13.6

Table II : Influence of the nature of the diamond powder suspension liquid used for ultrasonic pretreatment of the silicon substrates upon substrate surface roughness prior to deposition, on crystallite size and nucleation density. Operating conditions : 25 W/cm^3 (1.2 kW), 0.75% CH_4, T_s = 850 °C, p = 10 torr, hexane as diamond grit suspension liquid.

	Methanol			**Hexane**		
Powder grain size (μm)	R_a (nm)	d (nm)	N_D (cm^{-2})	R_a (nm)	d (nm)	N_D (cm^{-2})
≤ 0.25	2.4 ± 0.2	100	2×10^{10}	2.7 ± 0.2	50	7.5×10^{10}
8-16	3.9	170	8.5×10^{9}	3.5	100	1.6×10^{10}
20-40	5	300	4×10^{9}	5.8	220	8.6×10^{9}

Table III : Influence of CH_4 concentration in the H_2-CH_4 mixture. Operating conditions : 25 W/cm^3 (1.2 kW), 0.75% CH_4, T_s = 850 °C, p = 10 torr, hexane as suspension liquid.

	20-40 μm	**8-16 μm**	**≤ 0.25 μm**
% CH_4	R_a (nm)	R_a (nm)	R_a (nm)
0.5	13.7	12.3	7.4
0.75	12.1	11.0	6.2
1.0	10.7	10	5.6

Table IV : Influence of microwave power density in plasma on average roughness of 1 μm thick films. Operating conditions : 0.75% CH_4, T_s = 850 ° C, p = 10 torr, hexane as diamond grit suspension liquid, reactor in configuration I.

	20-40 μm	**≤ 0.25 μm**
Π (W/cm^3)	R_a (nm)	R_a (nm)
17 (0.8 kW)	20.3	-
25 (1.2 kW))	12.1	6.2
44 (2.1 kW)	7.9	-
59 (2.8 kW)	6.6	4

Table V : Average roughness and critical load for rupture and delamination of a 1 μm thick film as a function of Si orientation. Operating conditions : 59 W/cm^3, 0.5% CH_4, T_s = 850°C, p = 10 torr, 20-40 μm powder, methanol as diamond grit suspension liquid [12].

Orientation	R_a (nm)	F_c (nm)
Si(100)	9 ± 0.2	15 ± 0.9
Si(110)	4.7	7.3
Si(111)	2.6	4.6

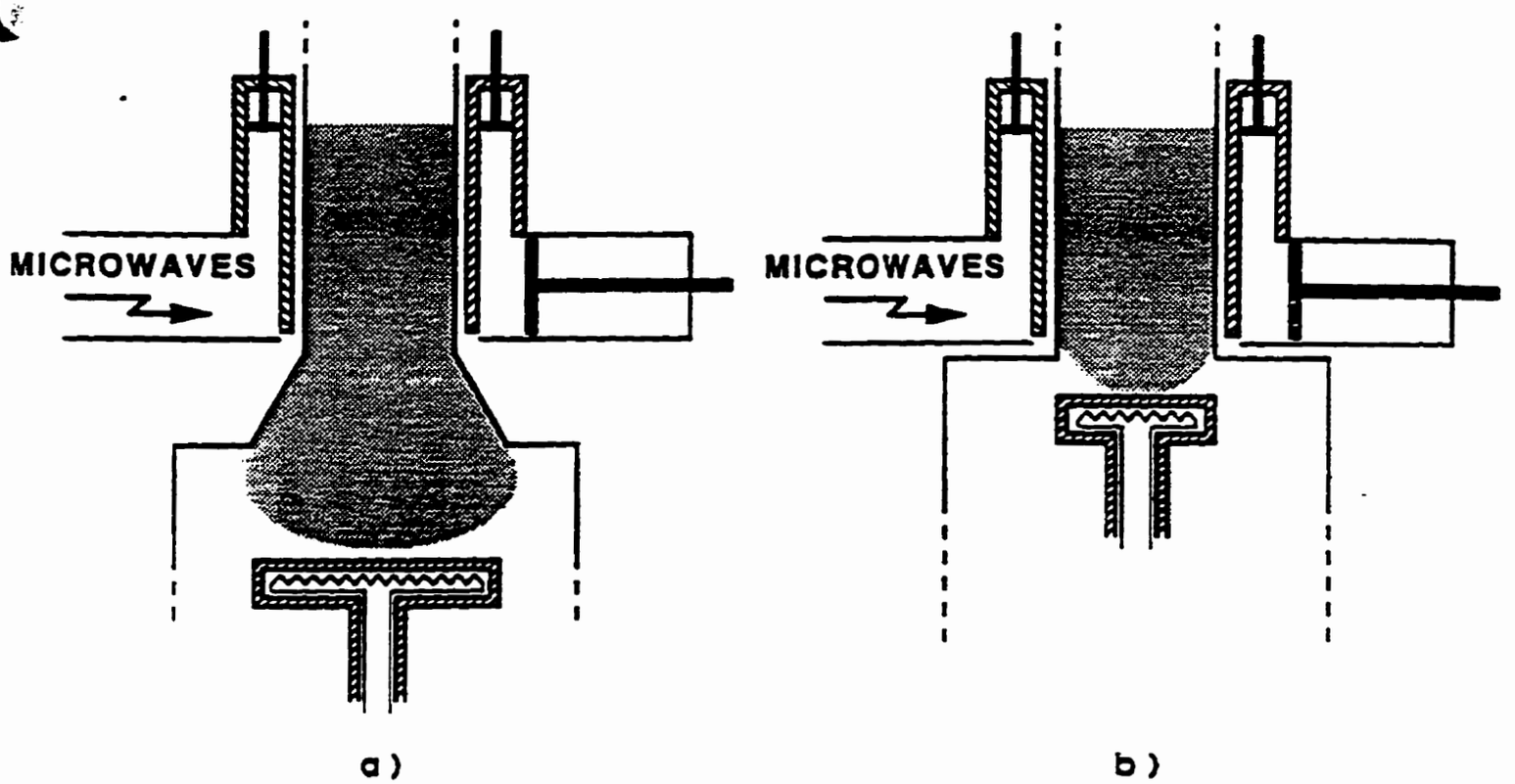

Fig. 1. Sketch of the reactor tube configuration showing how the diameter of the plasma hemisphere facing the substrate can be adapted to cover the substrate area: configuration I (a) and configuration II (b). For a given total absorbed microwave power, power density is higher with configuration II. The field applicator represented is a waveguide-surfatron wave launcher [35].

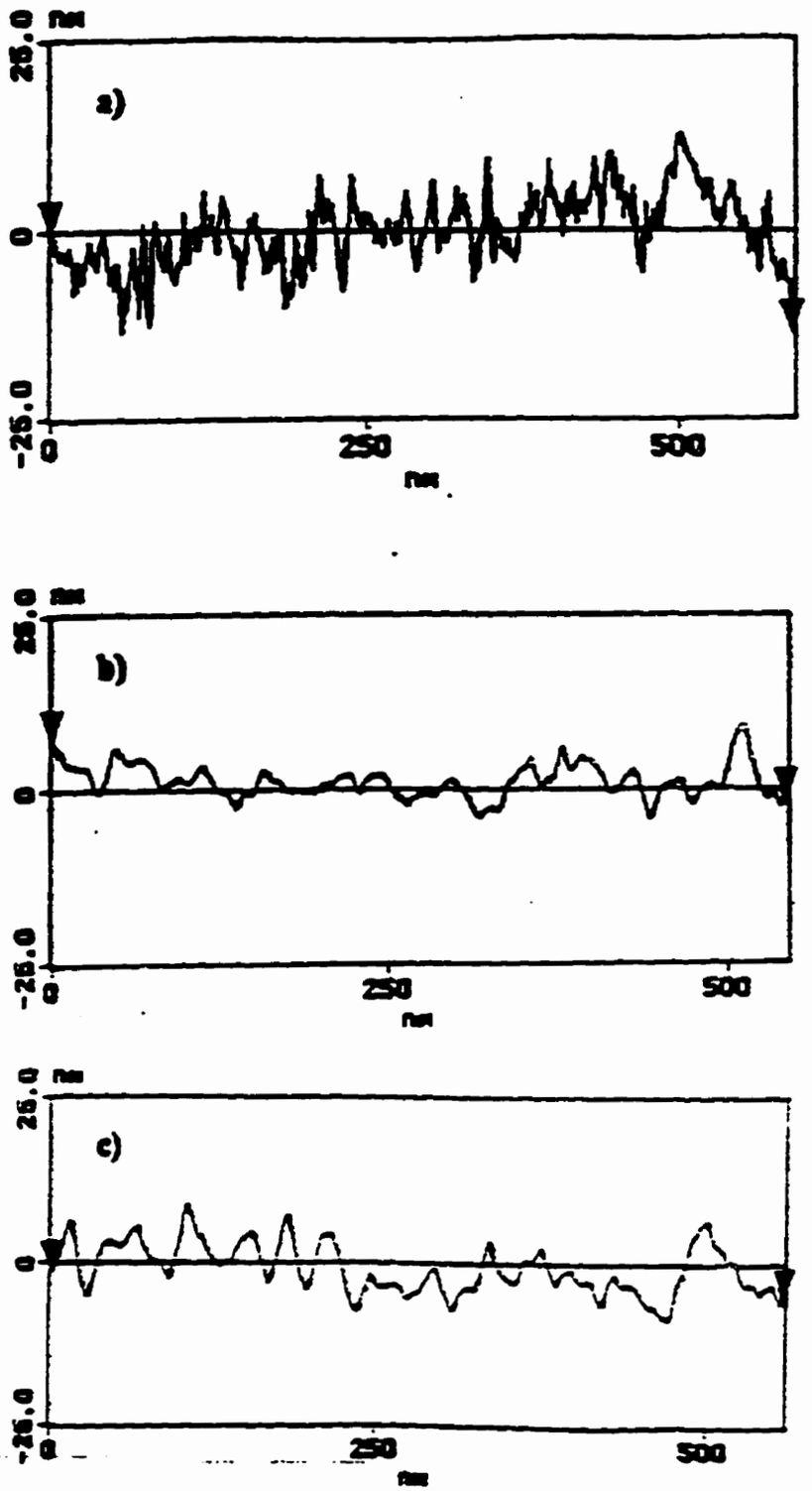

Fig. 2. Atomic force microscope recording showing that the smaller the grain size, the narrower and the deeper the holes created by ultrasonic impacts. Diamond grit sizes $\leq 0.25\mu m$ (a), 8 - 16 μm (b) and 20 - 40 μm (c).

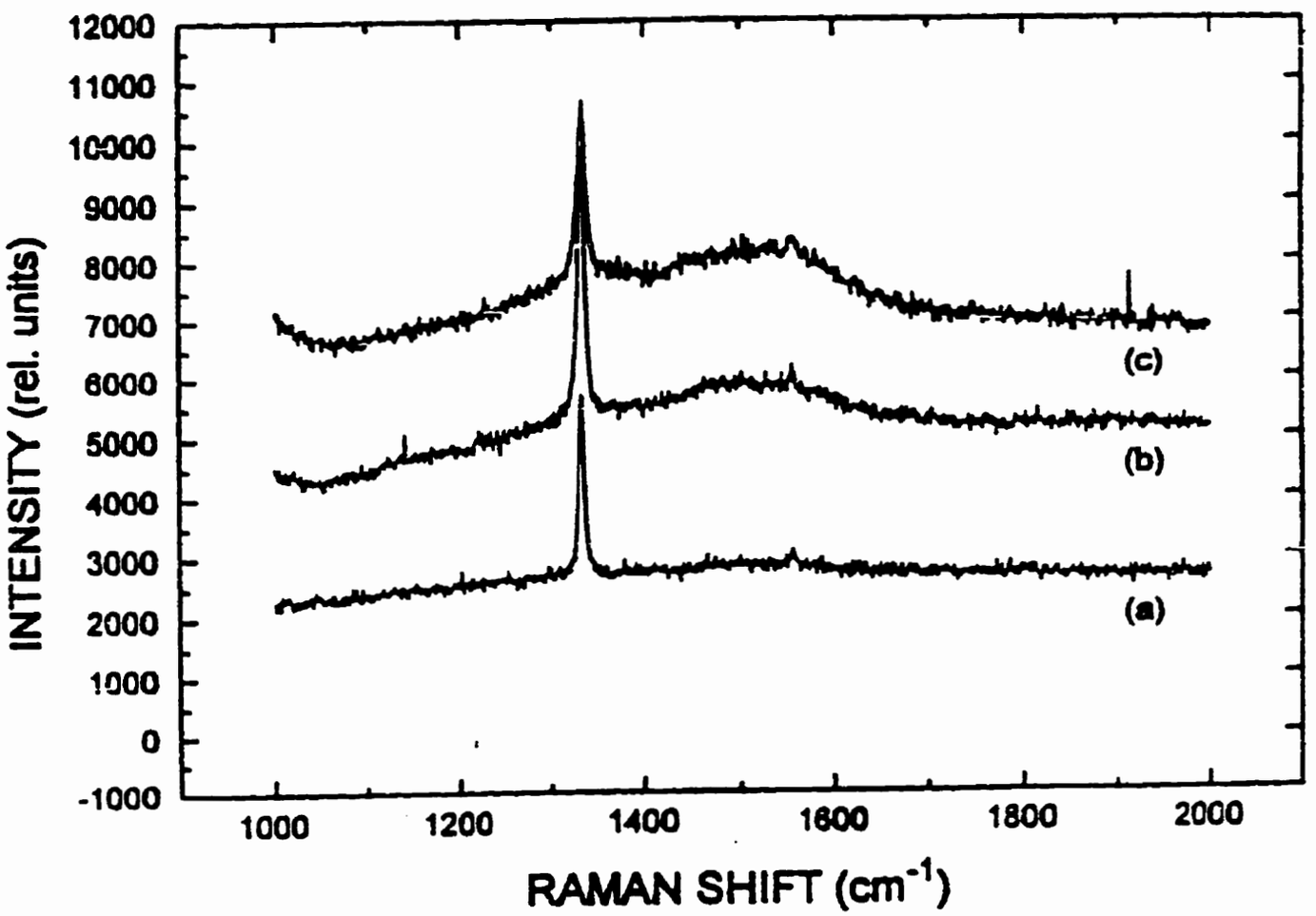

Fig. 3. Raman spectra of the diamond films deposited on substrates pretreated with diamond powders of three different sizes ($\leq 0.25\mu$m (a), 8 - 26 μm (b) and 20 - 40 μm (c)), followed by ultrasonic "cleaning" in methanol.

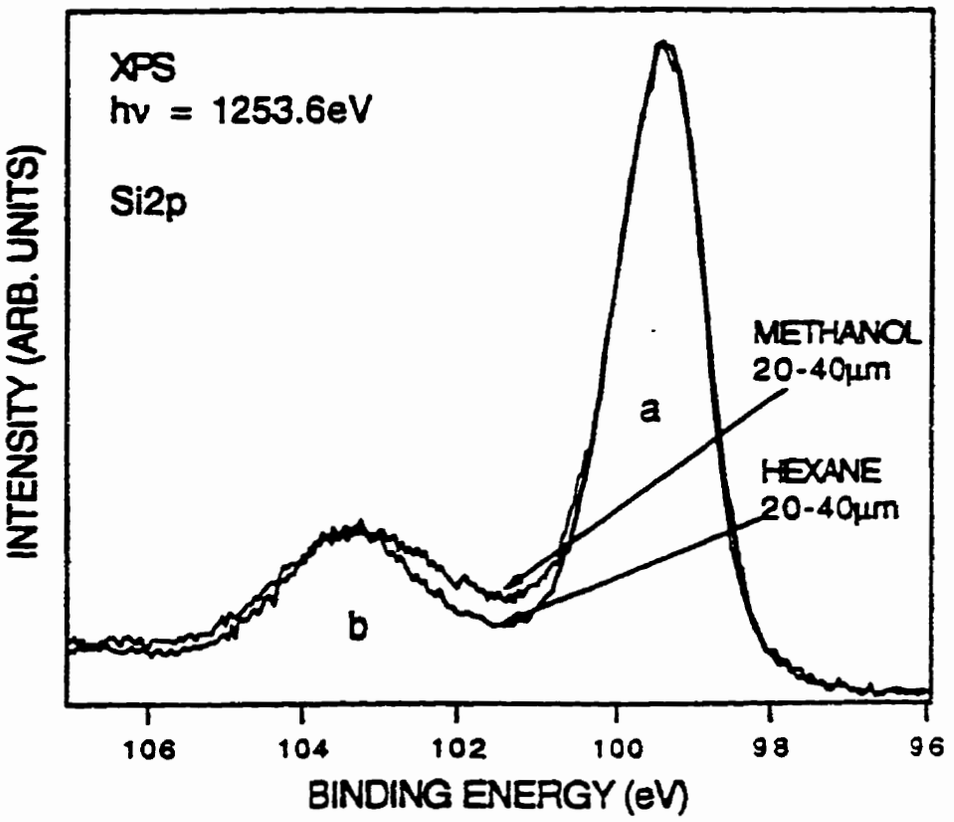

Fig. 4. XPS Si2p core level spectra of silicon substrates ultrasonically pre-treated in either methanol or hexane as the suspension liquid (20–40 μm diamond powder).

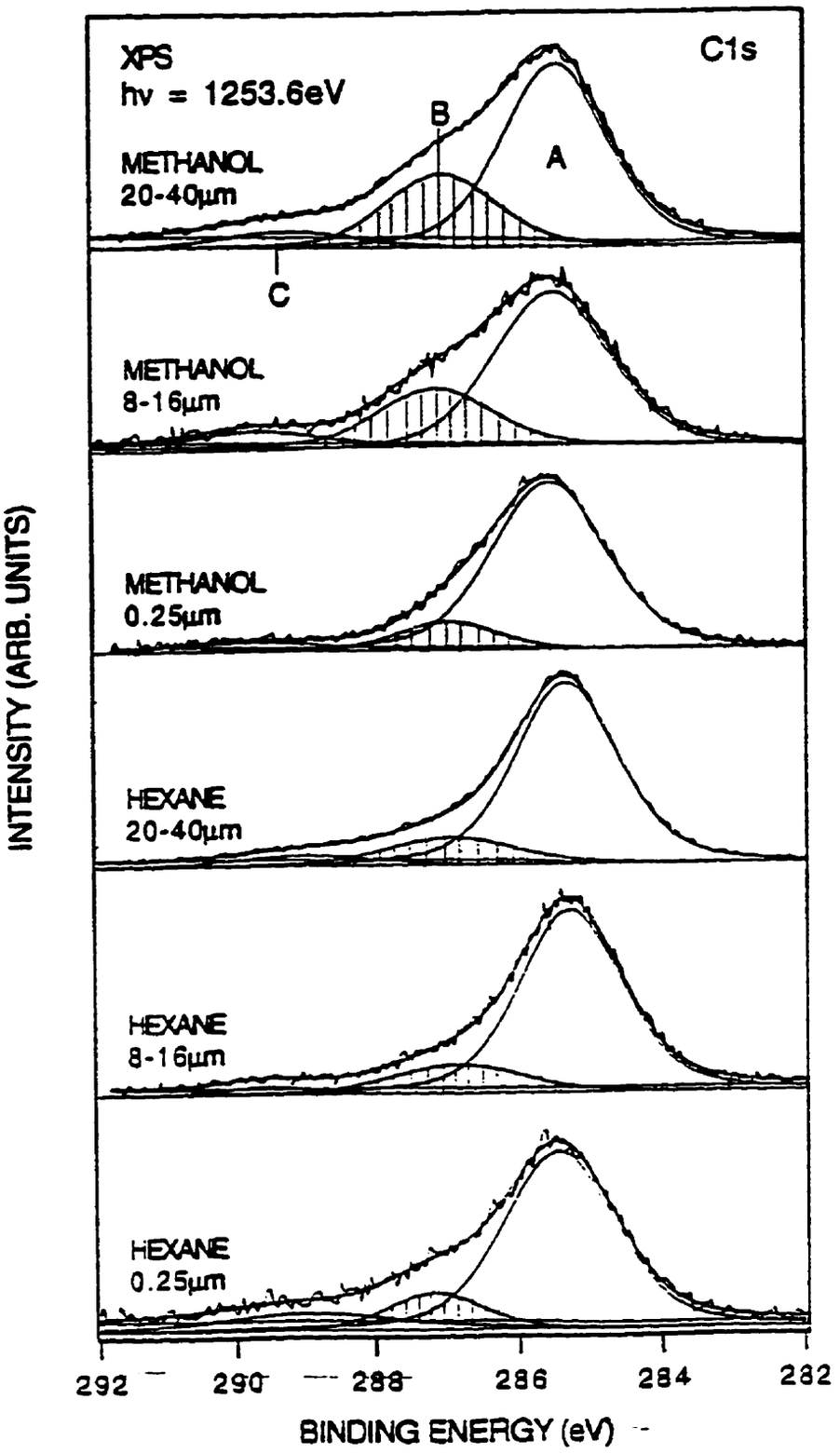

Fig. 5. XPS C1s core level spectra of silicon samples pretreated with different powder grain sizes using either methanol or hexane as the suspension liquid.

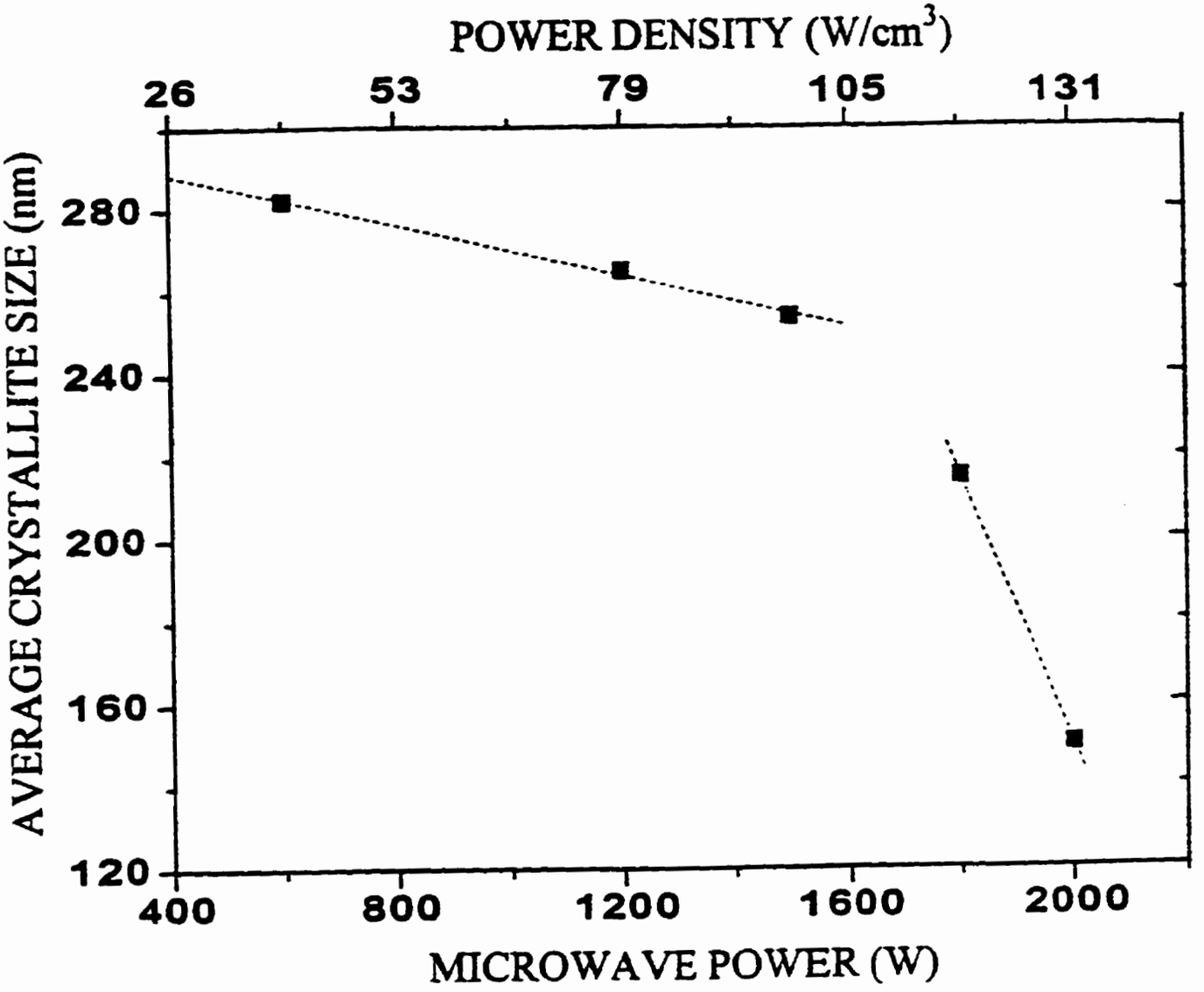

Fig. 6. Average crystallite size of a 1 μm thick film as a function of power density absorbed in the plasma. The data points can be fitted with two straight lines. Operating conditions: reactor in configuration II. T_s = 950 °C. $\%CH_4$ = 0.5. p = 10 torr. 20 - 40 μm diamond powder using methanol as the suspension liquid.

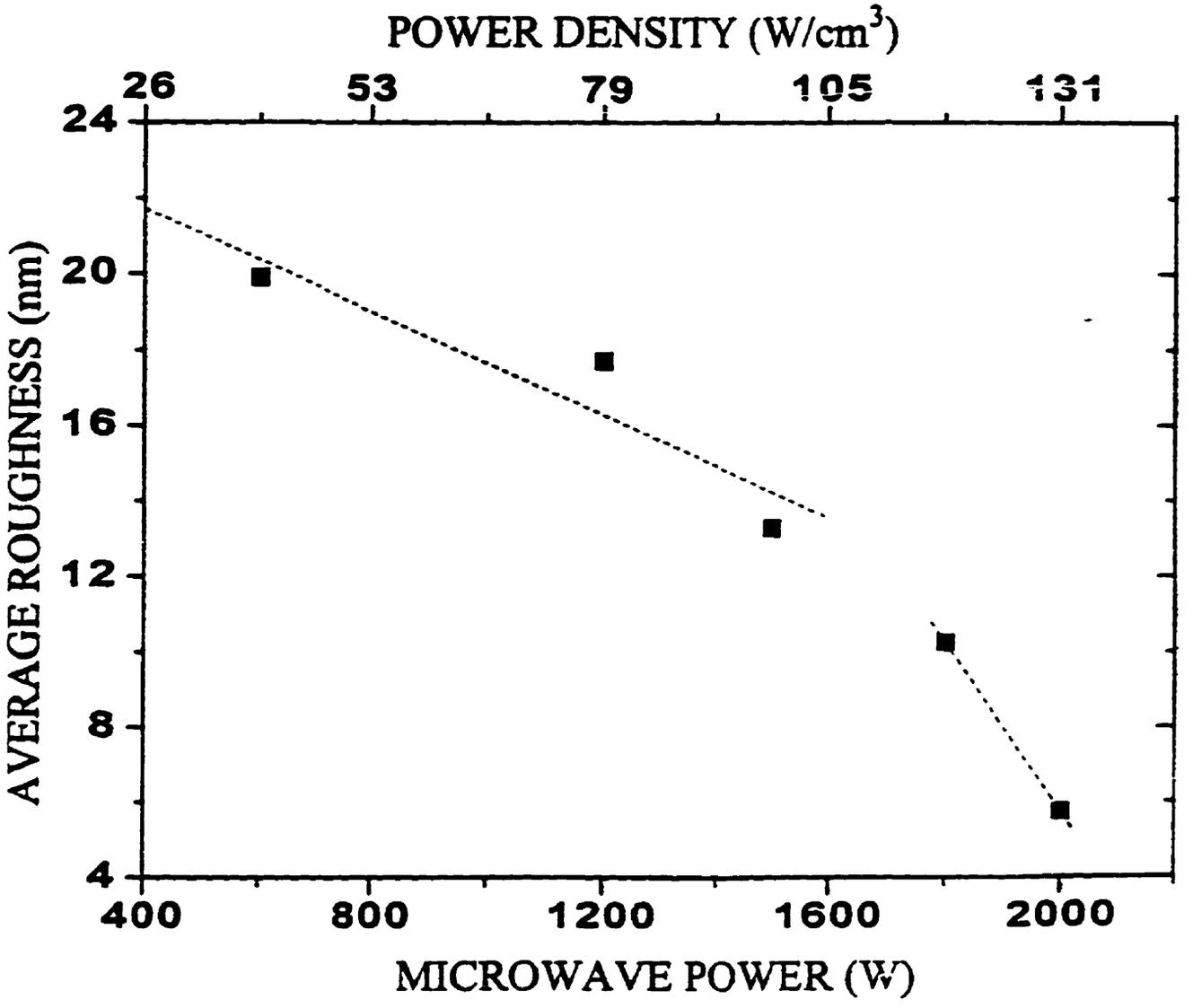

Fig. 7. Average roughness over a 1 μm thick film as a function of power density in the plasma. The data points have been fitted with two straight lines to try matching with the behavior of crystallite size with power density in Fig. 6. Same operating conditions as in Fig. 6.

CHAPITRE 7

Conclusion Générale

Chapter 7

Conclusion générale

Les travaux présentés dans cette thèse avaient pour but d'étudier divers aspects du dépôt de couches minces de diamant par chimie en phase gazeuse (CPG) assistée par un plasma de micro-ondes produit par une onde de surface électromagnétique. Cette activité s'est insérée dans un thème de recherche plus vaste au sein du groupe de physique des plasma de l'Université de Montréal, qui vise à contrôler et à étudier le dépôt par CPG classique et CPG assistée par un plasma produit par une onde de surface, de couches de matériaux ultra-durs ou de protections variées (e.g. nitruration) en vue d'applications industrielles.

Dans un premier temps, nous nous sommes particulièrement attachés à développer et mettre au point un nouveau type de réacteur à onde de surface pour le dépôt de couches minces de diamant (chapitre 2). Nous avons ensuite porté notre attention sur la maîtrise des conditions opératoires et sur une bonne connaissance des caractéristiques des couches de diamant ainsi réalisées. Cette étude nous a conduit à un contrôle rigoureux de la puissance micro-onde absorbée (exprimée en densité de puissance), de la vitesse de croissance de la couche et de la température du porte-substrat pour comparer avec les résultats publiés obtenus à partir de systèmes de type cloche à vide (*bell-jar*) ou à cavité résonnante. Nous avons vérifié que la puissance absorbée dans notre réacteur est, d'une part, totalement dépensée dans le plasma à la différence des systèmes "cloche à vide" et à cavité résonante et, d'autre part, que nous pouvions réaliser des densités de puissance plus élevées pour des puissances incidentes dans le réacteur comparables à celles de ces mêmes systèmes. La caractéristique peut-être la plus importante de notre réacteur concerne le découplage de la température T_s du porte-substrat d'avec la puissance micro-onde incidente: dans cette nouvelle configuration de réacteur, il n'est point besoin de

refroidir le porte-substrat pour travailler dans la gamme $600 \leq T_s \leq 1000\,°C$. Nous avons aussi observé que la rugosité des couches de diamant décroît lorsqu'on augmente la densité de la puissance micro-onde dans le plasma. Cette possibilité de réaliser des rugosités plus faibles que dans les réacteurs déjà existants de même qu'une meilleure adhérence sur des substrats métalliques (résultats non présentés dans cette thèse parce qu'il y a une demande de brevet en instance) semblent liées au fait que dans notre réacteur le substrat n'est pas chauffé par les micro-ondes. Lorsqu'il y a chauffage micro-onde du substrat, il y a généralement variation locale de T_s mais il pourrait aussi exister une température superficielle plus grande que celle affichée par le pyromètre optique pour l'ensemble du volume du substrat. d'où des conditions de dépôt différentes suivant la variation de T_s à travers le substrat[1]. Enfin, la force pondéromotrice en $\mid \nabla E \mid^2$ qui acélère les ions au sortir de l'hémisphere de plasma pourrait aussi être responsable de ces bonnes propriétés. Des articles très récents[2] montrent en effet l'action bénéfique d'une accélération des ions par polarisation du substrat.

Le chapitre III nous a conduit à une étude paramétrique des propriétés des couches diamant (qualité de la couche, taux de croissance, densité de nucléation et taille des cristaux) et du plasma (concentration en atomes d'hydrogène et température du gaz dans la couche thermique limite au-dessus du porte-substrat) en fonction de la concentration de méthane et d'oxygène, de la position du substrat et de sa température, de la pression du gaz, et de la densité de puissance micro-onde absorbée par le plasma. Nous avons trouvé que le taux de croissance est maximum pour $T_s = 930\,°C$ à une pression de 15 torr. Nous avons néanmoins obtenu des couches diamant avec des cristaux bien facettés et avec de défauts minimes dans un intervale de T_s plus large, 870-930 °C, et avec une concentration de méthane s'étendant de 0.25 à 1.50%.

Nous avons ensuite effectué (chapitre IV) une étude rigoureuse de la contamination en silicium des couches diamant. Une panoplie de diagnostics a été mise en oeuvre à cette fin (ERD-TOF, EMA, SIMS et XPS) et cette analyse a été comparée au spectre Raman des divers échantillon examinés. Nous avons montré que la concentration des

[1]Brevet: Stefan Feistritzer; Johann Kanz; Wilfried Schintimeister, US Patent Number:5,415,674 (16 Mai 1995)

[2]J. Robertson, J Gerber, S. Sattel, M. Weiler, K. Jung, and H. Ehrhardt; Appl. Phys. Lett. 66 (24), 12 June 1995

impuretés de Si était plus élevée sur un substrat de silicium pur que sur un substrat de silicium recouvert d'une mince couche de SiC. D'une façon générale, nous avons constaté que cette contamination venait de l'attaque par les atomes d'hydrogène du substrat (sans couche de SiC) et des parois du tube à décharge. La concentration en impuretés de Si mesurée est de l'ordre de 0.01% et 0.2% at. Une façon de réduire leur teneur est l'addition d'oxygène pendant le processus de dépôt: l'addition d'oxygène passive la paroi du tube à décharge mais neutralise aussi les atomes de Si qui provienennt du substrat sous la forme Si_xO_y ($x,y=1,2,3,...$). Finalement, on a constaté que l'ajout d'oxygène lorsque le substrat a été recouvert d'une mince couche de SiC augmentait plutôt la concentration de silicium dans la couche diamant. Une étude plus approfondie est nécessaire pour comprendre ce mécanisme de contamination. Enfin, nous avons mis en évidence que la présence d'impuretés de silicium causait la fluorescence observée sous forme de bruit de fond autour du spectre Raman de la raie diamant. La spectroscopie Raman est dans ce cas une méthode simple pour contrôler la présence de ces impuretés.

Le chapitre V a présenté une étude systématique des premiers instants de la croissance du diamant dans un plasma micro-onde. Pour cette étude, nous avons eu recours à la microscopie à balayage électronique (MEB), au microscope à force atomique et à la spectroscopie Raman. Nous avons montré que la densité de nucléation, la taille des cristaux, la qualité et l'adhérence de la couche diamant sur le substrat dépendaient de l'orientation cristalline du substrat de silicium. La différence de densité de nucléation entre le Si(100), le Si(111) et le Si(110) peut être expliquée par la contribution de deux effets: la topographie de surface des différentes orientations cristallines et la gravure préferentielle par l'hydrogène atomique de la surface le plus accidentée (Si(100)). Ce processus de gravure augmente en effet la distribution de défauts de surface, dont on sait qui ils favorisent la densité de nucléation. Cette augmentation de la nucléation favorise l'adhérence du dépôt au substrat. Par ailleurs, les défauts créés par le prétraitement par ultra-sons favorisent l'augmentation de la taille des cristaux mais ne semblent pas intervenir dans le mécanisme d'adherence.

À la suite de l'analyse de ces résultats concernant le prétraitment, nous avons effectué (chapitre VI) une étude approfondie de l'influence de la taille des cristaux de la poudre diamant du prétraitement sur la densité de nucléation, sur la taille des cristaux et sur la

rugosité de la couche diamant. Nous avons observé une forte augmentation de la densité de nucléation lorsque le diamètre moyen de la poudre diminue jusqu'à $0.25\mu m$. Par contre, la taille des cristaux et la rugosité moyenne décroissent lorsque la taille de la poudre diamant du prétraitement diminue. De cette façon, nous avons montré que la rugosité des couches diamant dépendait fortement du prétraitement du substrat mais aussi de la densité de puissance absorbée dans le plasma.

Cette thèse aura donc permis de proposer à la communauté scientifique un nouveau type de réacteur à plasma pour le dépôt de couches diamant. Ce nouveau réacteur est non seulement original mais il possède des propriétes remarquables qui, d'une part, nous ont permis de progresser dans la connaissance des mécanismes de prétraitement et de dépôt des couches diamant par CPG et qui, d'autre part, autorisent d'envisager la fabrication de couches diamant de haute qualité pour le revêtement de divers matériaux, notamment dans le domaine des outils de coupe. Ces travaux méritent d'être poursuivis, par exemple, par une modélisation électromagnétique du plasma hémisphérique. Par ailleurs, des études ont commencé en vue de la réalisation d'un réacteur fonctionnant à 915 MHz pour pouvoir recouvrir des substrats de plus grande surface. Enfin, des efforts sont déjà en cours dans le cadre d'une subvention stratégique pour apporter notre concours au développement industriel de ce procédé.

Remerciements

Premièrement, j'aimerais remercier le professeur Michel Moisan pour m'avoir accueilli dans le Groupe de physique des plasmas en qualité de directeur de Thèse et pour ses nombreux conseils indispensables au succès de ce travail.

Je tiens aussi à remercier les professeurs Michel Wertheimer et Ludvic Martinu (École Polytechnique) pour leur nombreux conseils et une collaboration enrichissante. Je remercie aussi la professeure Alix Gicquel (Université Paris XIII) pour son accueuil chaleureux et un fructueux stage dans son laboratoire au début de mes travaux de thèse.

J'aimerais remercier le Dr. Sabine Schelz de notre groupe pour la discussion des mes travaux et sa fructueuse collaboration.

J'aimerais remercier le Dr. Vladimir Trava-Airoldi (INPE - Brésil) pour sa collaboration et de nombreuses discussions.

Je voudrais aussi remercier le professeur Daniel Guay (INRS - Énergie et Matériaux) pour notre fructueuse collaboration qui a permis la caractérisation des couches diamant au moyen du microscope à force atomique.

Mes remerciements vont également au Dr. Éric Gat (INRS - Énergie et Matériaux) pour son aide, au Dr. S. G. Gujrathi pour les analyses ERD-TOF, et au Dr. P. Van der Heide (University of Western Ontario) pour les mesures SIMS.

Il m'est particulièrement agréable d'exprimer ici toute ma reconnaissance à l'aide précieuse de Messieurs François Roy, Robert Lemay, Robert Martel, Gaston Sauvé et Remy Grenier pour leur encadrement technique, leur collaboration amicale et sympathique, essentiels pour mener à bien ce travail dans un climat de bonne humeur.

A mes remerciements, j'associe l'ensemble des mes collègues de travail.

Enfin, je remercie le Ministère des Affaires Internationales du Québec (programme des bourses d'Excellence) et l'Université de Montréal pour leur soutien financier.

Qu'il me soit permis d'exprimer ma reconnaissance aux membres de mon jury de Thèse:

- à Monsieur John L. Brebner, qui m'a fait l'honneur d'être président du jury,
- à Messieurs Michael Wertheimer et Jean-Luc Meunier pour avoir accepté de faire partie du jury.

Enfin, j'associe également à ces remerciements l'ensemble du personnel administratif pour leur sympathie et leur disponibilité de chaque instant.